Measuring and modeling stormwater runoff from an interstate in a rural/forested watershed

by

Mitchell Forrest Moore

A dissertation submitted to the Graduate Faculty of
Auburn University
in partial fulfillment of the
requirements for the Degree of
Doctor of Philosophy

Auburn, Alabama
December 10, 2016

Keywords: Runoff, highway, groundwater, modeling, water quality, streamflow

Approved by

Jose G. Vasconcelos, Chair, Associate Professor of Civil Engineering
Wesley C. Zech, Professor of Civil Engineering
Xing Fang, Chair Professor of Civil Engineering
Prabhakar Clement, Professor of Civil Engineering
Latif Kalin, Professor of Forestry and Wildlife Science

Abstract

In hydrological research, roadways are often defined simply as an increased impervious portion of a watershed or a flow blocking structure. The research presented in this dissertation examines the effects of highway crossings on stream water quality, groundwater-surface water interactions, and stormwater runoff. Management of stormwater runoff from highways has been identified as an important aspect of highway development or redevelopment in recent years. Research to date has shown that stormwater runoff, including that from roadways, may have constituents that cause adverse impacts to aquatic ecosystems. Such investigations have focused either on characterizing the runoff directly generated on roads or on the effectiveness of various pollutant removal techniques. Unlike these works, the research presented herein focuses on impacts created by stormwater runoff from roadways measured in small headwater streams. This dissertation presents the results of an investigation on the impact of stormwater runoff from Interstate 59 (I-59) measured at the Little Cahaba Creek (LCC), a small headwater stream in Trussville, AL.

Water samples were collected at selected points and hydrological and water quality parameters were continuously monitored in selected stations. In addition to field measurements of streamflow, groundwater levels, and water quality parameters within the LCC, two hydrologic models (SWMM and GSSHA) were developed to explore the relationship between the interstate features and the watershed's response to rain events, including groundwater fluctuations. After model calibration, the relationship between observed streamflow and groundwater table

fluctuations was determined: bank storage was a dominant process in the near-stream subsurface. Comparisons of modeled data to measured streamflow and groundwater table elevation data are made for multiple major storm events. Both programs performed well in calculating the groundwater table elevation change due to stream bank storage.

Water quality upstream and downstream of the roadway was very good, with low concentrations of nutrients, suspended sediment, and other parameters and high biodiversity as measured in this study. Of particular importance, these parameters generally do not increase as the stream receives stormwater runoff from I-59. Additionally, the complex response of streamflow to rain events across the roadway could not be well defined through field measurement alone. Modeled data indicates that a substantial amount of groundwater table elevation change could be represented as bank storage at the downstream site, but the median drainage area captures and retains more runoff than could be modeled in this work.

Since groundwater-surface water interactions are often neglected in hydrological modeling, an accurate understanding of the location of the groundwater table is unlikely when this is not considered. With this in mind, the ability to properly design and install infiltration based stormwater volume reduction approaches will be severely reduced and unreliable. Future research should include the consideration of road-crossing hydrology. In particular, grass-lined medians are common in roadway development, yet it is unclear how much stormwater runoff could be captured in the subsurface of these drainage systems.

Acknowledgments

I acknowledge first the Alabama Department of Transportation for funding this research as a part of the project number 930837R, as well as ALDOT staff who have contributed towards the completion of our goals. This includes Wade Henry and Barry Fagan for their insight on stormwater runoff from roadways and for their advice and perspective on interstate drainage and design. The findings in this dissertation reflect the work done by the author, and do not reflect the views of the funding agency.

I would like to thank my wife, Lorena Vangjeli Moore, for her love, care, and support during the difficult times, as well as sharing in the happy times.

To my committee, many thanks are owed to the countless hours of collective advice, tough talks, challenges, support, encouragement, and training I have received from you.

Dr. Jose Vasconcelos, my dissertation advisor, has been an amazing mentor and helper during this research. Thank you for your hard work, availability, and faith in me as you have entrusted me with this task. You have been an amazing advisor, thank you.

Table of Contents

List of Tables

List of Figures

List of Abbreviations

1D	1-Dimensional
2D	2-Dimensional
Ψ_f	Capillary Suction Head
ADEM	Alabama Department of Environmental Management
ALDOT	Alabama Department of Transportation
ASCE	American Society of Civil Engineers
COD	Chemical Oxygen Demand
DEM	Digital Elevation Model
DO / LDO	Dissolved Oxygen
EDT	Estimated Detection Limit
EQ	Equation
ET	Evapotranspiration
FHWA	Federal Highway Administration
GSSHA	Gridded Surface Subsurface Hydrologic Analysis
I-59	Interstate 59
IC	Ion Chromatograph
K_{sat}	Hydraulic Conductivity
LCC	Little Cahaba Creek
µS	Micro-Siemens

MS4	Municipal Separate Storm Sewer System
NPDES	National Pollutant Discharge Elimination System
NSQD	National Stormwater Quality Database
NTU	Nephelometric Turbidity Units
ppm	Parts per million
Q	Discharge or Flow Rate
SM	Standard Methods
SUMSQ	Sum of Squares
SWMM	Storm Water Management Model
TKN	Total Kjedahl (organic) Nitrogen
TN	Total Nitrogen
TP	Total Phosphorous
TSS	Total Suspended Sediment
TS	Total Solids
USACE	United States Army Corps of Engineers
USEPA	United States Environmental Protection Agency
USGS	United States Geological Survey

Chapter 1 – Introduction

Watershed hydrology is the branch of science focusing on the distribution, characteristics, and processes of water within a defined area (i.e., watershed). Throughout the U.S., watersheds are defined at varying scales for water use and management. The geographic boundaries of a watershed are defined by the topography of the region, where ridgelines create a divide for the eventual delivery of rainfall to a common downstream endpoint in a river, stream, or other water body. Though the boundaries of a watershed are defined by the physical nature of the ground surface, the focus of watershed hydrology includes complex processes that affect one another in respect to the movement and quality of water resources.

Although the hydrologic cycle is a complex process, the major pathways of water and physical processes that occur are often lumped into the following set of categories: precipitation, infiltration, evapotranspiration, surface runoff, groundwater, storage, and rivers or streams, as seen in Figure 1.1. Precipitation is the driving force of streamflow and groundwater recharge; it can fall as rain or snow depending on climatic forces and varies in intensity, duration, and spatial distribution. Some of this precipitation will enter the soil via infiltration depending on soil characteristics, land use, and the physical nature of the surface and subsurface. Some, though not all, of this infiltrated water becomes groundwater where it is temporarily stored and typically travels more slowly than surface water. A large portion of precipitation will return to the atmosphere through evapotranspiration both before and after becoming streamflow or groundwater. The total amount of water that returns to the atmosphere through evapotranspiration (ET) is dependent on many factors including temperature, solar radiation, land use, plant types, soil characteristics, wind, and others. The majority of water that does not directly infiltration the soil initially becomes surface runoff as the water travels over the surface

of the ground towards a downslope stream, river, or other water body. In addition to water that is stored as groundwater, water may be stored in ponds, lakes, wetlands, and other surface features that can retain large volumes of water with relatively limited to no outflow. Streams and rivers are formed in the valleys between higher elevation areas, collect surface runoff, and convey flow towards a downstream or lower elevation point.

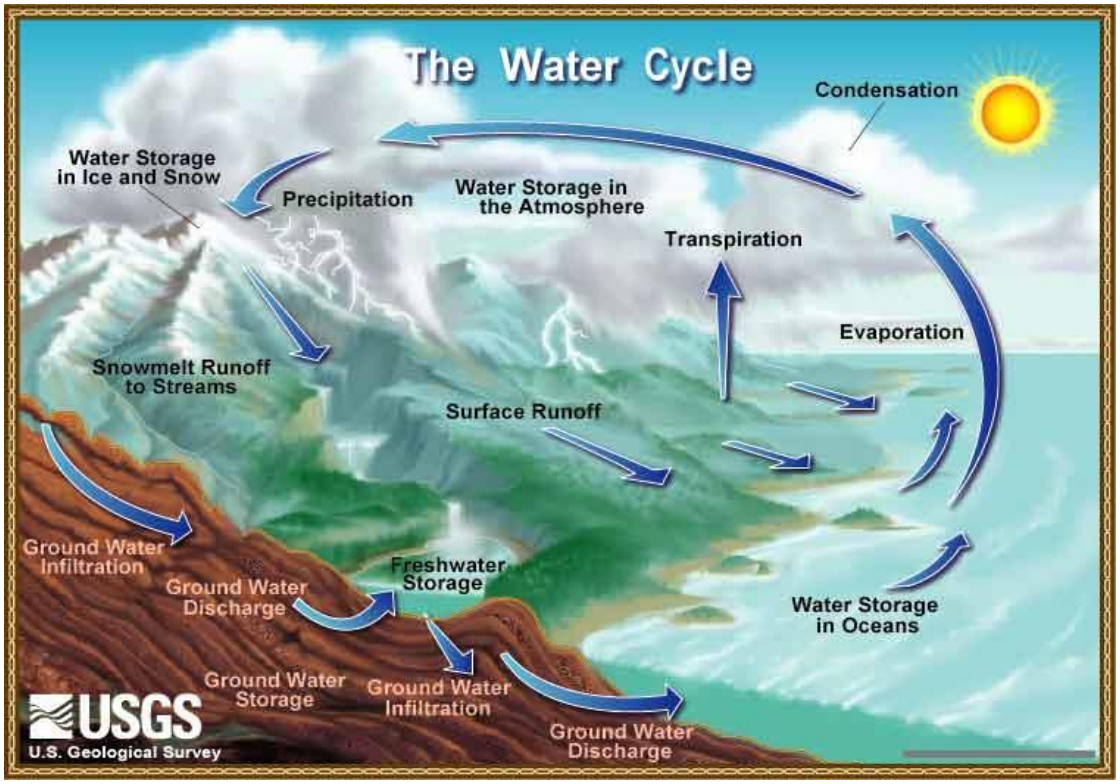

Figure 1.1 Major processes of the hydrologic cycle. Figure from USGS (2016).

Headwater watersheds are those regions where major rivers and streams derive most their flow. These are areas that contribute flow to 2nd and 3rd order streams, and have a more dynamic relationship between groundwater, hillslope, geomorphology, nutrients, and surface runoff than their downstream recipients of runoff (Gomi et al., 2002). Headwater watersheds experience most of the features of the hydrological cycle without any remote influences, particularly streamflow from a distant source. The present research focuses on such a headwater watershed,

and can consider the impacts of a major roadway with limited influence from other sources and land uses.

Although the above mentioned hydrological processes are broadly defined as separate systems, they interact with one another exquisitely, motivating both practical and philosophical research. As one of the most dominant processes, evapotranspiration rates drastically affect the others (Hanson, 1991). High evapotranspiration rates can encourage additional rainfall at a regional scale, increase infiltration capacity in soils, and decrease groundwater levels and baseflow conditions in streams and rivers. These latter effects are especially noticed in the absence of rainfall events over a prolonged period. Surface runoff and infiltration capacity of soils are typically inversely related, whereas higher rainfall intensity and duration is positively related with surface runoff. Groundwater and surface water levels can often interact with one another, and channels are either defined as losing or gaining depending on the direction of flow, either towards or away from the groundwater aquifer, respectively. Since these interactions are extremely complex, hydrologic researchers typically focus on a selected group of hydrological process and a smaller group of interactions.

Land use development tends to alter one or more hydrological processes, interactions, and water quality of a watershed, depending on the type of land use and development strategy. To minimize or mitigate the impact of land use development, particularly regarding the impacts of land development to runoff generation and changes in water quality, stormwater management practices can be employed as mitigation strategies.

1.1 Land Uses and Associated Impacts to Watersheds

Economic development is a leading driver for land use change in the U.S. and across the world, where naturally forested or grassland areas are converted to residential, agricultural, commercial or industrial land uses (Lambin and Patrick, 2011). In general, land uses can be lumped into two categories: developed, and undeveloped. Within each of these two categories, there are many different types of specific land uses identified that have similar characteristics, especially in regards to hydrological features, vegetation type, and imperviousness. During land use development, characteristics of the developed land is often compared to the undeveloped condition, such as is often the case for hydrological parameters (i.e., peak runoff rate, total runoff volume, infiltration rate, and groundwater levels).

Depending on the type of land use, in addition to those mentioned above, many characteristics of the developed area will change. Often, variations are similar within certain types of land use, so they are categorized together, though these groupings may vary depending on the use of the classification system. The national land cover database (NLCD, Homer et al., 2015) has 20 different land use categories, only four of which are for developed areas of varying intensities. The national stormwater quality database report (NSQD, Pitt et al., 2004) distinguishes five major land uses: residential, commercial, industrial, freeway, and open space. Residential land use varies by region, but generally has more impervious surfaces than undeveloped land use, and may have increased pollutant loads in stormwater runoff. Commercial and industrial land uses have much higher percent impervious areas, and have the potential for higher pollutant loadings than residential land use. Open space typically has better water quality in stormwater runoff, though it is developed land, due the lack of impervious surfaces and anthropogenic sources of pollutant loads. Table 1.1 shows some summary data from the NSQD

for the land uses mentioned here, and parameters of stormwater runoff that are relevant to this work.

Table 1.1. Summary of available data from the NSQD (Pitt et al., 2004) for varying land uses.

	Parameter	pH	Conductivity (μS/cm)	TSS (mg/L)	NH_3 (mg/L)	NO_3 (mg/L)	TN (mg/L)	TP (mg/L)
Overall Summary	Median	7.5	121	59	0.58	0.59	2.27	0.27
	Cv	0.1	1.6	1.8	0.8	0.7	-	1.5
Residential	Median	7.2	102	49	0.31	0.6	2.41	0.31
	Cv	0.1	1.6	1.8	1.1	1.1	-	1.1
Commercial	Median	7.4	107	43	0.5	0.6	2.6	0.22
	Cv	0.1	1	2	1.2	1.1	-	1.2
Industrial	Median	7.5	139	81	0.42	0.69	2.51	0.25
	Cv	0.1	1.3	1.6	1.3	0.92	-	1.4
Freeways	Median	7.1	99	99	1.07	0.28	3.35	0.25
	Cv	0.1	1	2.6	1.3	1.2	-	1.8
Open Space	Median	7.7	113	48.5	0.18	0.59	1.51	0.31
	Cv	0.08	0.5	1.5	1.24	0.9	-	3.5

Note: Cv is the coefficient of variation, defined as the mean divided by the standard deviation. pH is the measured of hydrogen ion activity, conductivity is a measurement related to the concentration of ions in the water, TSS is the total suspended sediment concentration, NH_3 is ammonia, NO_3 is nitrate, TN is total nitrogen, and TP is total phosphorous.

Roadways comprise an estimated 1% of the land within the U.S. (Watts et al., 2005) and often cross over multiple watersheds and water bodies (i.e. streams, wetlands, lakes, and ponds). According to the national land cover database, only 5.6% of the U.S. area is developed land use, when agricultural land is considered as separate (Homer et al., 2015). Thus, roadways may comprise approximately 10 to 20% of the developed land in the U.S. This type of land use change is of importance concerning the hydrological system, as it increases the impervious fraction of land cover and often leads to the installation of conveyance channels and basins that alter the natural response to rainfall (Zoppou, 2000). Previous work has shown that roadways, in some cases, can introduce additional nutrient loads in receiving water bodies (Pitt et al., 2004), and alter stormwater runoff and groundwater table elevations (Kahklen and Moll, 1999). Since roadways are so abundant, and exist within most watersheds, a clear understanding of the

hydrological variations caused by roadways must be achieved. Additional detail on the impacts of roadways to receiving water bodies are presented in Chapter 2: Literature Review.

1.2 Stormwater Management in Developed Watersheds

Since land use development alters the natural landscape and hydrological response of an area, various strategies are employed to reduce the associated impacts of land development. One strategy is developing Stormwater Management Plans, which can be viewed as a group of institutional, managerial, and engineering approaches that aim to maintain the integrity and stability of receiving water bodies and ecosystems affected by stormwater runoff (USEPA, 2005). Stormwater Management Plans include deployment of best management practices (BMPs), such as detention structures and drainage features, to reduce peak runoff rates and runoff volume, treat surface runoff and discharges, and encourage additional infiltration and groundwater recharge. The approaches used for stormwater management are often site-specific based on a variety of factors and are regulated by federal and state organizations.

To protect the nations water bodies, section 402 of the Clean Water Act of 1972 introduced the National Pollution Discharge Elimination System (NPDES). This program gave the Environmental Protection Agency (EPA) the ability set limits on discharges into bodies of water through a process of permitting regulations. These permits are applied at the federal and state level, and are considered general permits for land uses with similar disturbances and discharges or individual permits for specific entities. Regulations exist for most Municipal Separate Storm Sewer Systems (MS4s), which are any type of conveyance network or channel that conveys stormwater, not a combined sewer, that is owned by any city, state, town, or other public entity discharging into the nations waters. MS4s are categorized as Phase I (large and

medium MS4s) or Phase II (small MS4s) depending on the size of the municipality the system is designed for and population. Per the Code of Federal Regulations (CFR), Title 40, part 122.26(b)(4) and (7), large MS4s are those "located in an incorporated place with a population of 250,000 or more…" and medium MS4s are those "located in an incorporated place with a population of 100,000 or more but less than 250,000…", or otherwise designated by the director or the CFR.

In the context of roads in Alabama and the NPDES, the Alabama Department of Environmental Management (ADEM) recently issued MS4 permit coverage to the Alabama Department of Transportation (ALDOT) (ADEM, 2013). The permit, ALS000006, regulates stormwater discharges from ALDOT properties located within urban municipal boundaries designated as Phase I and Phase II MS4s. Among the elements and requirements of the permit is the need to implement controls to minimize impacts of stormwater during and after construction. To attain the goals of post-construction stormwater management, and considering that stormwater runoff impacts may also originate from other types of land use in the watershed, it is essential to obtain pre-development information on the hydrological and water quality characteristics.

ALDOT's MS4 permit is relevant in the context of the Birmingham Northern Beltline (BNB), an ongoing (84 km) road project carrying traffic around the north and west of Birmingham, Alabama (Figure 1.2). The proposed road alignment intersects a number of streams and rivers that are very important to the state including the Cahaba and the Black Warrior Rivers. One of the streams is the Little Cahaba Creek (LCC), a headwater perennial stream that is at the easternmost point of the BNB. Figure 1.2 indicates the location of the new road to be constructed and the location of the LCC watershed (black rectangle). The stream's watershed is currently intersected by Interstate 59 (I-59). While baseline information for assessing post-construction

stormwater runoff impacts in the LCC is needed, the existence of I-59 also provides researchers a chance to evaluate any long term post-construction impacts of I-59 on the LCC. In a larger context, this work also aims to understand the types of impacts of interstate stormwater runoff into underdeveloped watersheds sharing similar characteristics.

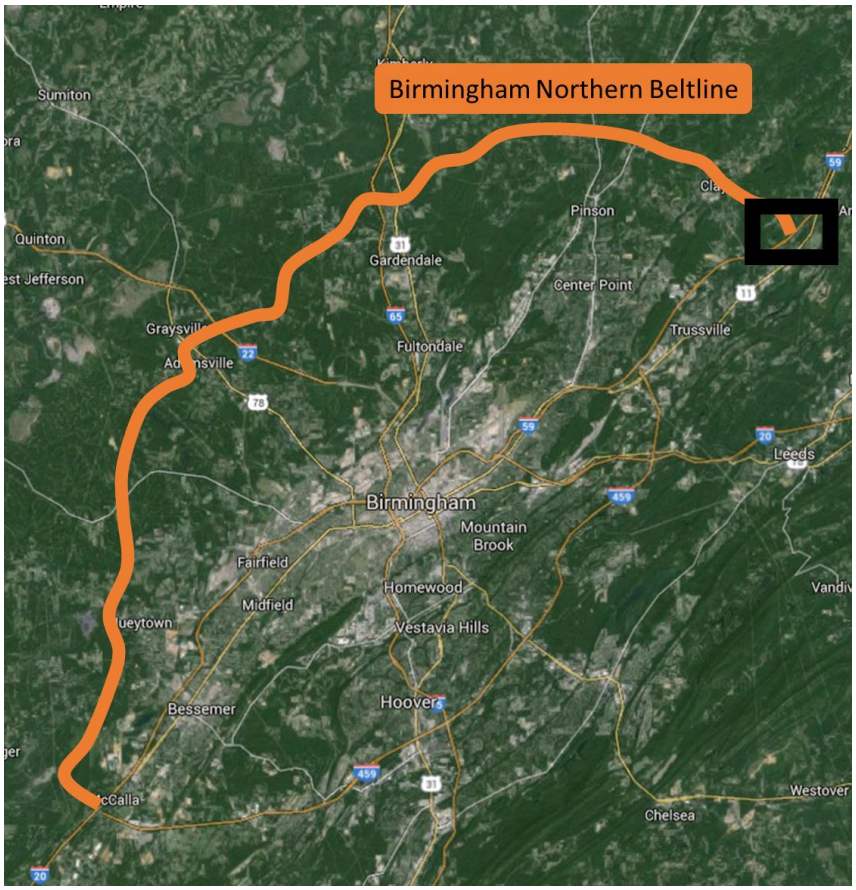

Figure 1.2 Proposed alignment of the BNB. Bold orange line indicates location of the beltline. Black rectangle indicates the location of research project and LCC.

1.3 Watershed Modeling Tools

Since the processes by which water travels through a watershed are complex and dynamic, models are often used to describe one or more of these processes. In the context of watersheds, these models will use single or multiple equations to simulate a hydrological response, such as a downstream flow rate, from an input feature, such as a rainfall hyetograph. There are many ways

to classify hydrological models, including: 1) conceptually- vs. physically-based; 2) lumped vs. distributed; 3) and event-based vs. continuous modeling. Physically-based models use equations that describe the physical processes that occur in hydrology, such as the rate of infiltration occurring in a soil with a given capillary head, porosity, and saturated hydraulic conductivity. Conceptually-based models, on the other hand, use equations with conceptual parameters to describe the hydrological process, such as the case of the well-known rational method, which solves for a downstream peak flow rate using a runoff/rainfall ratio coefficient. Lumped models represent a watershed as having a single downstream outlet and a single set of parameters describing the hydrological processes within the watershed. Distributed models, on the other hand, solve for various hydrological results at each defined spatial unit.

Since distributed models obtain many solutions within the model domain, the calculation time is longer than lumped models, typically. Additionally, distributed models are more complex than lumped, and they also typically use physically-based formulations, whereas lumped models often use conceptual formulations. Thus, in the hydrological modeling literature, models are often described as either conceptually-based lumped models or as physically-based distributed models. Event-based models are focused on calculating the hydrological response, such as downstream flow rate, from a single storm event. These simulations may require providing some information about the watershed before the event, such as antecedent moisture conditions, initial soil moisture content, and days since the most recent rainfall. Continuous models simulate watersheds over long periods of time, often at least one year, and typically incorporate seasonally-based data such as temperature, evaporation rates, cloud cover, and atmospheric pressure.

The development of hydrological models began with a focus on conceptually-based lumped models, in part due to the simpler computational setup, and lack of detailed data as inputs for the more comprehensive physically-based distributed models. Examples of lumped models are the Rational Method model, the United States Department of Agriculture (USDA) Technical Release 55 (TR-55) model, and the USDA Natural Resources Conservation Service (NRCS) Runoff Curve Number (CN) model. A brief description of the uses of these models follows. More detail, including model setup, equations, and variable definitions may be found in many hydrology textbooks (such as Viessman and Lewis, 2003).

The Rational Method is still currently used in many engineering calculations, as it calculates the peak runoff rate for small urban and rural watersheds using only one parameter to represent the runoff producing characteristics of the watershed. That parameter is the runoff coefficient, commonly depicted as *C*, which is representative of the fraction of runoff vs. rainfall for an area. There are a variety of sources in the literature for values of this coefficient, but in practice it is highly variable, with values from 0.5 to 0.95 (Viessman and Lewis, 2003). Though the exact limits for the maximum contributing area to a downstream outlet are not specified, some have recommended the limit be 0.81 km^2 (Thompson, 2006). The rational method is typically used to design structures that carry a maximum flow rate for a design storm, such as culverts under roadways or stormwater conveyance channels.

The NRCS-CN method was developed by the USDA, and is primarily used in agricultural settings. Depending on the hydrological group of a soil, land use, treatment, and hydrological condition of an area, a curve number is chosen from a table of established values. This number may be adjusted based on initial moisture conditions, and can be used as well to calculate the approximate abstractions of rainfall. Through the NRCS-CN method, a rainfall

event producing a specific depth of rainfall can be calculated to yield a specific depth of runoff. The CN method is more applicable for agricultural uses in that it produces only a runoff depth, a single value of total runoff. Additionally, this method is only applicable for headwater watersheds, that do not have any inflow from upstream land uses. This calculation will not yield a rate of runoff, or a flow hydrograph at a specific discharge point. Thus, for many non-agricultural engineering approaches, it is not as useful as other methods.

TR-55 is based on the CN method introduced above, but has additional calculations to describe the pathway of water in a watershed or catchment area. Like the rational method, TR-55 produces a peak runoff rate at a downstream outlet, as well as a hydrograph and has the potential to calculate sub-area routing when using the tabular method. This method has distinct advantages over the previously mentioned for engineering uses, since it can consider physical parameters of a subcatchment including the overland slope, flow length, and time of concentration. However, this approach is considered useful only for small areas, though the exact size is not specified.

Though lumped models, such as those described above, have been widely used in hydrological modeling and are a foundation for hydrological research, the growing trend of hydrological research has been away from lumped towards distributed models. This is due to: 1) the increased computational resources available for researchers through recent technological advancement; and 2) increased availability of detailed input data at varying spatial scales and resolutions. As a result of these advancements, numerical models, which rely on more complex formulations with a wide variety of parameters and that solve multiple equations successively and iteratively, are more commonly used in contemporary hydrological research. The following discussion introduces the reader to some of the most common hydrological models that rely on physically-based numerical methods. These models are currently in a state of continuous

improvement, and this discussion by no means aims to replace a deeper reading of user manuals, hydrology guides, and textbooks which better describe these.

The United States Army Corps of Engineers (USACE) has developed many hydrological and hydraulic models for varying uses, three of which are introduced here. The first is the Hydrologic Engineering Center's (HEC) Hydrologic Modeling System (HMS). HEC-HMS is a widely used hydrologic model that is capable of simulating infiltration, unit hydrographs, surface runoff, evapotranspiration, and other processes. This model is most often used in conjunction with other models to supplement the areas of hydrology that the model was not designed for, such as river hydraulics and groundwater interactions.

The second model from the USACE introduced here the River Analysis System (HEC-RAS). This model is often used in conjunction with HEC-HMS to introduce additional surface runoff into the system. HEC-RAS is capable of simulating steady flow surface water profiles, 1-D and 2-D unsteady flow, sediment transport, varying boundary conditions, water quality analysis and more. Typically, HEC-RAS is used in large river systems for floodplain analysis, sediment transport calculations, thermal loading studies, or major flood event simulations, and may not be suitable for small watersheds where groundwater interactions play a major role.

The last model from the USACE introduced here, and one selected for use in this research, is the Gridded Surface and Subsurface Hydrological Analysis tool (GSSHA). Originally developed as a surface hydrology model, GSSHA is a discretized two-dimensional (2-D) overland and one-dimensional (1-D) channel routing model. Groundwater table elevations are simulated with a 2-D groundwater surface equation (more details on this later in this dissertation). GSSHA is a physically-based model capable of simulating infiltration, spatially varying precipitation, overland surface runoff, exfiltration of groundwater onto the ground

surface, interactions between groundwater and channel surface water, lateral groundwater movement, sediment transport, and more. Due to the 2-D groundwater component, and physically-based calculations of runoff and flow routing, GSSHA is ideal for watershed studies where each of these components significantly impacts one another.

The USDA Agricultural Research Service (USDA-ARS) developed, with the Texas A&M AgriLife Research, the Soil and Water Assessment Tool (SWAT). It is used widely for large basin watersheds where the entire hydrologic cycle (yearly rainfall, evapotranspiration, groundwater, soil types etc.) impacts the watershed and water use of the area. This continuous model is often used for simulation of long-term impacts of land use change, predominantly in agriculture related uses. The soil/subsurface component of SWAT can model soil evaporation, plant uptake/transpiration, lateral flow of subsurface water, and percolation to the groundwater table. The surface component of SWAT can calculate surface runoff, stream flow, sediment and nutrient loadings, and many other agricultural related variables. Though the discretized SWAT model includes some surface and subsurface calculations, and represents continuous calculations of the hydrologic cycle, it uses a daily time step for calculations. In this case short-intense rain events will be averaged out through the entire day, and surface routing is largely limited. Thus for small watersheds that experience rapid delivery of surface runoff, SWAT's calculation of the above mentioned features is limited.

One of the most popular groundwater modeling tools used currently is the United States Geological Survey (USGS) Modular Finite Difference Flow Model (MODFLOW). This model is capable of calculating the three-dimensional (3-D) flow of groundwater through a distributed model framework. Due to the 3-D nature of the model, variations in the groundwater solution can be solved not only in the 2 lateral dimensions, which not all models do, but also can simulate

variations of groundwater with depth, which few models do. This is principally important at a regional scale, where there may exist large variations with depth where soil horizons have significantly different parameters. Additionally, bedrock may convey or limit groundwater movement at varying depths, as is generally the case for regional groundwater studies. However, MODFLOW is a groundwater model, and in order to characterize watershed surface runoff, it must be combined with other models to simulate surface and subsurface conditions. There have been many such combinations produced both by the USGS and other researchers.

The last model introduced here, which is also the second model selected for this research, is the Environmental Protection Agency (EPA) Storm Water Management Model (SWMM). SWMM is used in both event-based and continuous modeling, and is a semi-distributed model that breaks up the domain into subcatchments of similar hydrologic parameters. SWMM is capable of simulating infiltration, surface runoff, spatially-varying precipitation, groundwater storage, stream-groundwater interactions, sewer systems, closed-pipe flow, water quality, evaporation, surface storage, and low-impact development (LID) features. This model is largely used in urban settings, though it is capable of simulating under-developed watersheds as well. Common uses for SWMM are designing stormwater control measures, floodplain mapping of open channel flow, simulating combined sewer systems, and evaluating the effectiveness of BMPs for water quality. Since SWMM was designed for urban systems, there has not been much validation for the model in undeveloped watersheds. Additionally, the groundwater component is setup as a storage unit that creates a recession curve in surface water routing, rather than a distinct system with lateral transport and varying dynamics.

1.4 Motivation for this Research

As discussed above, there is widespread concern throughout the U.S. about the impacts of varying land uses on receiving water bodies. Currently, there is a limited amount of post-construction data on roadway stormwater management, particularly impacts measured within the stream rather than measured directly at the edge of pavement or within conveyance channels. More detail on the current state of research on the impacts of roadways on receiving water bodies will be discussed in Chapter 2: Literature Review. To assess what impacts, if any, exist in a post-construction freeway/interstate land use, field measurement and hydrologic modeling was performed on the LCC. Details of this watershed are presented in Chapter 3.

1.5 Research Objectives

1.5.1 Field Investigation of the LCC

The first objective of this work was to study the hydrological and water quality impacts of I-59 to the LCC. The study included field monitoring of nitrogen and phosphorus species, solids, dissolved oxygen, temperature and pH among other water quality parameters. Hydrological parameters monitored include rainfall, stream flow and groundwater levels. The overarching goal was to understand the potential impacts of the interstate or highway stormwater runoff to other headwater or underdeveloped streams that are intersected by roads. The second objective of this research was to quantify the concentrations of water quality parameters within the receiving water body. This was measured both downstream and upstream of the interstate to evaluate the impact of stormwater runoff from the roadway. These objectives are addressed in Chapter 3.

1.5.2 Modeling Stormwater Runoff and the LCC

To gain further insight on the hydrological response of interstate stormwater, SWMM and GSSHA models were developed for the LCC and I-59. Groundwater, streamflow, and rainfall data collected at this location were used to calibrate the models and represent some varying interactions between the groundwater table and streamflow, as well as drainage features associated with the interstate. There are three research objectives for the work presented in Chapter 4. The first objective was to discuss the similarities and draw comparisons between formulations and calibration parameters from the popular lumped model SWMM and the distributed model GSSHA. The second objective was to assess the extent that either model could reproduce the measured field data downstream of the roadway and within the interstate median, examining specifically stream flow and groundwater table variations. The third objective was to discuss causes for the differences in the results yielded by these models while simulating the selected watershed in the interstate area.

1.5.3 Resolving Pressure Transducer Errors

In addition, this work proposed a standardized methodology to reconstruct measured data from pressure transducers affected by temperature-induced errors. Such a procedure can transform valuable hydrologic data that has been corrupted by thermal artifacts into more usable time series data. In addition to rectifying previously collected datasets, the procedure can be applied in sensors that present relatively minor thermal artifact issues. This work is presented in Chapter 5.

1.6 Structure of the Dissertation

Following this introduction chapter, a review of relevant literature is presented in Chapter 2. The focus of that chapter is on the available body of research relevant to stormwater runoff from highways, the hydrological models chosen in this research, and uncertainties in streamflow and groundwater measurement. Following this literature review, an assessment of the current knowledge gaps is presented. Chapter 3 introduces the study site and is focused on field investigation of water quality and hydrological parameters of the LCC and I-59. Chapter 4 is focused on work done to model the LCC and I-59 using the previously mentioned SWMM and GSSHA computer models, as well as discussing some strengths and weaknesses of those programs. Chapter 5 presents work done to improve the quality of data collection from a widely and commonly used device for hydrological research. The major conclusions of this work are summarized in Chapter 6, as well as the limitations of this research and recommendations for future work.

Chapter 2 – Literature Review

2.1 Stormwater Runoff from Roadways

Human activities in watersheds, such as construction and urbanization, lead to impacts on land, streams, and other environmental systems. Stormwater drainage is one important cause of environmental impacts, both hydrological (e.g., increases of peak flows and runoff volumes) and in constituents in stormwater. In this context, roadways are a source of short and long term impacts, though in stormwater management most of the focus is placed on the short term impacts (Wheeler et al. 2006). Roadways and vehicular traffic can be potential sources of various pollutants from tire wear, brake linings, oil leakage, pavement degradation and atmospheric deposition (Shaheen 1975; Han et al. 2006). However, if there is secondary development in the watersheds where roads are located, these other types of land use will also create impacts.

Paved roadway surfaces decrease the pervious areas in watersheds, yet the relative area occupied by a given road often is relatively small. With regards to water quality impacts, various constituents may be present in the runoff from roadways (Shaheen, 1975; Tsihrinris and Hamid, 1997; Herngren et al., 2006). The National Stormwater Quality Database (Pitt et al., 2004) compares runoff constituent concentrations for different land uses with data collected across the United States. Relative to other land uses, runoff from roadways are a significant source of total suspended solids (TSS), oil and grease, chemical oxygen demand, organic nitrogen, ammonia, copper and petroleum hydrocarbons. Wu et al. (1998) determined that 20% of TSS loadings, 70% to 90% of nitrogen loadings, and between 10% and 50% of other constituents (chemical oxygen demand (COD), phosphorous, heavy metals, dissolved solids) in roadway stormwater runoff are sourced from atmospheric deposition, as opposed to vehicular traffic and road surfaces. In addition to this study, Schueler et al. (1992) determined that atmospheric deposition

accounts for 70 to 95% of nitrogen and 20 to 35% of phosphorous in stormwater runoff from roadways, indicating that vehicular traffic is not the sole input of nitrogen or phosphorous species in highway stormwater runoff. Federal Highway Administration (FHWA) sponsored research (Driscoll et al., 1990) presented summary data for a variety of stormwater roadway runoff related parameters from multiple states. The average values for parameters relevant to this study from this FHWA report includes: 143 mg/L of TSS, 432 mg/L of TS (total solids), pH (hydrogen ion activity) of 6.5, 103 mg/L of COD , 0.84 mg/L of nitrite (expressed as nitrogen), 1.79 mg/L of total organic nitrogen (expressed as nitrogen), and 0.435 mg/L of phosphate. In addition, Barrett et al. (1993) also present an extensive review of the literature on stormwater runoff pollution from highways in the U.S.

Impacts of these constituents on natural systems are site specific due to a high variability between measurements and the receiving water body characteristics. In North Carolina, Line et al. was able to prove that the construction of a new highway (HWY 2004-26 and HWY 2007-17) did not have a drastic effect on the turbidity downstream from the construction site due to their thorough documentation of the pre-construction water quality measurements (Line et al., 2009). Uses of low impact development (LID) and BMPs improve stormwater runoff from roadways. An interstate example of LID and green infrastructure (GI) comes from American Forest (2009) in the City of Albuquerque, New Mexico. The study found that increasing tree cover to 8%, from the current 6%, resulted in a significant decrease in stormwater runoff. Also swales where mulch, rock and native vegetation were used on Interstate 40 in Albuquerque directed, slowed and filtered stormwater coming from the interstate (LaBadie, 2010).

Additionally, work has shown that the majority of water quality impacts are within the first flush of highway runoff (Kayhanian and Stenstrom, 2005). Kayhanian and Stenstrom (2005)

have shown that treating the first 20% of surface runoff and diverting the rest is twice as effective at reducing pollutant concentrations as treating only 20% of the total runoff throughout the event. On a South Korean highway, the peak of pollutant concentration occurred 20 minutes after the rainfall event (Lee et al., 2011). Li et al. (2005) found that 40% of particles were discharged in the first 20% of highway stormwater runoff, and Lau et al. (2004) found similar results with organic matter. These studies reveal the need to focus on the timing of pollutant concentration as well as total surface runoff.

Another impact of increased surface runoff that may be attributed to paved roadways is the destabilization of stream channels. Streams can be easily eroded and transformed when a higher volume of water moves through the system over a shorter period of time. Gubernick et al. (2003) noted that culverts cause a significant problem for channels because sediment and woody debris is often impeded. The high rates of stormwater runoff roadway culverts are designed for often impede the natural movement of aquatic species. The federally endangered watercress darter in Birmingham, AL thrives where channel stability and natural levels of stormwater runoff allow for large vegetative growth (Duncan et al. 2010). For roadways, increases of stormwater runoff can be attributed to the increase of impervious surfaces, where a 50% increase in impervious surface can reduce the time of concentration by half and increase runoff by four times (Harned, 1988).

While few previous studies have highlighted impacts of roadway runoff to natural environments (Marsalek et al. 1999; Johnson et al. 2007), generalizations are not possible and field studies are necessary to characterize this in specific types of watersheds. In the context of streams, impacts from road runoff will often be combined with impacts from other land uses.

Thus, stream water quality changes caused by roadway runoff need to account for other potential sources of runoff.

2.2 Hydrological Modeling of Roadways

In addition to field measurement of stormwater runoff characteristics, hydrologic research often utilizes hydrological models to quantify stormwater runoff, estimate the impacts of various land uses, and predict the response of a changing hydrological system. Research on the impacts and hydrological response of roadways, including hydrologic modeling, is largely limited to logging roads in the Pacific northwest (Jones et al., 2000) or unpaved roadways in forested regions (Negishi et al., 2008). Other research performed on evaluating stormwater impacts of major highways typically focuses on constituents within runoff without a comparison of upstream versus downstream flows (Thomson et al., 1994) or the impact of roadways to flow patterns. Wang et al. (2011) modeled the effects of roadways using the Soil and Water Assessment Tool (SWAT), which is a model that has a daily time-step for calculations, noting the importance of incorporating roadway drainage features in hydrologic modeling. Kahklen and Moll (1999) determined that roadways have a definable impact on groundwater levels since drainage ditches, which are designed to route stormwater flow away from the road surface, intercept groundwater under a variety of settings (Jones et al., 2000). The findings in this list of existing research is dependent on the tools or models used and their inherent strengths and weaknesses.

As mentioned before, lumped models are more often used because they have a simpler model setup and require less computational effort. However, with the growing availability of remote sensing geo-referenced data and databases, as well as faster processing capability of computers, distributed models are becoming more commonly used by researchers and practicing

hydrological modelers (Zhang et al., 2016). After compiling work done by numerous hydrological model creators, Reed et al. (2004) noted that simulation accuracy is more likely dependent on the skill of the modeler, parameterization, and model formulation, rather than whether a particular model is lumped or distributed. Nevertheless, determining which hydrologic model best suits the needs of a research group, municipality, or engineering firm can be challenging consider the array of model alternatives and various modeling objectives.

SWMM and GSSHA are two hydrological models used in both research and consulting work in watershed modeling. In a comprehensive approach to solving highway runoff problems, the National Cooperative Highway Research Program used SWMM to evaluate the effectiveness of volume reduction approaches throughout the U.S. (Strecker et al., 2014). SWMM has been used in many cases to model stormwater runoff in small catchments (Tsihrintzis and Hamid, 1998), urban settings (Barco et al., 2004) and highways (Barrett et al., 1998). Although SWMM has been used largely for urban hydrological assessments, it has also been applied to modeling underdeveloped watersheds (Moynihan and Vasconcelos, 2014). By comparison, published research using GSSHA is not as numerous as SWMM, however the use of the model is gaining momentum in municipalities (Steele County, 2016) and environmental consulting firms (Trimble Report, 2013). GSSHA has been shown to be a dependable hydrological model for diverse watershed systems (Downer and Ogden, 2004), and comparable to other modeling programs (Kalin and Hantush, 2006).

Although these programs have been used for various hydrologic applications, a comparison between SWMM and GSSHA has not been made in the context of roadways, and their impact on surface and subsurface stormwater runoff. Zhang and Shuster (2014) present one of the few studies comparing SWMM and GSSHA. They modeled two small hillslope

catchments (0.47 hectare and 0.65 hectare) using long term simulations and a large dataset of rainfall-runoff observations. After model calibration, their simulations using SWMM and GSSHA produced runoff hydrographs that are comparable to observed data, however some modeled storm events did not produce any runoff hydrographs, even though observed data indicated otherwise.

Despite the plethora of rainfall-runoff research available, fewer research contributions attempt to couple runoff hydrographs with groundwater table fluctuations in simulations and calibrations (e.g., Sharif et al., 2010a). This may lead to a misrepresentation of the dominant runoff producing features, as noted in Seibert and McDonnell (2002). Seibert and McDonnell recommend accepting higher overall errors if subsurface flow conditions could be represented as well as surface runoff.

It is well known that roadways may impact the surface hydrology of natural streams in a variety of ways (e.g. increase in conveyance volumes and flow rates, lowering the local groundwater table, etc.). However, it is not known as accurately the impact roadways have with the coupled surface and subsurface runoff components in a small watershed. This is due in part to the fact that there has been limited research in hydrologic modeling focusing on both groundwater and streamflow in attempting to understand the behavior of small watersheds.

GSSHA has a stronger groundwater calculation component than SWMM, in the ability to represent the groundwater table with a 2-D solution where neighboring cells influence one another. Unlike GSSHA, SWMM averages the groundwater table elevation throughout the entire area of each subcatchment. Additionally, in SWMM, groundwater cannot be routed from one subcatchment to another, thus it lacks lateral transport of groundwater based on water table elevation differences. The lack of this lateral transport of groundwater in SWMM presents a

challenge for the hydrologic modeler, in cases where groundwater table dynamics are an essential part of the system hydrology of a watershed.

Even though published research is more limited for GSSHA than SWMM, it is feasible to assume that current SWMM users may become progressively more interested in considering distributed models such as GSSHA for developing hydrological studies. Due to the complex nature of groundwater and surface water interactions, attempts to model the impact of roadways on receiving water bodies without considering both of these systems may produce unsatisfactory results.

2.2.2 Hydrological Modeling with SWMM

SWMM is an open-source hydrological model, freely available to the public, and has been widely used in published literature for hydrological modeling. Early use of the model focused on surface runoff and the effects of urbanization in stream response (Warwick and Tadepalli, 1991). Tsihrintzis and Hamid (1998) modeled four small catchments (between 5.97-23.56 ha) in Florida with one primary land use in each catchment, including one comprised primarily of highway land use. They demonstrated the accuracy of SWMM simulation compared against measured data of stormwater runoff and water quality pollutant concentrations. Roadway stormwater runoff was also modeled by Hwang and Weng (2015) using SWMM to consider the effectiveness of swales on water quality pollutants in roadway stormwater runoff. SWMM is commonly used to assess impacts of development from pre-development conditions (Jang et al., 2007) and sewer systems. Temprano et al. (2006) used SWMM to model water quality pollutants within stormwater runoff of a combined sewer system in Spain, and found that more than 50% of TSS and organic nitrogen were captured by the first 30% of stormwater runoff.

Hydrological research with SWMM has focused on more diverse topics in recent years. Originally a dominantly surface water model, recently SWMM has been demonstrated to accurately simulate karst groundwater systems (Peterson and Wicks, 2006), and can be coupled with stronger groundwater simulation models (Tian et al., 2015). Additionally, SWMM has incorporated LID structures into the model structure (Rossman, 2010). With the increased attention that LID, BMP, and GI has received for resolving stormwater runoff issues in highly urban areas, research utilizing this new aspect of SWMM is proliferating. Current research on this topic includes simulating rain barrels and rain gardens (Abi Aad et al., 2010; McCutcheon and Wride, 2013), green roofs (Burszta-Adamiak and Mrowiec, 2013), bioretention cells (Sun et al., 2011) and LID watersheds (Rosa et al., 2015).

Other current aspects of SWMM research include modeling urban areas and large water bodies. Recently, SWMM has been used to model urban flooding in India (Bisht et al., 2015) alongside a 2-D hydrological model. Rai et al. (2016) simulated floods in the Brahmani river delta using SWMM with Nash-Sutcliffe efficiency values between 0.616-0.899, indicating that the model is simulating the observed data very well. In addition to these larger systems, SWMM was used to assess the impacts of land use change and variations in climatic forces in urban headwater streams (Wu et al., 2013).

2.2.3 Hydrological Modeling with GSSHA

Research using GSSHA for hydrological modeling is more limited than for SWMM, but covers a wide array of relevant hydrological issues. Early work was focused on Hortonian surface runoff hydrological modeling (Senarath et al., 2000), but later demonstrated that the model was capable

of simulating more complex runoff and subsurface hydrological responses (Downer and Ogden, 2004).

GSSHA has been used for complex hydrological problems, including glacier melting runoff studies in the Tibetan Plateau (Li et al., 2014), tropical storms in steep island terrains (Ogden, 2015), and flooding events in Texas (Sharif et al., 2010a; Sharif et al., 2010b; Hassan et al., 2013). Land use change simulations may be more intuitive when using GSSHA, compared to lumped models, due to the ability to spatially represent the location of land use change and the impacts on hydrological estimates (Zhang et al., 2013). Ogden et al. (2011) studied various parameters relevant to increased urbanization, including impervious area, drainage density, and subsurface storm drains using GSSHA's explicitly spatial representation of these elements. As flooding is a major concern for hydrological research, GSSHA has been used for multiple flooding studies including ungauged watersheds in the Philippine Islands (Pradhan et al., 2016), the impact of detention basins and soil storage on decreasing flood discharges (Smith et al., 2015), and rainfall focused studies (Wright et al., 2014; Yang et al., 2016).

Using GSSHA's spatial discretization, new radiation based temperature estimates have been utilized for snowmelt routines, accounting for more local variations than air temperature (Follum et al., 2015). Additionally, GSSHA is used for various rainfall simulations including utilizing radar-reflectivity based rainfall estimates (Habib et al., 2008a), hydrological response variations caused by different precipitation data sources (Chintalapudi et al., 2012; Chintalapudi et al., 2014), and the impact of rain gauge tipping-bucket errors (Habib et al., 2008b) on simulation accuracy. Additionally, GSSHA has been incorporated into web-based tools for teaching hydrology in a university setting (Habib et al., 2012) and for water resource decision applications (Jones et al., 2014). Although the computational engine behind GSSHA has been

developed since 1995 (Julien et al., 1995), the recent increase in published research using the model may indicate that obstacles limiting its use, like computation resources and data availability, are beginning to be overcome.

2.3 Uncertainty in Streamflow and Groundwater Measurement

As hydrological models become more widely used and trusted for accurate simulations, it is imperative to have high-quality data for calibration and validation of these models. Pressure transducers are one of the most common instruments in hydrological studies to measure continuous stream and groundwater levels. A variety of instruments have been manufactured that make this type of data collection simple and efficient. Most instruments fall into one of two categories: sensors that measure absolute pressure, and sensors that measure differential pressure (also termed vented pressure transducers). Pressure transducers are often used to measure groundwater levels, where the daily cycles of head change are associated with evapotranspiration (Nyholm et al., 2003; Zhu et al., 2011). Daily fluctuations in groundwater and surface water height may also be related to freezing and thawing conditions, daily rainfall, and changes in the hydraulic conductivity associated with temperature changes (Gribovszki et al., 2010). As Gribovszki et al. indicate, historically these daily cycles in streamflow and groundwater levels were not considered important aspects of a total water budget. However, with the widespread use of high temporal resolution models and ease of solving numerical models (such as that of Szilagyi et al., 2008), an accurate analysis of daily water cycles may be needed. Despite the widespread use, abundance, and variety of pressure transducers, there exists an error in pressure readings reported due to temperature fluctuations within the instrument.

There are a variety of errors and uncertainties in measuring stream or groundwater levels including, but not limited to, sensor error. Accuracies and errors associated with these instruments vary by brand and model type, but are often quite small compared to the range of use (for instance, the Onset® HOBO® U20-001-01 model with an error range of ±0.075%, 0.3 cm, for a range of up to 4 m). Fluctuations in the barometric pressure can cause the head in groundwater wells to misrepresent the groundwater elevation, as discussed by Spane (2002). Additional uncertainties include a groundwater delay response due to borehole storage, and barometric pressure variations through the unsaturated zone. Since pressure transducers are commonly used in outdoor environments, thermal fluctuations are unavoidable; but these fluctuations produce changes in the reported pressure readings that are not indicative of an actual change in pressure in the environment. In a classical study discussing this issue, Freeman et al. (2004) traced the source of this error to effects of temperature changes in the electronic components of these sensors. Regardless of the model, brand, or type, temperature fluctuations in the electronic components of pressure transducers often produce erroneous data. These errors can include sensor drift, hysteresis, changes in sensitivity, time constant, and others. As pointed out by Freeman et al. (2004), there are attempts to correct such errors during the construction and calibration of the instrument, but the solution does not always work for every instrument.

More recently, other investigations have identified thermal artifacts in data from a variety of pressure transducers. While recording data (with absolute pressure transducers) in the Los Rios Region in Southern Chile, Cuevas et al. (2010) noticed daily fluctuations in stream measurements related to thermal artifacts. In laboratory experiments, these fluctuations were on the order of 1.5 cm. Their recommended solution was to place the barometric sensor in a location that will experience the same temperature changes as the stream sensor in order to reduce the

pressure reading errors. Other research has also reported fluctuations in sensor measurements due to solar radiation (Cain et al., 2004; Liu and Higgins, 2015) and thermal variations (McLaughlin and Cohen, 2011). Other researchers argue that with proper care and maintenance, such as keeping vent tubes dry and sensors free of biofouling, some pressure transducers do not experience erroneous measurements associated with thermal artifacts (Gribovski et al., 2013).

It is not straightforward to determine if a particular instrument is experiencing thermally induced errors. If sensors are deployed in the field, only a secondary set of data by physical measurement and installation of another sensor would enable a reliable validation of a sensor's output. For some instruments, the thermal artifacts in pressure readings increase in amplitude over time. Thus instruments that are functioning within an acceptable error range at initial deployment may degrade before thermal artifacts are detected and corrections can be made, such as sensor replacement or redeployment. Additionally, instruments that are rated to work for 5 years or more may begin to experience erroneous measurements prior to their rated life expectancy.

2.4 Knowledge Gaps

The introduction of stormwater runoff into a receiving water body involves complex systems of seasonal climate change, flow variations, and other various interactions. The hydrology of a perennial stream or similar water body includes groundwater–surface water interactions, the intersection of various stream channels, evapotranspiration, and other nonlinear hydrologic functions. The stream water quality within such systems is further complicated by other processes indirectly linked to stormwater runoff such as riverbank erosion, topsoil erosion, upstream land use variability, and aquatic organism interactions. As a result of these

complexities, it is important to determine the impacts of stormwater runoff within the receiving water body, and not only at the edge of the roadway or within drainage structures.

2.4.1 Stream Water Quality Impacts

The task of determining the impacts of a roadway on a stream is not trivial, because a variety of data are necessary. This includes, among others, rainfall regime, soil and geomorphologic characteristics, runoff constituents, other types of land use in the watershed, and vehicular traffic volume. However, there is limited published research on the impacts of stormwater runoff from interstates or freeways measured within a receiving water body. The research that does exist typically focuses on one or two aspects of the hydrological or water quality impacts of roadway runoff, or the downstream concentrations of water quality constituents without a comparison of upstream concentrations. Thus, the extent of the impacts of roadway stormwater runoff to a stream's water quality is poorly known.

2.4.2 Hydrological Impacts

It is known that roadways may impact the surface hydrology of a stream in a variety of ways (e.g. increase in conveyance volumes and flow rates, and lowering the local groundwater table). However, it is not as well known the hydrological impact roadways have with the coupled surface and subsurface components in a small watershed. Researchers in the field typically focus on either groundwater or streamflow in attempting to understand this issue. Due to the complex nature of groundwater and surface water interactions, attempts to model the impact of roadways on receiving water bodies without coupling these systems may produce unsatisfactory results (Siebert and McDonnell, 2002).

2.4.3 Thermal Artifacts in Pressure Transducers

Although some researchers have identified the presence of thermal artifacts in pressure transducers, a standardized procedure for mitigating thermal artifacts in sampled data has not been presented in the literature. If it is determined that errors associated with temperature effects exist in a sensor, the only existing recommendation is to deploy the instruments in conditions that reduce temperature fluctuations as much as possible (Cuevas et al., 2010). While this is valid, such recommendations do little to address the errors in already collected data, which may be of crucial importance in many applications, or in applications that such fluctuations are unavoidable. There is currently no guideline on how to rectify erroneous data that has already been collected. For now, researchers must: 1) be content with data even though it not representative of the true values; 2) attempt to average the fluctuations, which would eliminate an evapotranspiration response and introduce a guessing element in the results; and 3) use a daily time-step in any calculations, thus ignoring the fluctuations that occur within 24-hour cycles. As pointed out earlier, the growth in watershed modeling studies has been aided by increasingly accurate field instruments and studies for model calibration/validation. In an effort to continue forward, it is imperative to determine a way to reduce this thermal artifact signal from existing and future pressure transducer datasets.

Chapter 3 – Assessing the Impacts of Stormwater Runoff from I-59 to the Little Cahaba Creek.

3.1 Introduction

Stormwater runoff from freeways has been characterized by higher concentrations of some water quality pollutants, including TSS and TN (Pitt and Maestre, 2004), than other land uses. Additionally, roadways may impact the natural hydrology of a watershed by reducing the groundwater table elevation and increasing surface runoff (Kahklen and Moll, 1999; Jones et al., 2000). The LCC was selected as the research site for this investigation of the impacts of stormwater runoff from a freeway into a receiving water body. The LCC is formed in a watershed of about 18 km^2, receiving runoff from mainly rural land with some minor residential development. Along the length of this watershed, I-59 crosses the creek at various locations, contributing runoff to the creek. This specific location was also selected because it is the proposed site of the intersection between the existing highway (I-59) and the BNB, which is currently at the early stages of construction. Data collected at this site can be used as a baseline for comparison to data related to runoff from future roadway construction and operation.

The LCC is a perennial stream, with a constant baseflow throughout the year in most of the stream network due to groundwater flows in part supplied by upstream reservoirs. Soils in this watershed are primarily hydrological group B, gravelly silt loam (moderate K_{sat}, saturated hydraulic conductivity), layered with fine grained clay layers (very low K_{sat}; Soil Survey Staff, NRCS). Because of this, there is a moderate amount of infiltration, yielding a relatively consistent groundwater influence on the watershed. Additionally, the soils are underlain by limestone, chert, and sandstone from the Knox Group, Sequatchie Formation and Chickamauga Limestone, and Red Mountain Formation. These units are adequate for conveying groundwater.

There is faulting and folding in the region, which the length of LCC parallels on the southeast portion of the watershed. These geologic features have produced springs in the area that feed lakes and ponds, contributing to the perennial flows in the creek.

Figure 3.1 shows the LCC watershed and I-59. The red circles indicate the location of the upstream and downstream sites reported herein, in which the LCC branch (with a drainage area of approximately 2.7 km^2) crosses I-59. The sites selected for this study, one upstream and one downstream of the interstate, were chosen in order to provide an initial estimate of the impact the interstate has on the quality and amount of stormwater runoff in the LCC. A secondary intermittent branch of the creek drains a smaller subcatchment (0.56 km^2) of the watershed and joins with the main branch within the median of I-59, as seen in the figure. This intermittent branch was not a part of the water quality sampling reported here. Data was gathered at a 2-week interval (nutrients, pH, TSS and turbidity).

3.2 Methodology

Various water quality parameters and hydrological parameters have been monitored during this study at selected sites in the watershed. The water quality parameters included in this study are: total suspended sediments, total solids, turbidity, temperature, pH, specific conductivity, dissolved oxygen, nitrate, nitrite, ammonia, total nitrogen, ortho- and poly-phosphate and total phosphorous. The hydrological parameters included in this study are: stream level, stream flow and velocity, and cross-sectional areas. Figure 3.1 shows the location of two sites of this study. This stream flows from the northwest to the southeast separated by I-59, which crosses the creek at several locations, and contributes runoff.

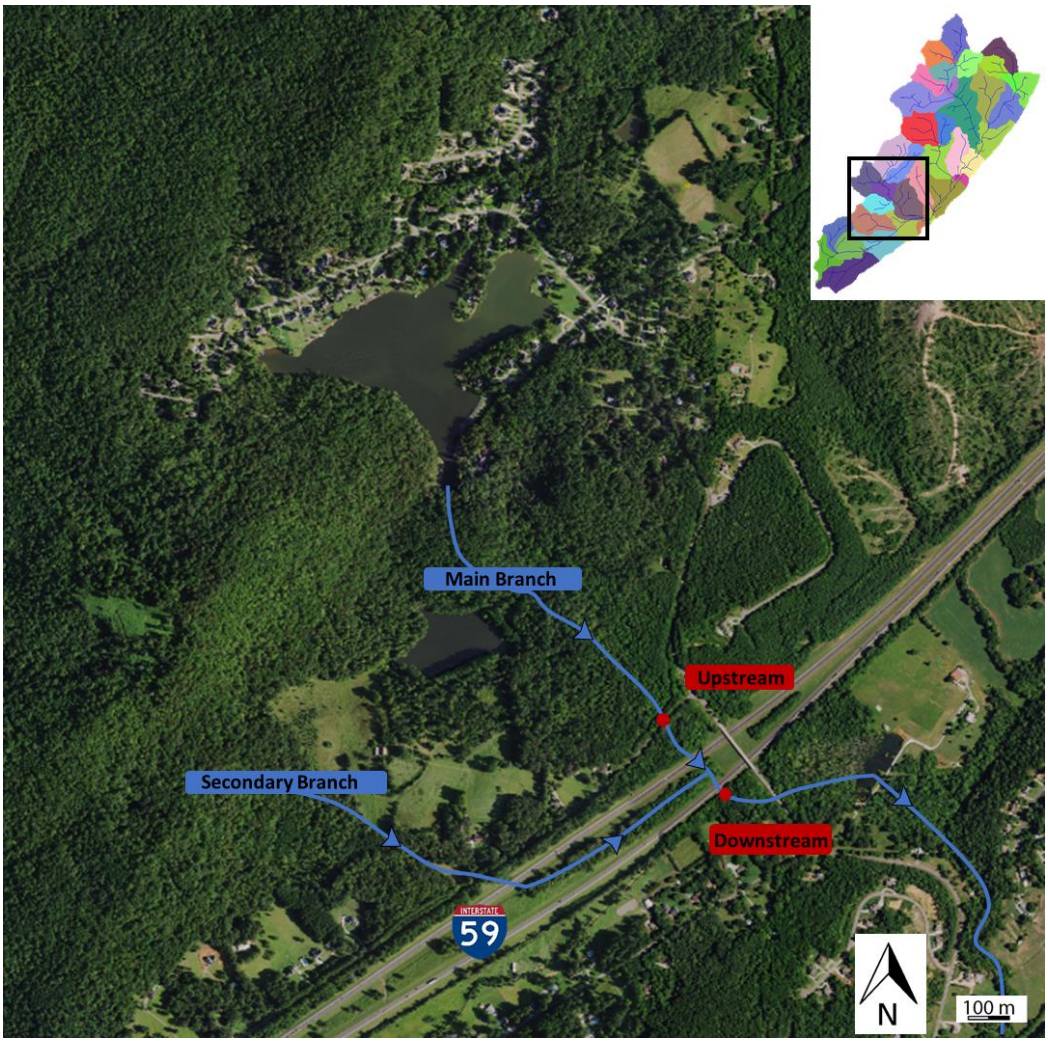

Figure 3.1 LCC watershed along the interstate I-59 corridor. Image from ESRI (2016)

At the upstream site, water samples were collected, the cross section was surveyed and stream levels were measured within a rectangular concrete culvert at every visit to develop head–discharge curves. An environmental sonde (Hydrolab®, DS5) and pressure transducers (Onset® HOBO®, U20-001-01) were also deployed at this station. The same general arrangement was also used at the site downstream from the I-59 crossing. Figure 3.2 shows the setup and location of equipment at the downstream site. The monitoring upstream aims to quantify the impacts of other land uses upstream from the interstate highway, namely open (mostly forested) terrain with some residential development.

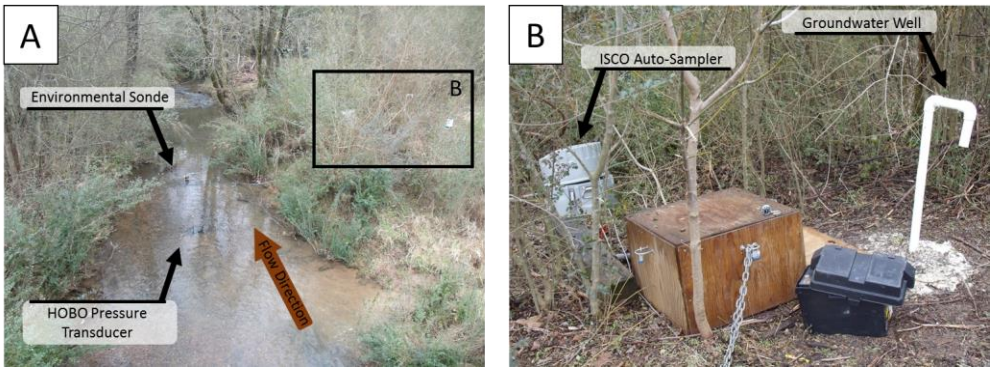

Figure 3.2. Downstream site monitoring equipment is identified by text boxes and arrows; for scale, the width of this stream is approximately 5 m.

3.2.1 Solids and Physical Parameter Monitoring

Commonly measured parameters in water quality studies are total solids (TS) and total suspended sediments (TSS). These parameters are among the simplest and most cost-effective measurements to quantify and qualify the impact of stormwater runoff. TS is defined as the amount (weight) of material in sampled water after all water has been evaporated at a constant temperature (approximately 103 °F, 39.4 °C, SM 2450B, Standard Methods for the examination of water and wastewater). TSS is defined as the amount of material remaining on a filter with a pore size of 1.2 µm (SM 2540D). TSS is a fraction or portion of the TS. Turbidity is a parameter that is related to the amount of suspended particles in a water sample which block light that passes through the water. Thus it can be seen as a sort of cloudiness factor that can be correlated to the TSS and TS of the sample. Turbidity was measured approximately every two weeks in the field and in the laboratory with a LaMotte® turbidity meter, as well as continuously in the field by a Hydrolab® probe. A calibrated Extech handheld pH meter and thermometer were also used to characterize these parameters in the streams.

TSS, TS and turbidity were sampled primarily in two ways during this research. First, biweekly, two grab samples (for repeatability) were collected from each of the sample sites for

analysis following the procedures outlined in Pitt (2007), regardless of rain event timing (typically intra-event). Duplicates for turbidity were measured, and if the readings varied by more than 5% to 10%, this was considered an error of measurement (such as disturbing the underlying sediment during sampling), and the samplings were repeated. Averaged values of these two readings are reported and used in the analysis. Additionally, pH and temperature were measured on site. Second, samples were collected by an ISCO® 6100 series auto-sampler positioned at each site. These instruments are activated by rainfall readings (values are defined by the user, in this case 2.54 mm, every 15 min) from an attached rain gauge. Once activated, the instrument pumps water from the stream through an attached hose line into a set of bottles within the auto-sampler. A volume of 800 mL of sample was collected in these bottles at intervals of 15 min. Thus with 24 bottles, six hours of samples were collected in certain rain events. By defining the rainfall dependent start time as the same for each sampler, the same amount of rain at each site should activate the auto-samplers at the same time. Due to interception of rainfall and spatial differences in rainfall distribution, the upstream and downstream samplers did not always turn on at the same time. The samples were brought to a water quality laboratory at Auburn University where TS and TSS parameters were measured following the SM 2540 procedures.

3.2.2 Continuous Water Quality Monitoring

To continuously monitor the water quality in LCC, two Hydrolab® DS5 environmental sondes were deployed at the upstream and downstream sites. At the downstream site, the sonde was deployed at a location that allowed for the mixing of flows coming from roadside ditches and the median. At the upstream site the probe was placed >30 m away from the interstate highway to

minimize any effect from the road runoff in its measurements. Parameters were continuously measured at 30 minute intervals by these two probes.

Every two weeks two newly calibrated probes were deployed, replacing the previously deployed sensors to ensure the quality of the data. Calibration of these probes consisted of adjusting the DO, turbidity, specific conductivity and pH sensors to a known value or regulated buffer solution. Table 3.1 shows the accuracy levels for each parameter measured by the probe.

Table 3.1. Sampling sensors and measurement accuracy for the Hydrolab® Environmental sonde.

Hydrolab® Sonde Parameters	Accuracy
Temperature Sensor	±0.10 °C
Specific Conductance Sensor	±1% reading; ±0.001 mS/cm
pH Sensor	±0.2 units
Dissolved Oxygen (LDO) Sensor	±0.02 mg/L for >8 mg/L
Self-cleaning Turbidity	±1% up to 100 NTU

3.2.3 Nitrogen and Phosphorus Species Measurements

Nitrogen and phosphorus species were measured from the grab samples collected every 2 weeks (intra-event). Samples were collected, preserved, and tested with a Hach® DR/890 colorimeter, for a full year from March 2013 to March 2014. The major nitrogen species include nitrate (NO_3), nitrite (NO_2), ammonia (NH_3), and organic nitrogen. This work measured nitrate, nitrite, ammonia, and total nitrogen using Hach methods 8192, 8507, 8155 and 10071 respectively. By subtracting the three nitrogen species measured from the total nitrogen measured in the lab, the organic nitrogen fraction could be determined. Phosphorus species consists of ortho-phosphate, poly-phosphate, and organic phosphate. Similar to the analysis of nitrogen, ortho- and poly-phosphate was measured, as well as total phosphate in the lab, according to the Hach methods 8048, 8180 and 8190 respectively. By subtracting ortho- and poly-phosphate from the total phosphorus measured, the organic phosphorus could be determined.

To promote quality control of nutrient concentration measurements, the samples tested for nitrogen and phosphorous concentrations were analyzed in an ion-chromatograph (IC) column during the initial months of the research. The point collection data was tested with an IC column from Dionex Products. The first full run of water samples and standards showed an average error of ~22%. The IC column was run with standards with the following concentration: 0.25 mg/L of NO_3, 1.0 mg/L of NO_3, 2.0 mg/L of NO_3 and 0.5 mg/L of PO_4, 1.5 mg/L of PO_4, and 3.0 mg/L of PO_4. All the standards had a R^2 coefficient in the range 0.9993 to 1.0. As the investigation progressed, IC column and colorimeter results showed increased consistency.

3.2.4 Hydrology Characterization

Continual measurement of flow in a stream is often accomplished by the construction of a weir, using a pre-existing structure, or by integrating the velocity and area relationship of the stream. To minimize impacts to the stream, in this work current meters and a Teledyne ISCO 2150 area-velocity sensor were used. During the initial months of this study, at both upstream and downstream sites, cross sections of the channel were surveyed at regular spatial intervals. The water depth at each stream segment was measured as well as water velocity using a Global Water current meter. Integration of the velocity and area over the width of the channel yields the flow rate using equation 3.1:

$$Q = \sum_{i=1}^{n} A_i V_i \qquad \text{(Eq. 3.1)}$$

Where Q is the channel flow rate (m^3/s), n is the total number of cross sections, i is the interval section, A is the cross-sectional area (m^2), and V is the velocity (m/s). In addition to measurements within the channel, water height within the interstate culvert outlet yielded critical

depth discharge condition and a simple flow determination. Figure 3.3 shows the data points and curves collected and calculated with Equation 3.1.

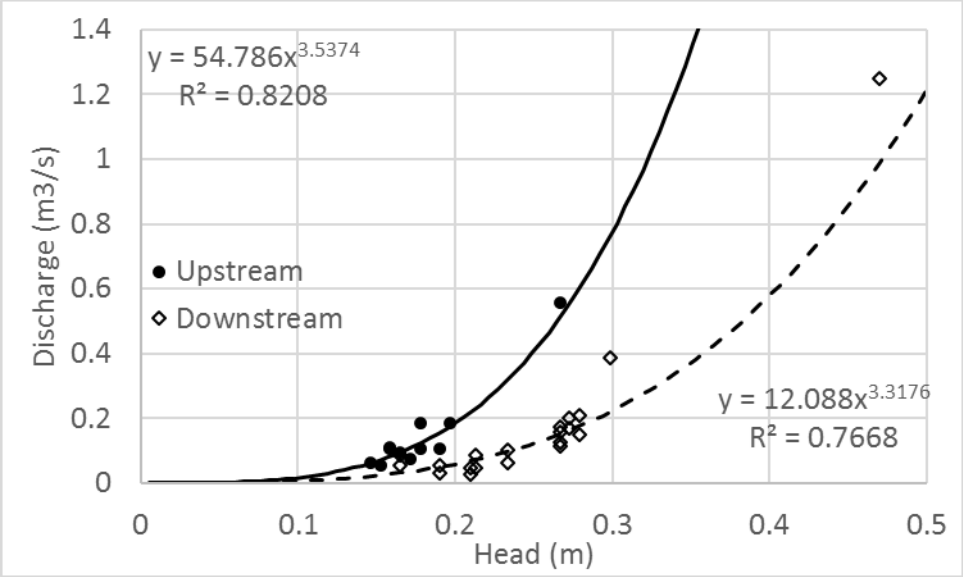

Figure 3.3. Head–discharge curve for the upstream and downstream sites.

These head-discharge curves were used with HOBO® pressure transducers to determine flow rates with a 30-min interval. These transducers measured the pressure experienced by the sensor, which included both the water pressure and the changing atmospheric pressure. To compensate for atmospheric pressure, an additional pressure sensor was deployed nearby so that these atmospheric pressure changes could be discounted in the readings. In addition to the stream level measurements, two HOBO® RG3 rain gauges were installed in the LCC watershed. One rain gauge was in a nearby field (350 m from the downstream site in Figures 3.1 and 3.2) and another in an open space to the northeast (approximately 4 km away); these were placed to capture the spatial variation of rainfall in the LCC watershed.

3.3 Results and Discussion

3.3.1 Traffic Data

A continuous traffic meter (ATR-163) operated by ALDOT at a point 3.2 km from the research site provided a 1-hour interval series of traffic flow during an average week (Figure 3.4). This data was collected to determine if water quality parameters, such as TSS, nitrogen, etc., had a relationship with the number of cars travelling through the area during a given time interval. Measurements from three months were used to derive an average traffic and standard deviations for the traffic at each hour. This in turn was used to estimate the vehicle count between consecutive rainfall events. This vehicle count was compared to the water quality parameter turbidity results taken upstream and downstream of the interstate, as is discussed below.

The number of hours between rain events was compared to the level of turbidity. This relationship yielded a decaying trend, while the relationship of turbidity and the traffic amount between rain events showed no correlation between the two. To improve the relationship between turbidity and time or turbidity and the traffic amount, the turbidity was multiplied by the total rainfall depth per rain event raised to the power of 1.5. By multiplying the turbidity by the total rainfall depth, Figures 3.5 and 3.6 can represent the storm size and intensity. In other research, White and Bernhard (2014) did not find great correlation between elapsed time between rain events and water quality impacts of stormwater runoff from an interstate in south Alabama; however, a time-based approach improved the relationship shown here. The exponent 1.5 yielded the best relationships between turbidity and time and turbidity and traffic.

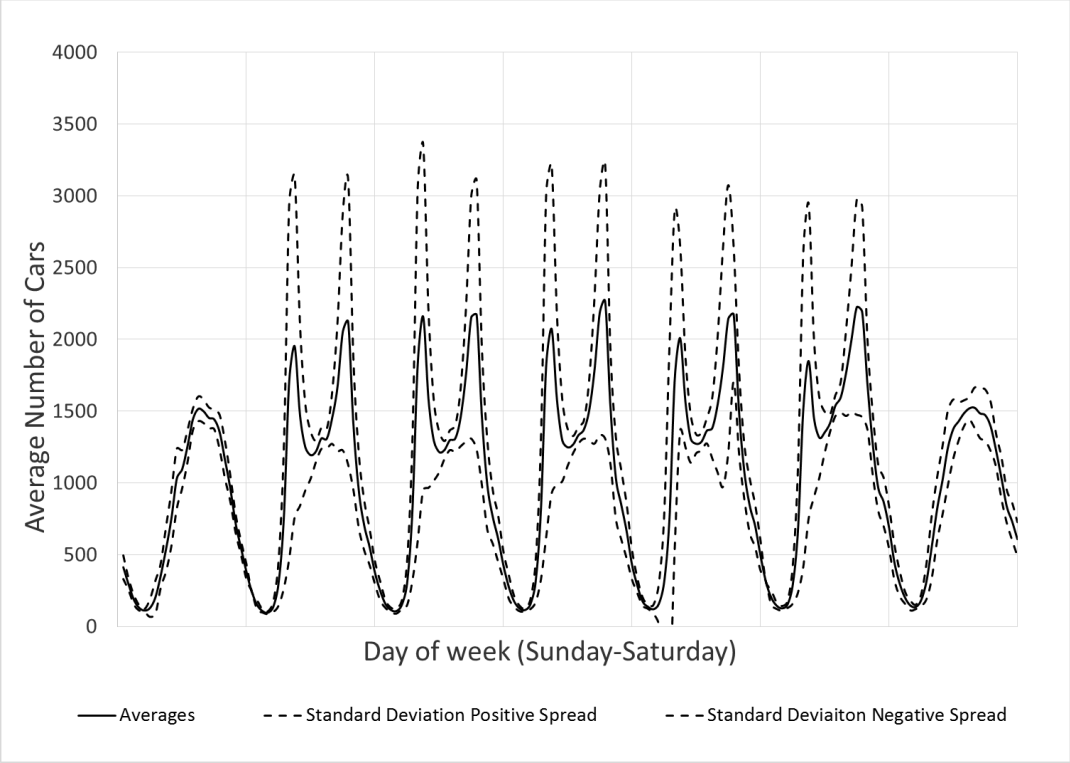

Figure 3.4. Average daily traffic over 1 week on I-59 north of Birmingham, Alabama mile post 140.2.

Another measure was taken to improve the quality and correlation between these variables. At times the upstream environmental sonde data consistently reported higher base levels of turbidity than the downstream location. This difference in the base levels of turbidity could be attributed to the deployment of the upstream environmental sonde, which could cause sediments to accumulate near the sensor interfering with turbidity values. To account for this error in deployment, the level of turbidity upstream was reduced by the difference in the initial turbidity level downstream and upstream. The relationships between turbidity and time and traffic are show in Figures 3.5 and 3.6.

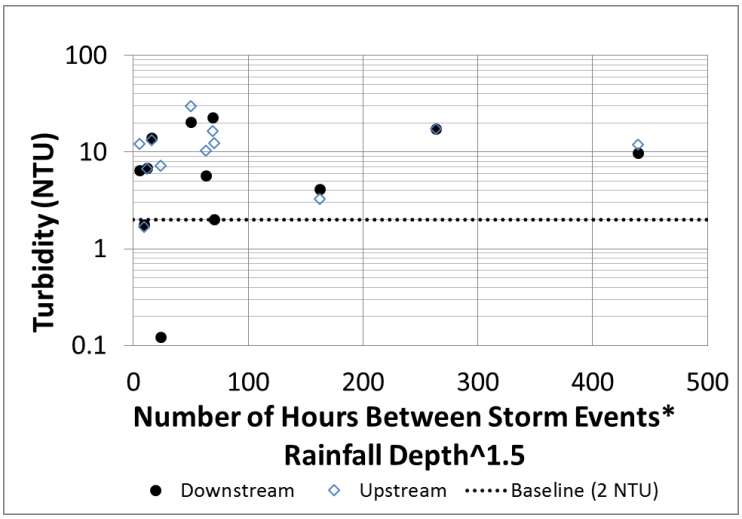

Figure 3.5. Turbidity compared to the number of hours between rain events and rainfall depth.

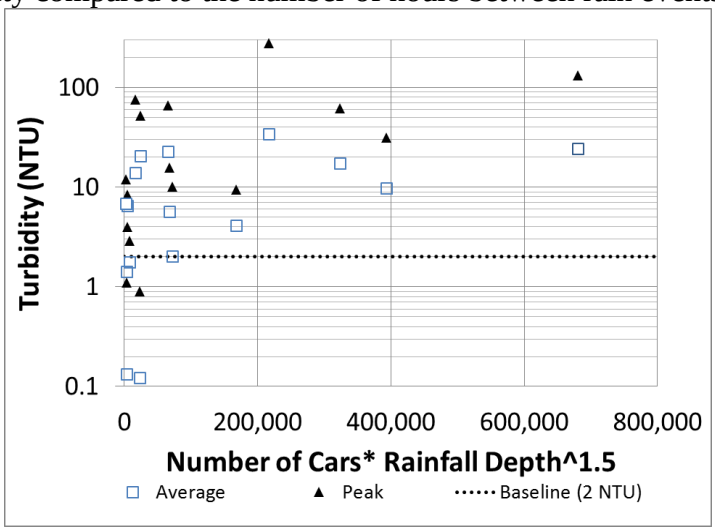

Figure 3.6. Turbidity compared to the number of cars between rain events and rainfall depth.

3.3.2 TSS and Turbidity Measurements

Rainfall events sampled with the auto-samplers in three dates are presented here: 10/07/2013, 11/01/2013, and 2/21/2014. In these events, there is a good correlation between the rain intensity and the increased amount of turbidity and TSS due to the increase in stream flow and runoff. The increase of TSS and turbidity in the upstream site was generally minor, but the increase at the downstream station was much more pronounced. The source for this could either be the road

runoff itself or another intermittent catchment that contributes to LCC between the upstream and the downstream site (referred to as the secondary branch).

TSS, turbidity and rainfall measurements for both upstream and downstream sites are shown in Figures 3.7 to 3.9. In all of these events, the TSS and turbidity at the upstream site did not exceeded 7.2 mg/L and 3.6 NTU, respectfully, whereas the downstream location reached values of 500 mg/L and 110.8 NTU. Note that in these figures the scales for turbidity and TSS vary for each event, due to the high variation of these parameters during different rain events. The event on 2/21/2014 represents a more typical relationship between TSS and turbidity, where the TSS and turbidity upstream samples are on the same scale of magnitude as the downstream samples. The delay between the rain event start and the peak of the TSS/turbidity at the downstream station varied between 1.5 hours and 3 hours.

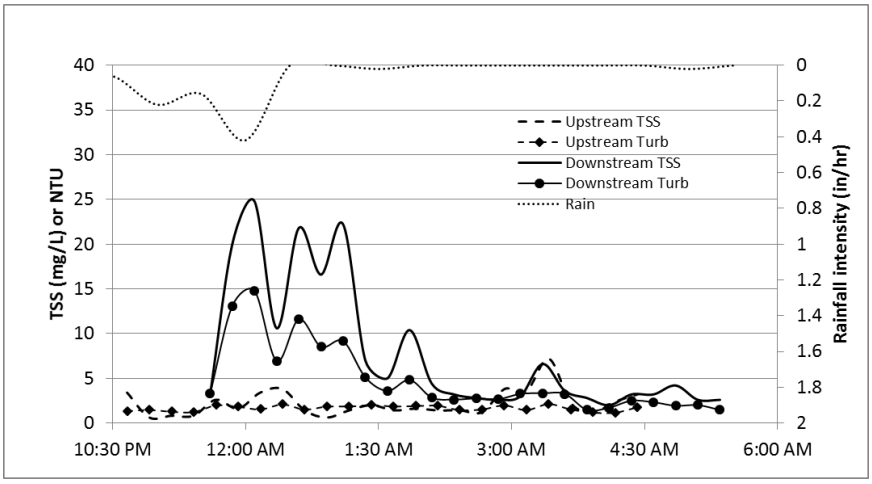

Figure 3.7. TSS and turbidity measurements for a rain event on 10/06/2013.

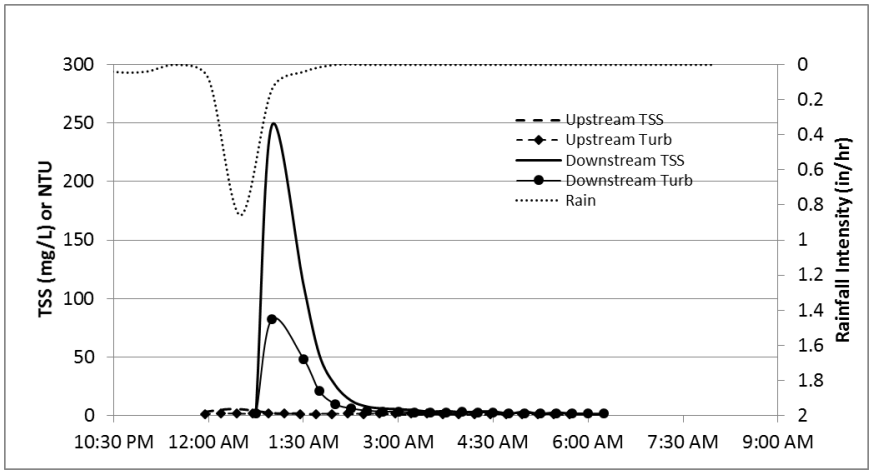

Figure 3.8. TSS and turbidity measurements for a rain event on 11/01/2013.

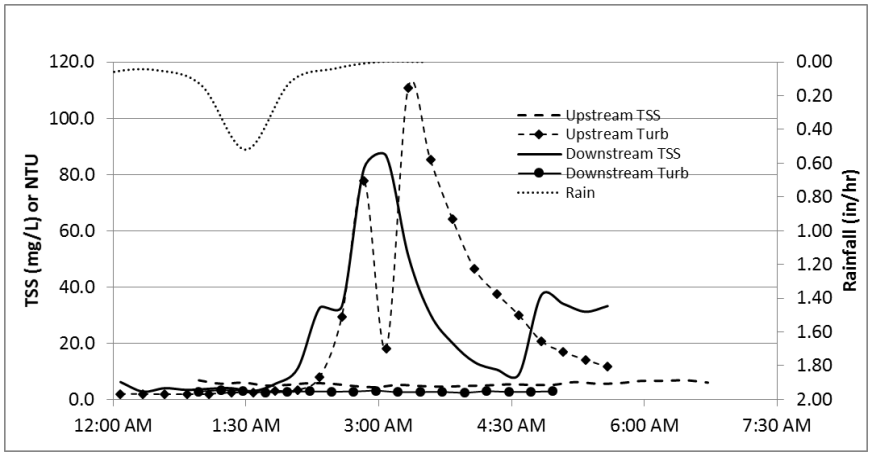

Figure 3.9. TSS and turbidity measurements for a rain event on 2/21/2014.

Figure 3.10 shows the overall correlation between the TSS and turbidity. This relationship was derived from the TSS and turbidity results found in the Auburn University lab by taking all the points from the adequate auto-sampler sets as well as the stream grab samples. There is significant scatter in the TSS and turbidity relation for the range of TSS between 1 and 8 mg/L, though the scatter decreases outside this range. Most TSS and turbidity results at the upstream site were under 32 mg/L and 16 NTU respectively. Results for the downstream site, however, could exceed 64 mg/L of TSS and above 32 NTU during rain events. As mentioned earlier, this could have been caused by the interstate or conveyance channel runoff or by another LCC tributary that merges with the stream between the upstream and downstream sites.

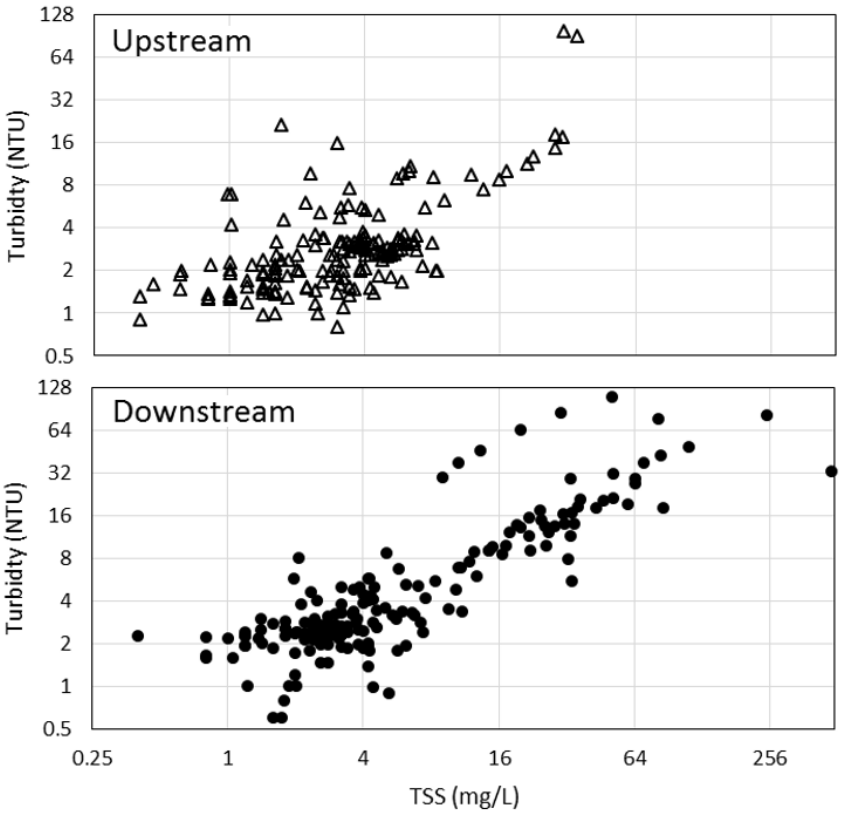

Figure 3.10. Turbidity vs TSS measurements for both sections of the stream (note the significant difference in scale for the TSS between sites).

For the physical parameters collected in the 2-week interval point sample collections, the TS tended to be greater when collected more than 72 hours after a rain event. TSS upstream of the interstate tended to be greater within the 72 hours following a rain event while the TSS downstream of the interstate tended to be greater after 72 hours following the rain event. The average turbidity across all sites tended to be greater for the samples collected within 72 hours of a rain event. Table 3.2 presents statistical data from the upstream and downstream sites for these parameters.

To determine if the increased turbidity and TSS concentrations downstream of I-59 were caused by the roadway features or by the secondary upstream site, investigation into the conditions of the secondary site was conducted. Figure 3.11 shows the location of the major sites discussed in this study, including the location of the secondary branch of the LCC that travels

through the median of I-59, connecting with the main branch. Additionally, Figure 3.12 shows the conditions of the stream channel after crossing underneath the small side road labeled "Arrowhead Lane" in the previous figure.

Table 3.2. Summary of available sediment statistical data for the upstream and downstream sites.

Physical Parameter	Site	Average	Standard Deviation	Occurred within 72 hours of event		Occurred after 72 hours of event	
				Average	Standard Deviation	Average	Standard Deviation
TS (mg/L)	Upstream	116.6	32.8	112.9	38.6	120.9	23.5
	Downstream	118.8	32.6	111.1	36.6	127.8	24.1
TSS (mg/L)	Upstream	12.6	26.4	16.8	34.9	7.6	6.3
	Downstream	3.2	10.0	2.1	11.8	4.5	7.2
Turbidity (NTU)	Upstream	3.4	3.2	3.7	3.4	3.0	2.7
	Downstream	3.8	2.8	4.3	3.3	3.0	1.7

The secondary branch channel banks are unstable at this location, with frequent sediment removal from local scour. Plants are undercut in these images, which points to the recent nature of these events. In addition, the water in this location, although at this time flowing, was very turbid. Turbidity and TSS data were collected from the secondary and downstream site during the rain event on 6/11/2014, and this data is shown in Figure 3.13. The peak turbidity data point in the secondary site, at 6:41 pm, was above the detection limit (999 NTU) for the instrument used in this study. The downstream site data has a similar distribution of peak sediment concentration, though 15 minute delayed. This would be the expected trend as higher sediment concentration water travels from the secondary site location to the downstream location.

Considering the high TSS concentrations, high turbidity levels, and the correlation with downstream data timing, it is likely that the sporadically high levels of TSS and turbidity measured at the downstream site originated from this secondary location, not the roadway. Due to these high sediment concentrations upstream of the roadway in the secondary location, any contributions from the roadway would be covered by the higher signal, and unknown.

Figure 3.11. Aerial view of the two channels of the LCC as it crosses I-59 (image from Bing Maps). The 3 sites of data collection are indicated by white circles labeled Upstream, Median, and Downstream.

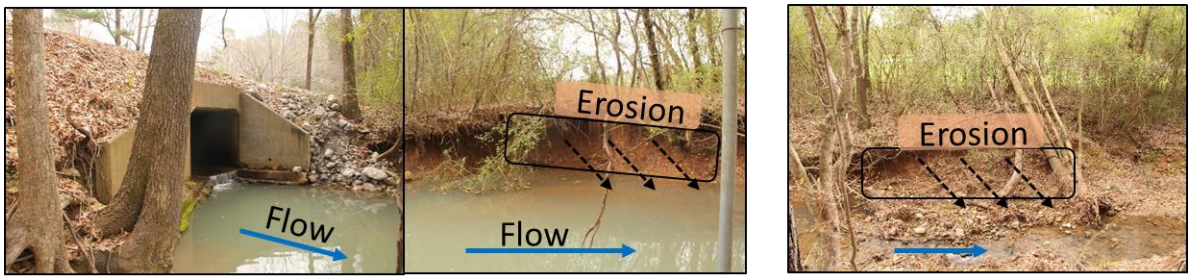

Figure 3.12. Photos of the secondary branch after passing Arrowhead Lane. Channel banks at this location are experiencing erosion, indicated by living trees uprooted and sliding down the banks.

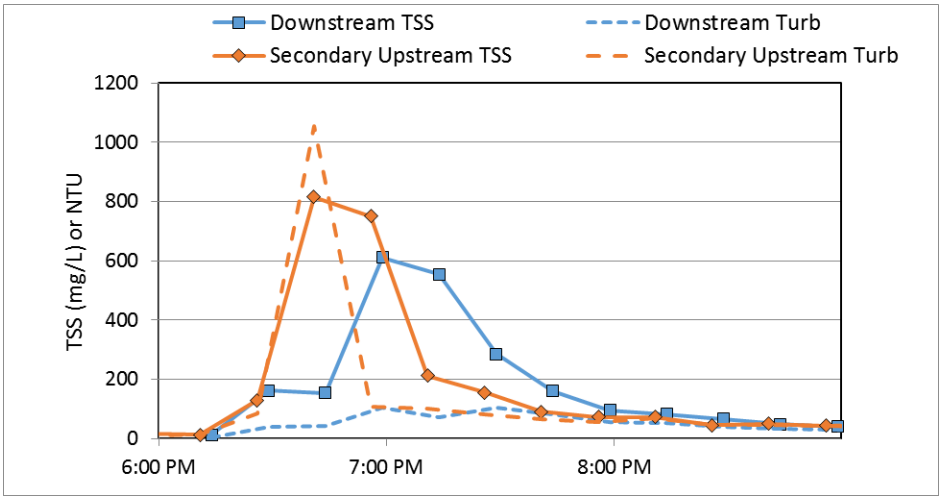

Figure 3.13. TSS and turbidity data from the secondary branch upstream of I-59, and downstream of I-59.

3.3.3 Results of Nitrogen and Phosphorus Species Measurements

Figures 3.14 to 3.17 are a comparison of the upstream and downstream nutrient levels: nitrate (NO_3), ammonia-nitrogen (NH_3-N), total nitrogen (TN), and total phosphorous (TP), respectively. These figures represent measurements over 12 months, with estimated detection limits (EDT) and the degree of accuracy for each Hach test measurement represented in the figure caption.

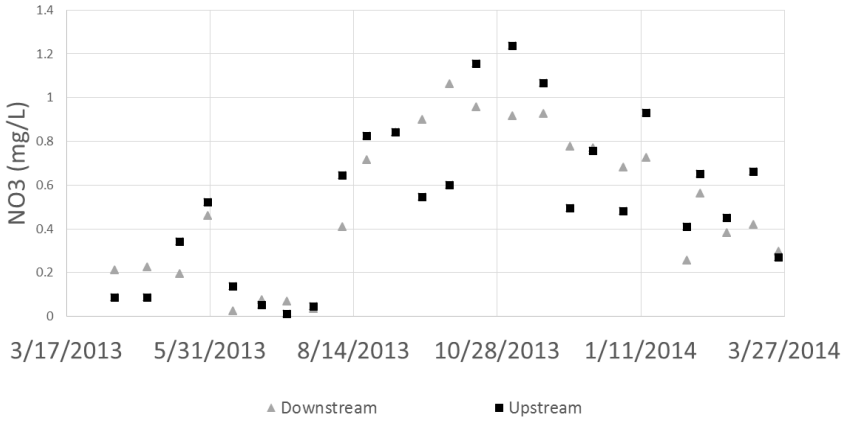

Figure 3.14. Upstream and downstream sites NO_3 results expressed as N (EDT: 0.01 ppm NO_3-N; accuracy: ±0.03 mg/L).

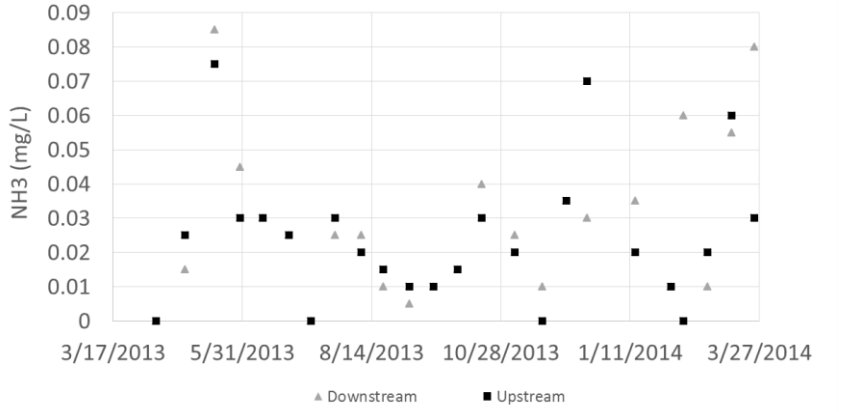

Figure 3.15. Upstream and downstream sites NH_3–N results expressed as N (EDT: 0.07 ppm N; accuracy: ±0.02 mg/L).

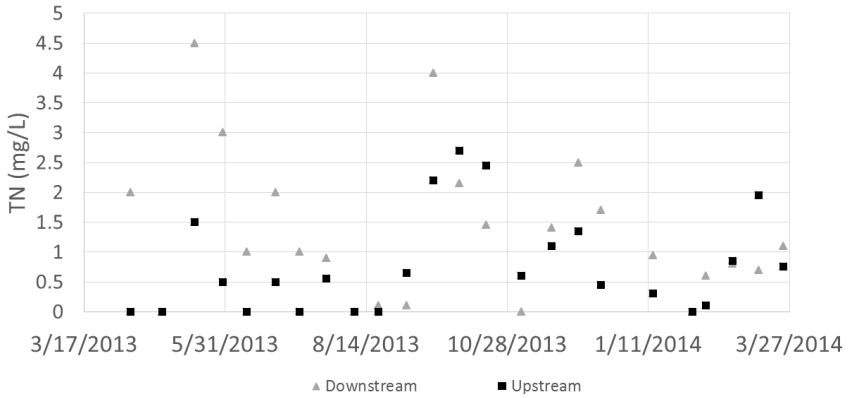

Figure 3.16. Upstream and downstream sites total nitrogen results (EDT: 2 ppm N; accuracy: ±0.05 mg/L).

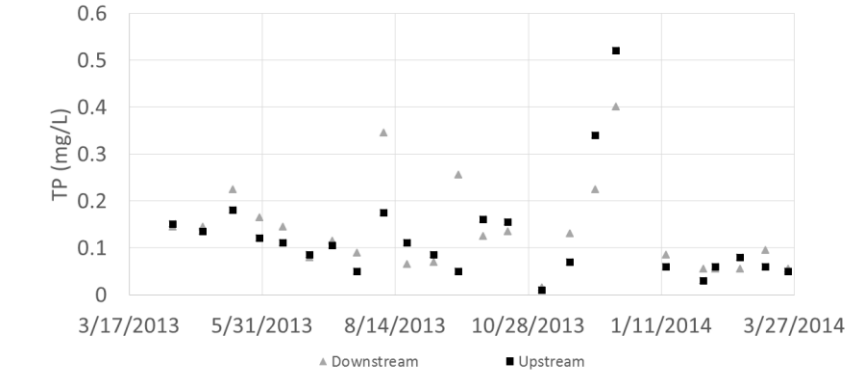

Figure 3.17. Upstream and downstream sites total phosphorus results (EDT: 0.07 ppm PO4; accuracy: ±0.07 mg/L).

TN, TP and NH_3 all show no major seasonal variations. The level of NO_3 rose from August to January by approximately 1 ppm. The collected data also indicates that overall there was no significant increase of nutrients between the upstream and downstream stations across the interstate highway. The downstream station, however, occasionally contained higher levels of TN than the upstream station, but the levels of TN were more consistently below the estimated detection limit of the instruments used (2 mg/L). This indicates that, in general, the concentration of TN in the LCC is low. The occasional increase in TN measured downstream of the roadway could be caused by atmospheric deposition in the paved area, or by vehicular exhaust. Since

vehicle exhaust contains nitrogen oxides, such as NO and NO_2, and NH_3 (AQEG, 2004), vehicle exhaust may be a contributing factor to this increase in nitrogen (Capea et al. 2004). If this increase in nitrogen was caused by vehicular exhaust, plant growth and development near the interstate may increase with increased traffic of the BNB highway (Capea et al. 2004). Other than TN, nutrient levels were generally low and often below the detection limits from the methods used in this study.

Over the collection period of point samples (from March 2013 to March 2014), the overall average and standard deviation was calculated for each of the seven N and P species: NO_3, TN, NH_3, NO_2-N, TP, PO_4^{3-} and poly-phosphate. Averages and standard deviations were calculated for the all samples by grouping results according to the amount of time passed since the most recent rain event. The collection points taken within 72 hours of a rain event were separated from the samples that were collected when a rain event had occurred more than 72 hours before collection. In addition, results from all samples were characterized in terms of average and standard deviation.

In general, all samples contain relatively small concentrations of N and P species. For nitrogen species, results from all sites were in general larger for samples taken after 72 hours following a rain event (Table 3.3). These values are consistent with the National Stormwater Quality Database version 1.1 (Pitt et al., 2004), shown in Table 3.4.

For phosphorous species, the upstream and downstream sites were found to have greater values on average within 72 hours of a rain event. Many possible factors can contribute to this presence of phosphorous species during rain events such as weathering phosphorous materials in streambeds or organic or inorganic material from nearby land (such as fertilizers). Table 3.3 summarizes the statistical data for the nutrients discussed herein.

Table 3.3. Summary of nutrient statistical data for the upstream and downstream sites. All values are in mg/L.

Physical Parameter	Site	Average	Standard Deviation	Occurred within 72 hours of event		Occurred after 72 hours of event		Error	Detection Limit
				Average	Standard Deviation	Average	Standard Deviation		
NO_3	Upstream	0.528	0.350	0.506	0.348	0.552	0.351	0.03	0.01
	Downstream	0.499	0.327	0.450	0.314	0.556	0.333		
TN	Upstream	0.794	0.805	0.521	0.691	1.067	0.819	0.5	2
	Downstream	1.312	1.187	0.927	0.778	1.729	1.394		
NH_3	Upstream	0.026	0.021	0.030	0.018	0.023	0.023	0.02	0.07
	Downstream	0.032	0.029	0.035	0.028	0.028	0.029		
NO_2-N	Upstream	0.007	0.008	0.003	0.003	0.012	0.010	0.003	0.005
	Downstream	0.006	0.008	0.003	0.003	0.010	0.010		
TP	Upstream	0.162	0.199	0.249	0.258	0.082	0.041	0.06	0.07
	Downstream	0.218	0.296	0.308	0.384	0.121	0.067		
PO_4^{3-}	Upstream	0.484	0.445	0.522	0.545	0.443	0.295	0.05	0.05
	Downstream	0.583	0.474	0.770	0.565	0.379	0.208		
Poly-Phosphate	Upstream	0.445	0.337	0.458	0.296	0.431	0.376	0.05	0.05
	Downstream	0.499	0.303	0.490	0.330	0.510	0.269		

Table 3.4 Stormwater runoff water quality data from the National Stormwater Quality Database.

Land Use	Parameter	Median	Cv
Mixed Open Space	pH	7.9 units	0.08
	Conductivity	113 µS	0.5
	TSS	48.5 mg/L	1.5
	NO_3	0.7 mg/L	0.8
	NH_3	0.51 mg/L	1.2
	TN	2.21 mg/L	–
	TP	0.25 mg/L	1.1
Mixed Freeway	pH	7.7 units	0.1
	Conductivity	353 µS	0.6
	TSS	88 mg/L	1.1
	NO_3	0.9 mg/L	0.7
	NH_3	1.07 mg/L	–
	TN	3.2 mg/L	–
	TP	0.34 mg/L	0.7

3.3.4 Environmental Sonde Results

The continuous measurement of DO, specific conductivity, pH and turbidity has provided insights into other impacts on LCC from the presence of I-59. Figure 3.18 shows the variation of some parameters for a rain event on 8/4/2013. Since Alabama has a warmer climate, and salt is not generally used for de-icing roads, runoff from the interstate should not result in significant

conductivity levels. This data shows that runoff from I-59 contains low and insignificant conductivity levels.

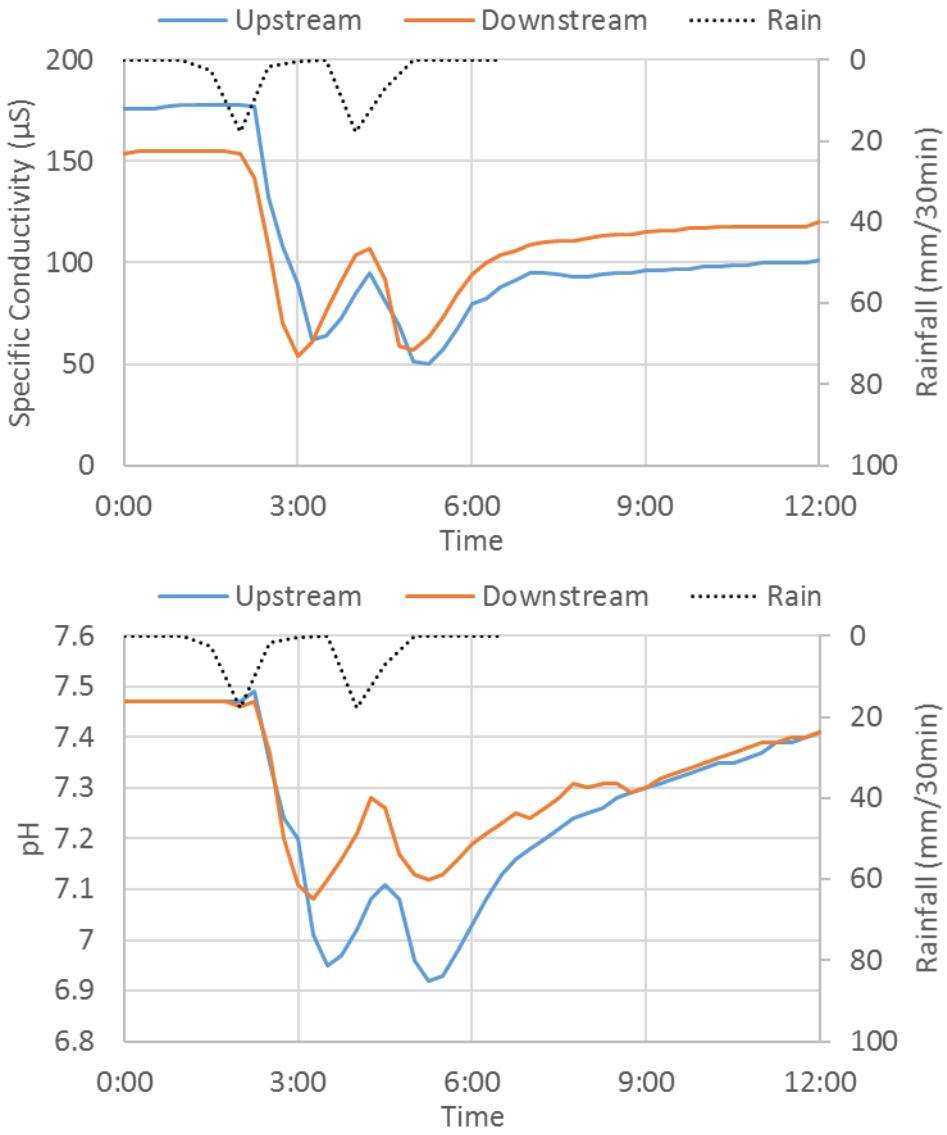

Figure 3.18. Stream responses measured on 8/04/2013 by the Hydrolab® DS5 environmental sondes in LCC.

Three parameters' values were observed to change across I-59 during rain events: pH, dissolved oxygen and turbidity. The pH results show generally a decrease during rainfall, which was due to the lower pH of rainfall (4.7 to 5) consistent with results from the National Atmospheric Deposition Program (2014). However, the pH decreases significantly more

downstream than upstream from the interstate highway. The pH decreases approximately 0.4 units before the highway and an additional 0.1 units across it. Dissolved oxygen generally increases across the highway during rain events. Specific conductivity decreases 40 µS to 60 µS during rain events, but does not significantly vary across I-59.

3.3.5 Macroinvertebrate Assessment

In addition to the water quality parameters shown and discussed above, an investigation into the biological response to water quality in the LCC was performed following the guidelines of the Alabama Water Watch stream biomonitoring manual. At the upstream and downstream site locations, macroinvertebrate species were collected, identified, and recorded to identify the diversity of organisms living in the LCC. Organisms identified in this procedure are the following, listed according to Taxa (I, II, and III): (I) Stonefly, Mayfly, Caddisfly, Riffle Beetle, Water Penny Beetle, Snail; (II) Dragonfly, Damselfly, Cranefly, Blackfly, Filtering Caddisfly, Hellgramite, Scud, Sowbug, Crayfish, Asiatic Clam; (III) Midge, Aquatic Worm, Leech, and Pouch Snail. The diversity and abundance of different macroinvertebrates indicates the biologic response to water quality in the LCC. Organisms belonging to Taxa I are the most intolerant species, and Taxa III are the most tolerant. Abundance of Taxa I and II organisms indicates high water quality. Macroinvertebrate species were collected and counted on March 23, 2015; data forms for this sampling are included in the appendix of this dissertation. Both upstream and downstream sites had a diverse population of Taxa I and II macroinvertebrates, scoring very high on the water quality index as defined by Alabama Water Watch. Upstream of the roadway had a stream quality assessment value of 32, and downstream had a value of 28; larger than 22 is

considered excellent. Thus, the water quality in the LCC was considered excellent both upstream and downstream of the roadway.

3.3.6 Hydrologic Measurement Results

Average rainfall in the Birmingham area varies between 7.6 cm to 15.25 cm per month, with typical lows in the summer (NOAA, 2002). Generally, there was little difference between the two rain gauges' rainfall measurements at this location, though they are approximately 3.5 km away from each other. Thus, data from the nearest rain gauge (<0.35 km from the stream-interstate highway crossing) is shown in Figure 3.19 for the first year of study. During this year, average rain events with intensities of approximately 1.3 cm/h occurred throughout the year, with less frequent rain events in the late summer and fall (late August to October). The most intense rain events (up to ~5 cm/h) occurred in the early summer months (June and July). These were not unusual rain events, as the 1-year return period for 60-minute duration rainfall produces approximately 3.8 cm/h intensity rains for this area (NOAA, Atlas 14).

Figure 3.19. Rainfall series measured within the LCC watershed, near the I-59 crossing.

Throughout most of the year, the LCC has base flows around 0.14 m^3/s to 0.23 m^3/s. The downstream portion of the creek typically has a base flow increment of 0.57 m^3/s to 0.85 m^3/s compared to the upstream portion due to groundwater contributions and the intersection of another small tributary of the creek that drains a 0.57 km^2 portion (rural area) of this watershed.

Although there are many rain events in this area of Alabama (Figure 3.19), the stream does not always show significant responses to all of them, as presented in Figure 3.20. Abstraction and infiltration in the forested portion of the catchment decrease runoff volume, particularly during the warmer season when the rain events have relatively long antecedent dry periods and low intensities. As Figure 3.20 shows, there was increasing noise in the pressure transducer data over time, which led to an investigation into the sensitivities of these instruments to variations of temperature. The results of that investigation are presented in Chapter 5.

Figure 3.21 presents flows for a rain event on 07/10/2013 derived with the H–Q curve. This event is representative of a typical rain event and stream flow response. A few other rain events in 2013 had relatively larger rainfall depths, and the stream responded with a rise in stream levels of >1.5 m. For these events, the developed head–discharge curve is invalid, because measurements were performed at lower flows.

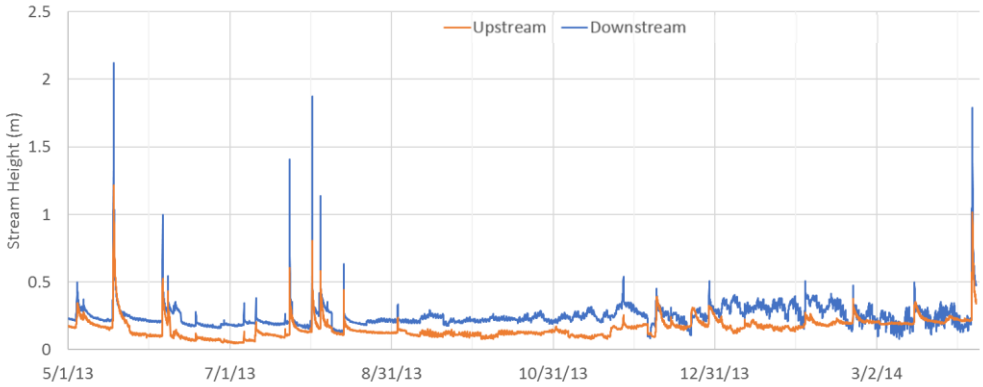

Figure 3.20. Stream stage height of LCC upstream and downstream of I-59.

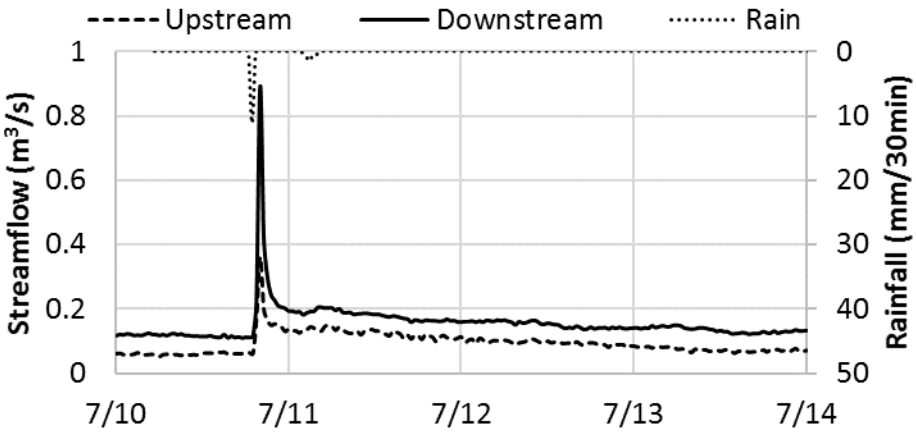

Figure 3.21. Calculated flow of LCC upstream and downstream of the interstate on 07/10/2013; the event had 1.5 cm of rain.

In addition to surface water measurements, groundwater table elevations at the upstream and downstream locations were measured with a near-stream observation well. These two wells were installed approximately 5 m from the edge of the stream bank. Additionally, a groundwater observation well was installed in the middle of the interstate median, approximately 20 m from the edge of the stream bank. Figure 3.22 shows the groundwater table response to rain events for the months of September to October, 2014. Before the event of 9/15/14, the groundwater table was below the observation well in the median, and the elevation during that time was unknown. From this figure, it can be seen that the groundwater table near the stream bank at the upstream and downstream location was typically at a constant elevation in the absence of rainfall. Additionally, the magnitude of response for the groundwater table rise and the surface water rise is comparable, suggesting they are well-connected.

The median groundwater table has a more complicated response, with a more delayed recession curve, and even a much larger increase than either of the other two sites. Though constructed areas like roadways are often sources of increased stormwater runoff, the

groundwater table response in the median suggests that the drainage features of the interstate have the capacity to capture and effectively "hold" stormwater for a long period of time.

The stream flow definitively increased as it received additional runoff while crossing the interstate. A relevant question is how much of this runoff was caused by increased imperviousness of the interstate and its associated structures as compared with natural pre-construction conditions. This question was addressed in section 4.2.5, with the aid of computer modeling. Another question is whether this increased runoff is proportional or not to the increased catchment area, irrespective of land use. The following section seeks to answer this second question.

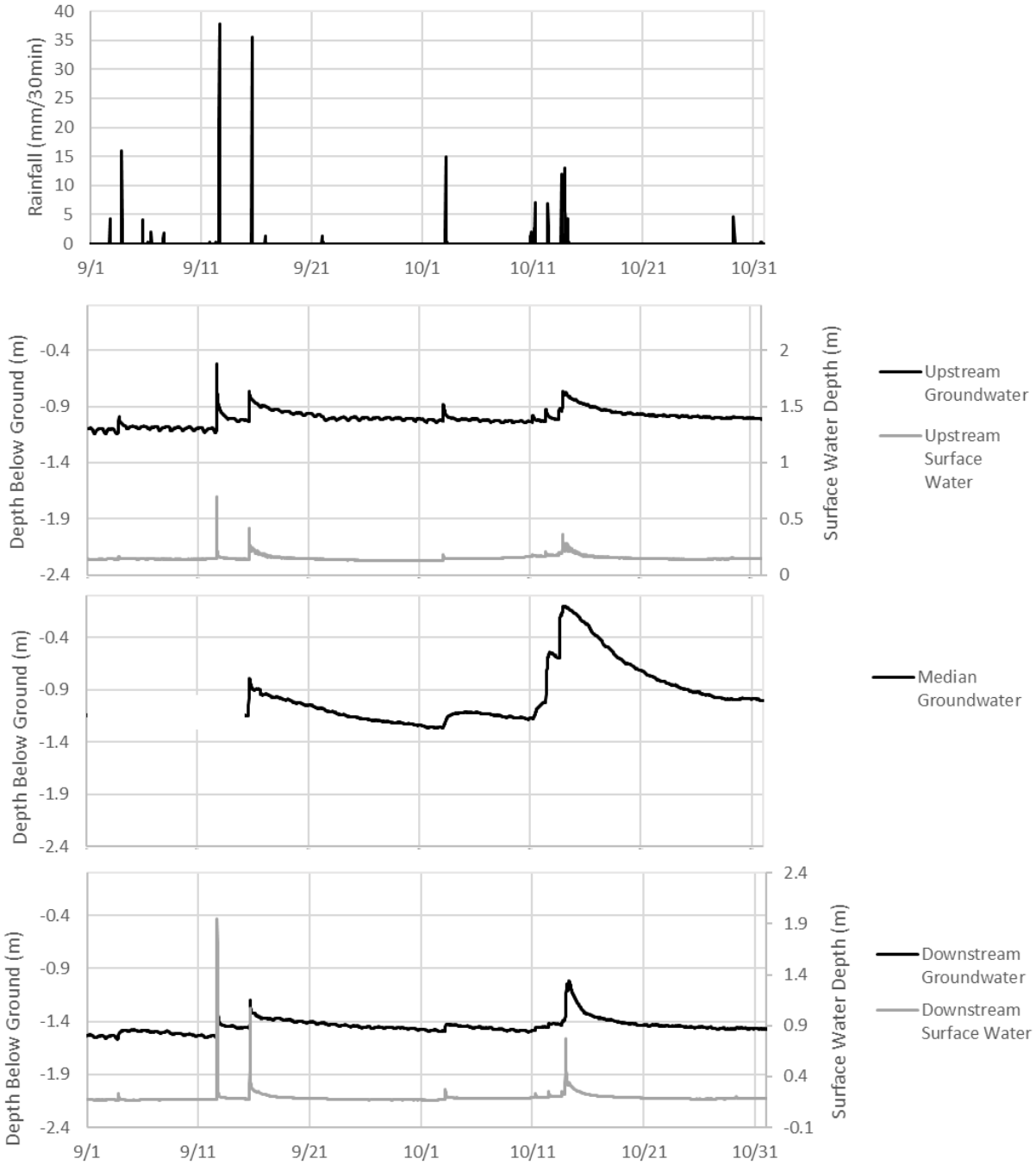

Figure 3.22. Groundwater table and channel surface water response to rain of September-October, 2014.

3.3.7 Volumetric Runoff Coefficient Calculations

Calculations of the volumetric runoff coefficient for selected events were conducted to obtain insights to the effect of the road on the flows measured in the stream. A constant base flow (the

minimum value prior to the rain event) was removed from the volume calculations. Integration of the stream flow rate, Q, over time yields the volume of water linked to the rain event as runoff (assuming that groundwater flows are moving much more gradually through the watershed). The volume of rainfall was determined by multiplying the rainfall depth for each time interval by the area of the contributing watershed, and summing the volume of rain over time. Any rainfall loss, such as interception losses, will result in a lower volumetric runoff coefficient.

The subcatchment area is different for the upstream and downstream portions; the area contributing to the upstream portion of the stream is about 2.7 km^2, whereas the downstream portion of the stream has an additional 0.57 km^2 contributing to the runoff. At each time interval, the volumetric runoff coefficient was determined as the cumulative volume of runoff divided by the cumulative volume of rainfall for each station. The following equation was used:

$$C_v(t) = \frac{\sum_{i=1}^{N}(Q_i - Q_{i-1}) * \Delta t}{\sum_{i=1}^{N} P_i * A_s} \qquad \text{(Eq. 3.2)}$$

In EQ-3.2, $C_v(t)$ is the volumetric runoff coefficient (unitless) evolution over time, Q_i is the runoff rate (m^3/s) at a specific time interval, Q_{i-1} is the runoff rate (m^3/s) at the previous time interval, Δt is the length of the recorded time interval (s), P_i is the rainfall depth (m) during the time interval, and A_s is the surface area (m^2) of the contributing catchment. Figures 3.23 and 3.24 show results of these calculations, the evolution of the runoff coefficient over time. The event shown in Figure 3.23 included 1.5 cm of rain, while the event in Figure 3.24 had a total rainfall of 3.84 cm. One advantage of these calculations is that they represent not the peak runoff of an area, but the volume of runoff reaching a downstream point, including the recession limb of the hydrograph.

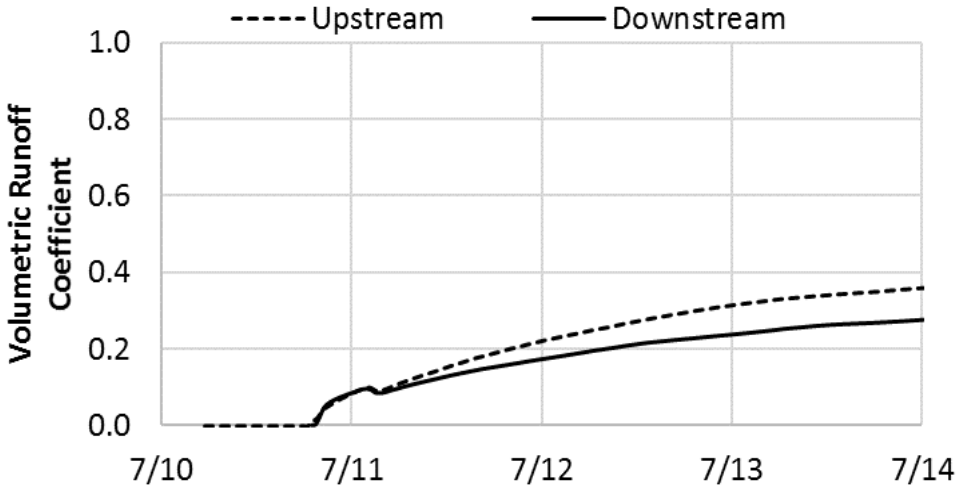

Figure 3.23. Volumetric runoff coefficient variation for a rain event on 7/10/2014.

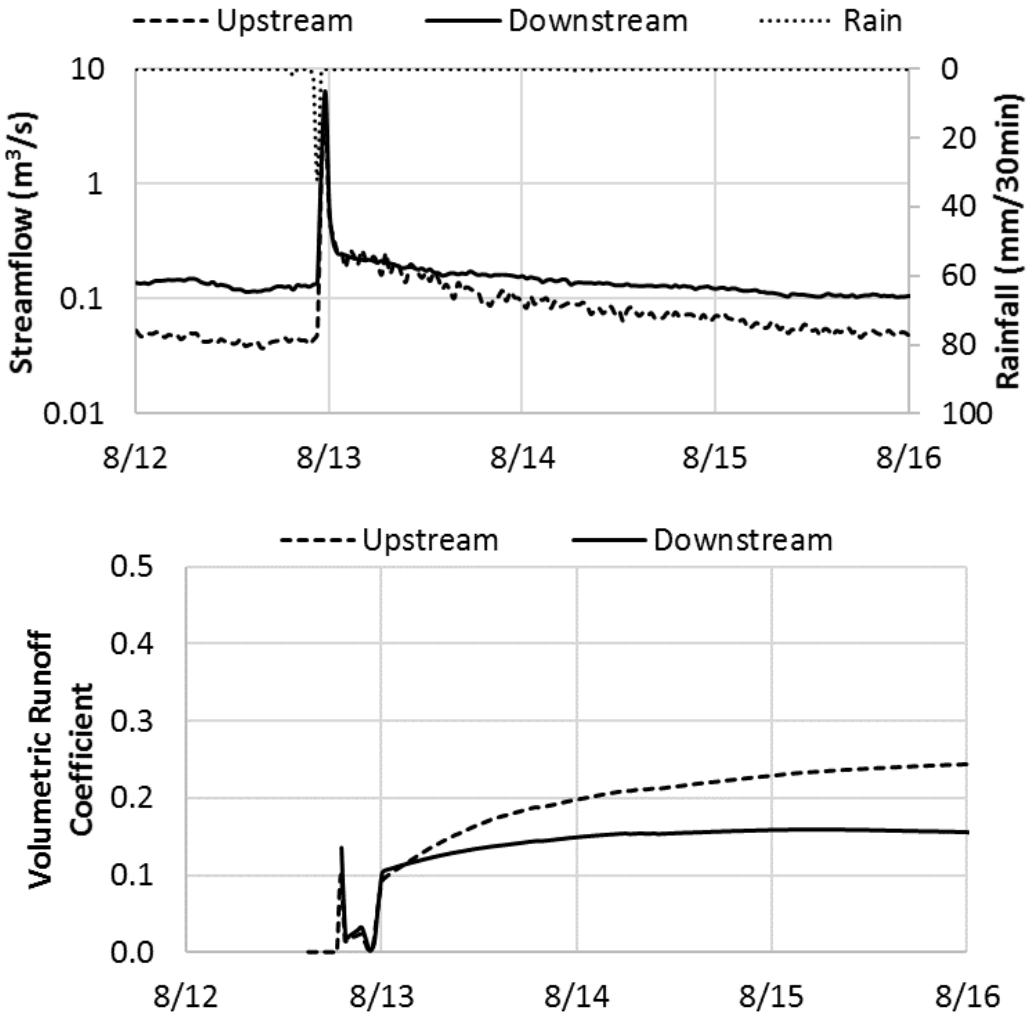

Figure 3.24. Hyetograph, stream flow and volumetric runoff coefficient variation for rain event on 8/12/2013.

In Figure 3.23 the initial stages of rain events there was a rapid increase in the runoff coefficient as more areas of the watershed contribute runoff at both upstream and downstream sites. Gradually the runoff coefficient began to approach values in the range 0.16 to 0.36 for the downstream site and 0.25 to 0.50 for the upstream site. Considering the paved area of the interstate, such a result is at first counterintuitive as it would be expected that the increased imperviousness from the roadway surfaces would increase the runoff coefficient, not decrease it.

Two factors may have a role in reducing the volumetric runoff coefficient across the interstate in the presented cases. First, the tributary of the creek (the secondary branch) that joins the stream between the upstream and downstream site drains a forested area with potential for large abstractions, such as tree canopy interception, which could decrease runoff contributions from that portion of the watershed. There is also potential for significant infiltration in the flat region of the interstate drainage area, decreasing the fraction of overland flow. In addition, a substantial portion of the highway right of way is vegetated with trees and bushes, which may encourage infiltration through root connections and macropores. Further work is discussed later in this document to determine the causes of these results, including discussion of shallow groundwater tables and interactions with surface water, and modeling of the ungauged portion upstream of the secondary branch.

Another interesting observation is the significant differences between the observed runoff coefficients from these two selected rain events. There are many variables that may yield different runoff coefficients between major rain event events. A key parameter pointed out by earlier studies (Hoffman et al., 1984; Irish et al., 1995) is the antecedent dry period. Longer dry periods are typically associated with higher values of initial abstractions and infiltration, which would significantly reduce runoff volumes. A key parameter is antecedent moisture conditions,

which is associated with the antecedent dry period. For the event shown in Figure 3.23, July 10th, there were about 3-4 days since the last rain event. The event on Figure 3.24, August 20th, had about 8 days since the previous rain event. This difference may impact the volumetric runoff coefficient values for these two events.

3.4 Concluding Remarks of Field Investigation of the LCC

Past investigations have shown that runoff from roads may include increased levels of nutrients and suspended solids among other constituents, as well impacts to local hydrology of streams. This study focused on measuring such impacts to the LCC at a point where it is crossed by I-59. Development of the local watershed was limited, with some residential areas, farmland and forested areas. Since the majority of stormwater runoff was conveyed as overland or natural subsurface flow, with little to no hard-piping, abstractions and water quality are relatively higher than in more urban watersheds. As runoff from other land uses may also cause impacts to the stream, all characterization has been performed at a site upstream from the road, and another site immediately downstream from the interstate crossing.

While there were significantly larger values for the turbidity and TSS parameters at the downstream site during rain events, these higher levels were likely sourced from the secondary upstream location. There was no significant increase in nitrogen and phosphorus species across the interstate. The exception was total nitrogen, which occasionally had higher concentrations downstream of I-59, which may be due to organic nitrogen since the other nitrogen species were very low. Rain events have also caused a drop in specific conductivity and in pH, but this effect was noticed in both sites across the interstate. Additionally, biological assessments indicate that the LCC has excellent water quality.

Additionally, based on volumetric runoff coefficient calculations, the runoff/rainfall ratio had a lower value downstream from the roadway when compared to the upstream region. This result is somewhat counter-intuitive, considering the relative increase in imperviousness caused by paved surfaces and potentially reduced infiltration of compacted soils. It is speculated that increased infiltration due to flatter slopes associated with the interstate ditches and medians had effectively reduced runoff values. Considering the response of the groundwater table in the interstate median, this seems likely. Compared to the land upstream of the roadway, which has 10% to 30% surface slope, the roadway has a drainage slope of approximately 5%. The upstream and downstream groundwater table elevations seem more strongly tied to surface water height than median groundwater table elevations, and were likely responding to rain events via the process of bank storage. This process will be explored more in Chapter 4.

Chapter 4 – Modeling Interstate Runoff with SWMM and GSSHA: Comparing Surface-Groundwater Interactions

During the field investigation task of this research, counter-intuitive hydrological results were found in regards to the total streamflow downstream of the interstate. The volumetric runoff coefficient calculations indicated that, for some rain events, the proportional volume of runoff produced by the roadway and secondary branch of the LCC was smaller than the forested area upstream of the main branch. To more accurately assess the hydrological impact of the roadway, as well as the ungauged secondary branch, a smaller subcatchment of the LCC was selected for the modeling research discussed here.

The humid, subtropical climate of Alabama ensures an ample supply of groundwater and streamflow throughout the watershed. Previous work done in this watershed focused on measurable effects of I-59 on stormwater runoff as it crosses over the creek (Chapter 3), as well as an attempt to model a larger portion of the watershed with SWMM (Butler et al., 2016). Complex features exist along the main branch of the creek, including steep elevation changes, fluctuating groundwater tables with exfiltration on the ground surface, and retention ponds on residential properties. The watershed area upstream of this area was not modeled in this work, but is rather represented in the hydrological models as a boundary condition with an inflow hydrograph. This region is indicated in Figure 4.1(b) with cross-hatching. During the data collection phase of this research, various sensors were installed within this subcatchment of the LCC upstream of I-59 to accurately quantify the inflow of stormwater from various areas of the research site.

4.1 Methodology

4.1.1 Research Site and Data Collection

Figure 4.1 indicates the research site, as well as the location where flow was measured upstream and the locations of other site monitoring stations. Figure 4.1(c) shows a closer view of the channel network as it crosses I-59. The four sites discussed in this work are identified as Upstream, Median, Downstream, and Secondary. The location labeled "Secondary" consists of an intermittent stream and is described here because only visual observations were made at this location during field visits, not via measured data as is the case for the other 3 locations. This portion of the watershed delivered occasional but intense runoff to the stream.

Both upstream and downstream sites were equipped with an ISCO area-velocity sensor (model 2150 flow module), a HOBO® pressure transducer (model U20-001-01) for in-stream head monitoring, and a near-stream groundwater observation well, which was placed approximately 5 m from the stream bank at each site. The interstate median site was equipped with only a groundwater observation well approximately 20 m from the stream bank. In each of the three groundwater monitoring wells, HOBO® pressure transducers were installed to measure pressure head. A HOBO® rain gauge (model RG3) was installed for rainfall measurements approximately 350 m from the downstream site, as well as an additional above ground HOBO® pressure transducer for barometric compensation. Rainfall and stream gauge field data was collected for approximately 2.5 years from March 2013 to January 2016. The ISCO area-velocity sensors as well as the groundwater monitoring wells were installed in July 2014.

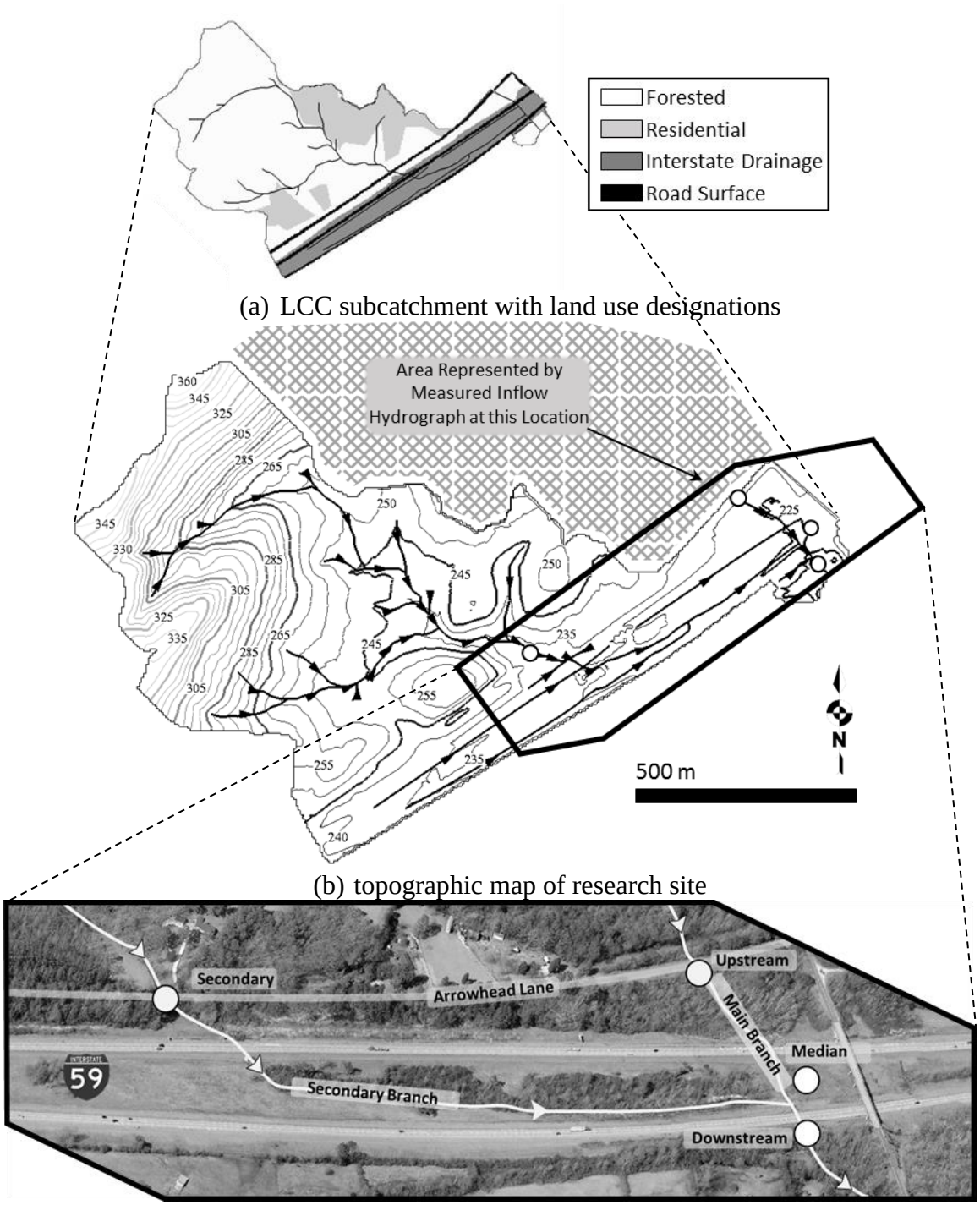

(a) LCC subcatchment with land use designations

(b) topographic map of research site

(c) aerial view of channel intersections with I-59 and data collection locations labeled (Image from Bing Maps)

Figure 4.1. Various views of the LCC watershed and research site location.

In addition to data collected in the field, soil maps and digital elevation models (DEMs) were retrieved from available sources. Soil type distribution shapefiles were downloaded from the Soil Survey Geographic (SSURGO) database available from the National Resource Conservation Service (NRCS). High resolution (1 m) DEMs were used from the United States Geological Survey (USGS). Due to limitations on land use geospatial data accuracy, land use was determined by visual inspection of satellite imagery. There were only four land uses defined in this area: (1) forested, (2) residential, (3) road pavement, and (4) interstate drainage via grass lined swales. Figure 4.1 shows the distribution of these land uses.

4.1.2 Governing Equations

The models SWMM and GSSHA share various commonalities in their representation of hydrological processes. The following discussion is not intended to supplement or replace the more thorough explanations in the models' reference guides (Downer and Ogden, 2002; James et al., 2016). Rather, an introduction of the basic governing equations is presented as a foundation for subsequent discussion on the impacts of these equations on hydrological modeling between the two programs. As mentioned earlier, GSSHA is a 2-dimensional hydrologic model, and it divides the watershed into grid cells of equal size. Figure 4.2(a) shows the discretized form of the LLC watershed modelled in this study.

To capture the effect of the roadway, the GSSHA model was divided into a total of 34,999 cells of 5 m by 5 m. Typically, GSSHA users are recommended to use larger grid sizes (i.e., 30 m and above), however, this is a small watershed and the need to capture the smaller elements of the roadway and ditches during this research led to using a smaller grid size. SWMM divides the watershed into subcatchments of homogenous parameters. Figure 4.2(b) shows this

study's watershed representation in SWMM, where the model was divided into 21 subcatchments, ranging from approximately 13,000 to 167,000 m^2 in surface area.

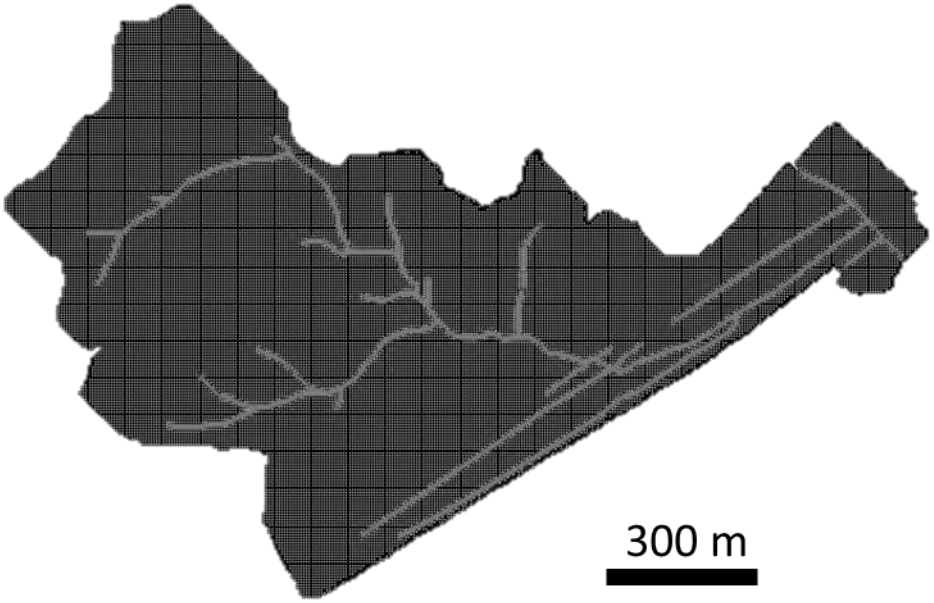

(a) GSSHA

(b) SWMM

Note: Images correspond to the area shown in Figure 4.1.

Figure 4.2. Model discretization of the watershed of the LCC

Many different hydrological processes are modeled within SWMM and GSSHA; Table 4.1 summaries the processes and methods used in this work. SWMM and GSSHA both solve Manning's equation for overland flow calculated from the overland depth. Since SWMM calculates the overland flow in a 1-dimensional scheme, the area term in Manning's equation introduces a unique *W* parameter, which is the representative width of the subcatchment (James et al., 2016).

$$q = \frac{1.49 * W * S^{1/2}}{A * n}(d - d_s)^{5/3} \quad \text{(Eq. 4.1)}$$

In Equation 4.1, q is the overland flow rate per unit surface area (m/s), W is the subcatchment's width (m), S is the average slope of the subcatchment (m/m), A is the surface area (m^2), n is Manning's roughness coefficient (unitless), d is the depth of water in the overland plane (m), and d_s is the depression storage (m). The width parameter may be adjusted to represent a shorter or longer time of concentration for overland flow to the desired outlet. Slope and subcatchment areas are quantifiable parameters, and thus are not typically adjusted. Depression storage and the Manning's roughness are user input values, and there are a variety of estimates for this parameter dependent on land use or other classifications. The depression storage parameter accounts for rainfall abstractions and removes a depth of water from the overland flow calculations, though this depression storage water is available for infiltration and evapotranspiration calculations. The depression storage parameter was adjusted in this work primarily to capture the amount of rainfall that, in measured data, does not produce surface runoff, but does infiltrate to alter the groundwater table elevation.

GSSHA has a similar overland flow scheme, except that it solves the equation in a 2-dimensional scheme as follows:

$$p_{i,j}^{n} = \frac{1}{n}\left(d_{i,j}^{n}\right)^{\frac{5}{3}}\left(S_{fx}^{n}\right)^{1/2} \quad \text{(Eq. 4.2)}$$

$$q_{i,j}^{n} = \frac{1}{n}\left(d_{i,j}^{n}\right)^{\frac{5}{3}}\left(S_{fy}^{n}\right)^{1/2} \quad \text{(Eq. 4.3)}$$

$$d_{i,j}^{n+1} = d_{i,j}^{n} + \frac{\Delta t}{\Delta x}\left(p_{i-1,j}^{n} + q_{i,j-1}^{n} - p_{i,j}^{n} - q_{i,j}^{n}\right) \quad \text{(Eq. 4.4)}$$

In Equations 4.2 through 4.4, inter-cell fluxes are defined as p and q in the x- and y-direction, respectively. S_{fx} and S_{fy} are the friction slope in the x- and y-direction, respectively. Δt and Δx are the time and space step used within GSSHA. Thus, both SWMM and GSSHA calculate overland flow applying a depth-discharge formulation based on Manning's equation. Yet, SWMM has no equivalent form for Equation 4.4 to calculate the overland depth. In both models depth was recalculated every computational step by updating the variables after evaporation, rainfall, outflow, and infiltration are considered.

SWMM and GSSHA can both calculate infiltration through a variety of methods. Since SWMM was designed as an urban stormwater model, formulation alternatives for infiltration include those used in urban settings: Horton's, Green-Ampt, and the curve number. GSSHA uses primarily the Green-Ampt equation, but also includes a version of Richard's Equation.

Table 4.1. Summary of the processes modeled in SWMM and GSSHA, and the methods used in this paper to describe these processes.

Process	SWMM	GSSHA
Depression storage	Two Parameter (assigned by land use, varying by impervious %)	Single parameter (assigned by land use)
Infiltration	Green-Ampt Equation	Green-Ampt Equation
Groundwater	2-Zone mass balance, single reservoir	2D groundwater surface
Overland runoff	1D Manning's	2D Manning's
Channel flow	1D Diffusive Wave	1D Diffusive Wave
Surface water & groundwater interactions	5-Parameter conceptual groundwater flux equation.	Darcy Equation
Evapotranspiration	Average daily value (State climate office of North Carolina, 2016)	Not used (initial moisture conditions calibrated for event-based simulation)

The Green-Ampt equation as written by Mein and Larson (1973) is:

$$f_p = K_s\left(1 + \psi_f \frac{\theta_d}{F}\right) \quad \text{(Eq. 4.5)}$$

This equation can then be solved by integration into the form:

$$F^{t+\Delta t} = K_s \Delta t + F^t + \psi_f \theta_d ln\left[\frac{F^{t+\Delta t} + \psi_f \theta_d}{F^t + \psi_f \theta_d}\right] \quad \text{(Eq. 4.6)}$$

Where, f_p is the infiltration rate (cm/hr), K_s is the saturated hydraulic conductivity (cm/hr), Ψ_f is the capillary suction head at the wetting front (cm of water). Θ_d is the moisture deficit, equal to the saturated moisture content (unitless fraction; often considered equal to porosity) minus the initial (or current) moisture content (unitless fraction), and F is the cumulative infiltration since the beginning of the rain event (cm). GSSHA calculates the next infiltration rate, $f_p^{t+\Delta t}$, by plugging this new cumulative infiltration, F, back into Equation 4.5. SWMM differs in that the average infiltration rate over a time step, f_{AVE}, is then calculated as follows:

$$f_{AVE} = \frac{F^{t+\Delta t} - F^t}{\Delta t} \quad \text{(Eq. 4.7)}$$

Thus, SWMM uses an average infiltration rate over the computational time step, and GSSHA uses an updated infiltration rate at the next time step.

Another difference between these two models' implementations of the Green-Ampt equation is related to the discretization of the overland plane, and the subsurface component. For GSSHA, if small cell sizes are used that can accurately represent the spatial distribution of impervious surfaces (i.e., roadways), then the infiltration parameters can be reduced to inhibit infiltration. If larger cell sizes are used, an "area reduction" component is added to the computation that reduces the infiltration by a user-determined fraction. Similar to this second method, SWMM reduces the surface area available for infiltration with a user-defined impervious area fraction. SWMM can route surface runoff from the impervious area onto the

pervious area, which is the pathway for stormwater from the road surface onto the drainage area and conveyance channels. The infiltrating water is then added the subsurface of the subcatchment uniformly, not specifically under the pervious fraction. This seems to be the case as well for the area reduction format of GSSHA for simulating pervious areas, though this is not clearly specified. Differences between the implementation of the Green-Ampt equation also exist in the redistribution or recovery of soils after rain events cease; however, the work presented herein comparing these two models does not focus on long-term simulations but rather individual events.

Channel flow modeling in this study was accomplished by solution of the 1-dimensional continuity and momentum equations (St. Venant equations):

$$\frac{\partial A}{\partial t} + \frac{\partial Q}{\partial x} = q_L \qquad \text{(Eq. 4.8)}$$

$$\frac{\partial Q}{\partial t} + \frac{\partial}{\partial x}\left(\frac{Q^2}{A}\right) + gA\frac{\partial h}{\partial x} + gA(S_0 - S_f) = 0 \qquad \text{(Eq. 4.9)}$$

Where A is the cross sectional area of the flow (m^2), Q is the channel flow rate (m^3/s), and q_L is lateral flow from overland and groundwater contributions (m^2/s), h is the water depth (m), S_0 is the channel bed slope, and S_f is the friction slope. If the inertial terms, $\frac{\partial Q}{\partial t} + \frac{\partial}{\partial x}\left(\frac{Q^2}{A}\right)$, are dropped from Equation 4.9, it results in the zero-inertia wave form of channel routing, adopted by GSSHA in routing calculations. SWMM is capable of solving both the zero-inertia and the full version of Equation 4.9. To more closely compare these two programs in this study, the diffusive wave equation was adopted here for channel SWMM modeling.

Another important distinction between the solution of these channel routing equations for SWMM and GSSHA is the variation in discretizing the channel domain. SWMM represents the channels in a junction and link system, where channels have a uniform geometry between nodes,

typically with no discretization between junction; on the other hand, GSSHA represents channels on a discretized fashion (i.e., cell by cell). Because the length of a conduit is variable in SWMM according to the stream topology, spatial derivatives are usually evaluated across the entire reach length. In contrast, GSSHA adopts uniform cell spacing for numerical stability as it routes channel flow through a finite volume approach. Due to this approach, surface runoff and groundwater (q_L) interact with each segment within channel reaches in GSSHA. In SWMM, these lateral flow contributions (q_L) enter the channel routing domain at the junctions (not links). In SWMM, flow is calculated in the channels by combining the continuity and momentum equation and head is calculated in the nodes from the continuity equation.

Groundwater is accounted for by SWMM and GSSHA in very different ways. SWMM models groundwater primarily from conservation of mass in the unsaturated and saturated zones as a function of fluxes of infiltration, evapotranspiration, stream-interaction, and loss to deep groundwater. These are either user-defined values or calculated as functions of porosity and available moisture content, depth of the water table, and depth to the bottom of the aquifer. Since GSSHA is a 2-dimensional coupled surface and subsurface model, it can account for groundwater levels and flows in the same 2-dimensional grid that is setup for overland flow modeling.

Using the solution of the 2-dimensional free surface groundwater equation discussed by Trescott and Larson (1977), GSSHA represents groundwater in form as follows:

$$\frac{\partial}{\partial x}\left(K_{xx}B\frac{\partial E_{ws}}{\partial x}\right)+\frac{\partial}{\partial y}\left(K_{yy}B\frac{\partial E_{ws}}{\partial y}\right)=S\frac{\partial E_{ws}}{\partial t}+W_S(x,y,t) \qquad \text{(Eq. 4.10)}$$

Where K_{xx} and K_{yy} are the hydraulic conductivities (cm/hr) in the x- and y-directions, respectively. B is the thickness of the saturated media (m), which may also vary in the x- and y-directions. E_{WS} is the elevation of the groundwater surface (m), which may vary at each

computational cell. *S* is the storage term, which is calculated as the change in volume with respect to the change in head. This is a function of porosity, a user-input parameter in GSSHA. W_S is the flux term for sources and sinks; in this application that is largely infiltration from the solution of the Green-Ampt equation and inputs from channel interactions. In GSSHA's application of this equation, both the *S* and *B* terms are time dependent, and calculated implicitly by updating the values based on the change in groundwater head (Downer and Ogden, 2004). If the water surface elevation E_{WS} rises to or above the elevation of the ground surface at any cell, infiltration ceases and exfiltration will occur for that cell. Since SWMM does not currently route groundwater between subcatchments, there is no equivalent for Equation 10 in its computation.

Surface-groundwater interactions play an important role in the context of the LCC watershed studied in this work. Both SWMM and GSSHA model these interactions as a function of the elevation of surface water and groundwater levels. The equation for stream-groundwater interactions in SWMM takes the form:

$$f_g = A1\left(h_{gw} - h_{cb}\right)^{B1} - A2(h_{sw} - h_{cb})^{B2} + A3 * h_{gw} * h_{sw} \quad \text{(Eq. 4.11)}$$

Where f_g is the groundwater flow rate (m^3/m^2) from the aquifer to the channel (or reverse if the value is negative), h_{gw} is the elevation (m) of the groundwater table conceptually-averaged over the area of a designated subcatchment, h_{cb} is the elevation (m) of the channel bottom represented at the receiving channel node, h_{sw} is the elevation (m) of the surface water at the receiving channel node. The groundwater elevation is considered as the average of the maximum and minimum groundwater elevation that would exist in the subcatchment (James et al., 2016). *A1*, *A2*, *A3*, *B1*, and *B2* are user-defined parameters that require calibration. This approach is highly conceptual, since the groundwater elevation is the average value for the entire subcatchment and this interaction occurs only at the receiving junction, not the length of the channel. The

groundwater interaction equation in GSSHA is based on McDonald and Harbaugh's (1988) equation and takes the form:

$$f = -\frac{K_{rb}}{M_{rb}}(E_r - E_{ws}) \quad \text{(Eq. 4.12)}$$

Where f is the groundwater flow per unit area (m/s), K_{rb} is the riverbed's hydraulic conductivity (cm/hr), M_{rb} is the thickness of the riverbed sediment (cm), E_r is the elevation of the river water surface (m), and E_{WS} is the elevation of the groundwater surface (m) at each defined computational cell. In contrast to SWMM, GSSHA calculates this flow as an input value in the flux term "W_S" of Equation 10 above for the cells that are defined as stream cells. The groundwater flow, f, is incorporated in the continuity equation (Equation 8) for channel flow modeling as part of the lateral contributions (q_L). This calculation occurs at every cell along the user defined linear stream network. This would increase or decrease the elevation of the water surface at the stream boundaries, and the propagation of this change would occur according to the groundwater equation discussed above.

4.1.3 Comparing Calibration Procedures for SWMM and GSSHA Models

Considering that model calibration is a fundamental step in the application of hydrological models, the focus of this section is to explain how the calibration of a SWMM model translates to a GSSHA model in the context of a simulation of a small headwater watershed containing a roadway. In particular, the discussion focuses on the features that are similar between these two models and that are the essential steps for developing a working hydrological simulation. When focused on hydrologic modeling, calibration often consists of changing parameters that Liong et al. (1991) calls "traditional" and "nontraditional" parameters. Of the common parameters for adjustment in SWMM or comparable models (e.g. Dent et al., 2004), those chosen for calibration

in this study were: Manning's overland roughness (n), subcatchment width (W), depression storage (d_p), infiltration parameters (K_s and Ψ_f for Green-Ampt), Manning's channel roughness (n_c), and the groundwater-surface water interaction parameters from Equation 4.11. The subcatchment width and groundwater parameters *A1* and *A2* are SWMM model-specific variables. The depression storage, roughness coefficient, and groundwater parameters were assigned and varied by land use, which is shown in Figure 4.1. This portion of the LCC is relatively small (0.875 km^2), and the soil types in the area are so similar that variations do not affect the solution significantly in this study. The degree of development in the watershed would affect the hydrologic character of the area, including the infiltration rates of the soils. Due to development, compaction of natural soils will reduce the hydraulic conductivity and increase the suction head in soils with significant clay material, which is the case in the LCC. The Green-Ampt infiltration parameters were assigned by soil characteristics determined by degree of development for both SWMM and GSSHA. The forested region of the LCC was assigned as no development, residential areas were considered limited development, and the roadway portion was considered fully developed.

Calibration in this study was done manually to represent both streamflow and groundwater table elevations since automatic calibration is typically done to better represent one or the other. Calibration was performed by adjusting the parameters mentioned above to minimize selected error metrics using surface water and groundwater measurements, for single, discrete-events. Tables 4.2 and 4.3 show the calibrated values, which are within the ranges of these parameters reported in literature (Downer and Ogden, 2002; Dent et al., 2004; Amoah et al., 2012; James et al., 2016). There are no infiltration parameters for the roadway since paved surfaces are represented by the impervious fraction in SWMM.

The setup and calibration of SWMM is similar to the GSSHA model in many of the fundamental processes. For the purposes of this study as many parameters as possible were kept the same for both programs after calibrating the models including: depression storage, infiltration parameters, and groundwater hydraulic conductivity and porosity (K_{gw} is 25 cm/hr, θ_{gw} is 0.5). Additionally, the bottom of the aquifer was set to an elevation of 0 m (sea level), which causes a variation of the thickness of the aquifer (B in EQ-4.10) In addition, some other parameters were set by physical dimensions of the models and correlate to the same values including: ground surface area, overland slope (elevation), channel geometry and slope. Though the variables are similar between the models, their implementation in the governing equations varies slightly. In GSSHA, the imperviousness of the roadway was simulated by reducing the K_{sat} parameter in roadway cells to 0.00001 cm/hr, creating an effectively impervious surface.

Table 4.2. Calibration parameters assignment by land use for SWMM.

Land use	Depression Storage (Eq. 4.1) (mm)	Manning's Roughness *n* (Eq. 4.1)	Groundwater Parameters *A1* & *A2* (Eq. 4.10)
Forested	10	0.3	0.0008
Low-Density Residential	2	0.15	0.0008
Interstate Median	2	0.1	0.5
Roadway	1	0.02	0.5

Table 4.3. SWMM and GSSHA calibration parameters assignment by soil characteristic and degree of land development.

Degree of Development	Infiltration (Eq. 4.5)	
	K_s (cm/hr)	Ψ_f (cm)
No Development	0.25	50
Limited Development	0.05	80
Fully Developed	0.05	95

The parameters that varied during the calibration process in GSSHA from the SWMM set of parameters are the overland and channel Manning's roughness coefficients, and the surface

water–groundwater interaction parameters. The values for these parameters in GSSHA are shown in Table 4.4. In the same way as SWMM calibration, the groundwater-surface water interaction parameters' values vary upstream of the roadway due to the difference in groundwater table elevation versus channel elevation. Upstream of the roadway in the secondary branch, the terrain is characterized by hills, and the groundwater table was below the channel throughout the year. Comparing Figure 4.3 with Figure 4.1, the groundwater elevation ranges from 223.5 m near the interstate to 238.5 m in the forested region, whereas the ground elevation ranges from 225 m near the interstate to 360 m in the hillier, forested region. As a result, in the upstream areas, exchange between the channel and aquifer is primarily in the direction of the aquifer, which affects the interaction term's value (Hatch et al., 2010).

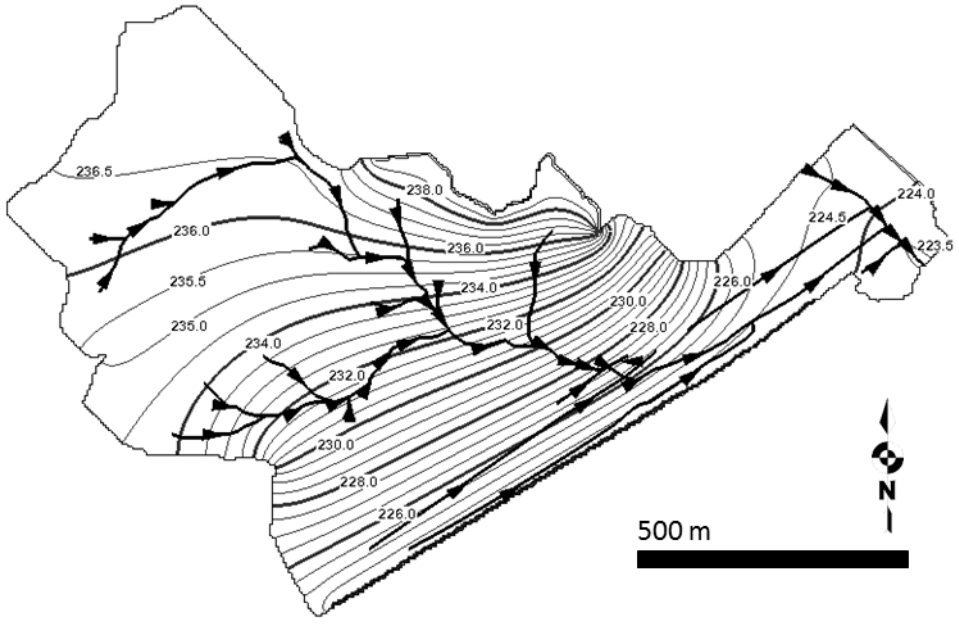

Figure 4.3. Contour map of the initial groundwater table elevation modeled in GSSHA.

Table 4.4. Parameter assignment by land use for GSSHA (showing only the parameters that varied from the SWMM model).

Land use	Manning's Roughness	Groundwater Parameters	
Forested	0.1	K_{rb} (cm/hr)	4
Low-Density Residential	0.08	M_{rb} (cm)	50
Interstate Median	0.05	K_{rb} (cm/hr)	100
Roadway	0.02	M_{rb} (cm)	50

In addition to those shown in Table 4.4, the Manning's roughness coefficient for channel flow varied between SWMM and GSSHA in some regions of the model. In SWMM the coefficient was calibrated to 0.075 for all channels in the interstate median area, and 0.02 upstream from the secondary location. The higher value for the interstate area was used to account for energy loss at roadway crossing culvert inlets and outlets, and channel merging in the interstate median. In GSSHA the coefficient was calibrated to 0.075 throughout the watershed. The calibration of these coefficients achieved runoff hydrographs with similar peak runoff rate and volume compared to measured data, as well as comparable groundwater table fluctuations in terms of head difference and duration.

In addition to the aforementioned parameters, the initial soil moisture conditions were adjusted and calibrated in GSSHA for each storm event considering the preceding storm events, antecedent dry period, and evaporation potential. For events in the summer where rainfall had not occurred for more than 7 days and high daily temperatures allow for excess evaporative potential, the initial moisture was adjusted to or near the wilting point of the soil (0.250). For events in the winter or late fall, where temperatures are low, or if a rain event of at least 20 mm had occurred within 3 days, the initial moisture was adjusted to or near the field capacity (0.387). In GSSHA simulations, a warm-up of 12-hours simulation time was used for each event to allow stream and groundwater conditions to equilibrate. SWMM, on the other hand, was run for two

months per simulation period desired, because SWMM can incorporate a simple daily evaporation value for internal adjustment of moisture conditions (James et al., 2016). Evaporation values in SWMM were taken from data available from the State climate office of North Carolina (2016), which has compiled data from the weather station at the Birmingham municipal airport. Their method for calculating the potential evapotranspiration values is based on the Penman-Monteith combination method using solar radiation, temperature, relative humidity, and wind speed. For example, for September storm events, the SWMM model was run from August 1st to October 1st with daily evaporation estimates for antecedent moisture adjustment.

4.1.3.1 SWMM Calibration Process for the LCC and I-59

Both SWMM and GSSHA are complex hydrological models, and users should have a fundamental understanding of hydrological theory for accurate simulations. New users are recommended to the applications manuals provided by the model developer websites. Because both application manuals detail model setup up to the point of incorporating basic overland processes, infiltration, and channel routing, this discussion will begin after that point in model setup. In this section, calibration of a SWMM model is broken into five steps.

The first step in calibrating the SWMM model of the LCC and I-59 was to choose values to assign for calibration parameters. There are many parameters within SWMM to adjust that affect the simulation accuracy and prediction of surface flow through channels and groundwater table elevations. The following is a list of parameters that were adjusted during calibration of the SWMM model: channel and overland roughness; subcatchment width; Green-Ampt infiltration parameters (K_{sat} and Ψ_f); aquifer K_{sat} and Ψ_f; groundwater parameters A1, A2, B1, and B2;

depression storage; groundwater seepage rate; and channel inlet offset. SWMM has many more parameters that could be adjusted during simulations but were not in this modeling effort, including: subcatchment slope, channel dimensions, other aquifer properties (porosity, hydraulic conductivity slope), percent imperviousness, depth to the bottom of the aquifer, and evapotranspiration rates. During this first step, proper judgement was used to assign values to these parameters, as well as consulting published literature for the ranges of these as used in SWMM and other hydrological models. After values were assigned, the model was run.

The second step in model calibration was to compare modeled data to observed data. The primary focus of most hydrological models in engineering applications is on surface runoff. In this work, the first observed dataset considered for simulation accuracy was the downstream hydrograph. Comparisons between this observed dataset and modeled data for SWMM occur with the node in the model downstream of I-59. Two other sets of observed datasets were the downstream and median groundwater observation wells. These observed datasets were compared to the groundwater table elevation for the subcatchment downstream of I-59 and the median of I-59, respectively. The modeled datasets were exported to an Excel spreadsheet, plotted on the same charts as observed data, and listed at the same time interval as observed data for error calculations.

At this second step of the calibration process, an evaluation of the modeled vs. measured data was performed. During earlier stages of calibration, basic comparisons were made between the datasets for peak flow rate, total volume of surface runoff, and groundwater table elevation rise and drawdown. Then the process moved to step three. However, at later stages of calibration, if the modeled data was within the desired limits of error calculations, then the process moved to

step five, to be discussed after steps three and four. The criteria for calibration error or accuracy is discussed later in this document, in section 4.1.4.

The third step of the SWMM calibration was to identify parameters to adjust in the next model run. If the modeled hydrograph was more spread out over time than measured data, the manning's roughness coefficient was reduced to allow more rapid delivery of surface runoff. If the modeled peak flow rate or total flow volume was low, the Green-Ampt infiltration parameters were altered to reduce infiltration on the surface by reducing K_{sat}. If the groundwater table did not rise in modeled data as much as measured data, the A1 and A2 variables of the groundwater equation were increased. During the calibration process these parameters were adjusted either one at a time, or many during one model run, which leads to the fourth step.

The fourth step of the SWMM calibration process is to consider the interaction between parameters that are being adjusted. Increasing the channel roughness coefficient will primarily delay the stream hydrograph and increase the stream water depth, but secondarily increase the flow of water in the groundwater interaction equation. Decreasing the overland roughness coefficient will primarily increase overland flow velocity, but also secondarily decrease total infiltration and increase surface runoff. Although the parameters are defined and bound within the solution of separate equations, in the SWMM computational setup these parameters often affect the solution of other equations. During this fourth step of the calibration process, other parameters were identified that balanced the secondary influence of the intended primary changes. After this step, the process was repeated going back to step one, choosing the values for calibration parameters.

As an alternative pathway between step two and three, if the modeled and measured data are within desired limits of error associated with all of the datasets, the fifth step of calibration

was to choose another rain event for simulation. If the previous simulation was focused on a high-intensity rain event, then the next simulation focused on a low-intensity event. Alternatively, if the previous simulation was focused on an event following a relative drought with many antecedent dry days, the next simulation focused on an event with fewer antecedent dry days. Using the existing calibrated parameters, the SWMM model was run, and the process returned to step two.

Because SWMM was run with evapotranspiration estimates for soil moisture accounting between rain events, a single model run of SWMM can contain the solution for all of the events during the calibration period. During later stages of calibration, when the calibrated parameters were more finely adjusted, all of the calibration events were compared against measured data during each model run and parameter adjustment. For simplicity, a flow chart of this process is presented in Figure 4.4. In this chart, the main pathway was as follows: 1) choose the values for calibration parameters and run the model; 2) compare datasets and determine model error; 3) identify the parameters to adjust; and 4) consider what interaction those parameters may have with others, and repeat the process until the modeled data error is low. The alternative pathway was to evaluate the calibration parameters for other rain events and repeat the process until the model cannot be improved by parameter calibration any further.

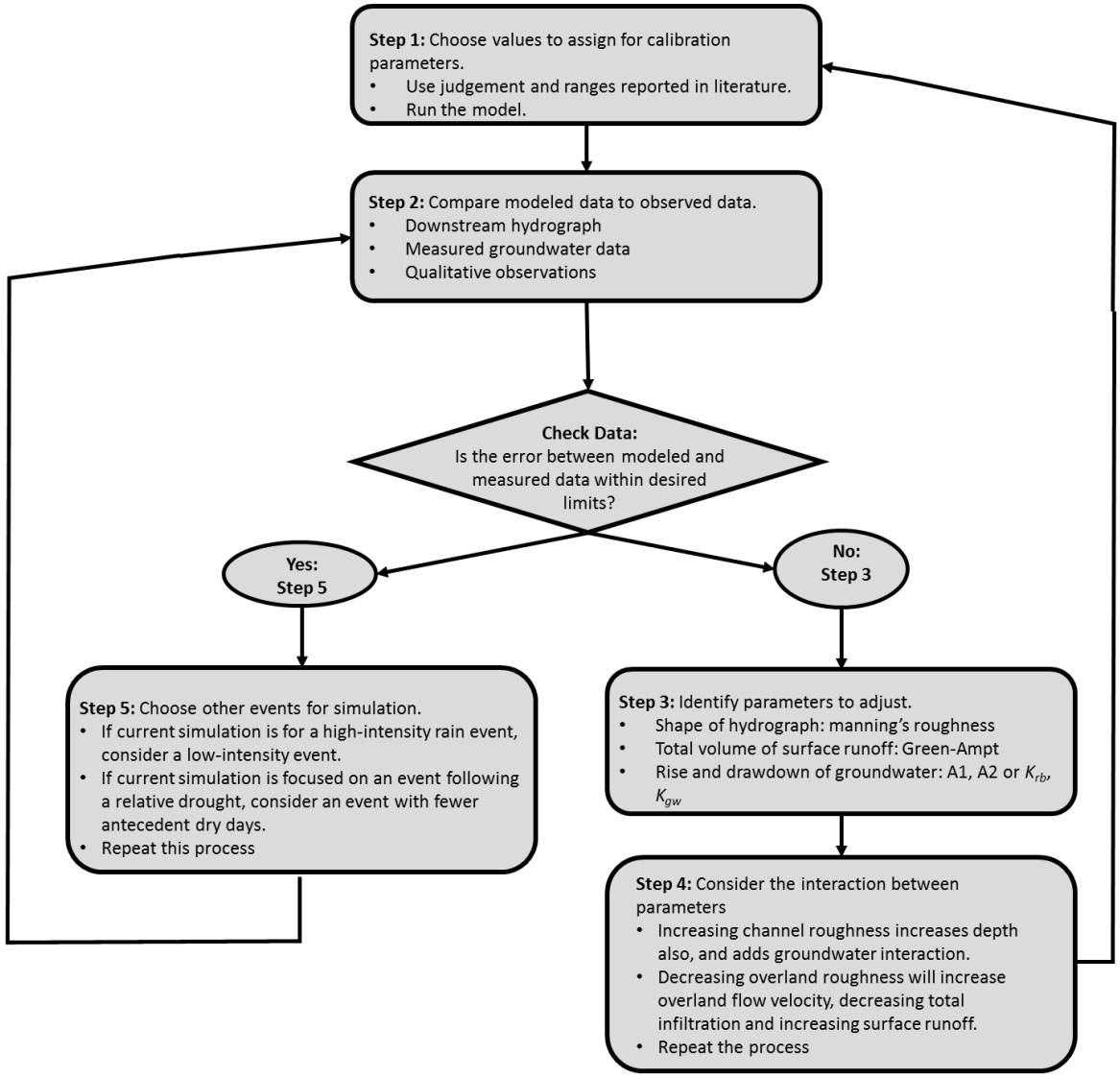

Figure 4.4. Flow chart of the calibration process for SWMM and GSSHA.

4.1.3.2 GSSHA Calibration Process for the LCC and I-59

The method of calibration for GSSHA followed the same pathway as SWMM shown in Figure 4.4, though the selection and adjustment of calibration parameters was different. The first step of GSSHA model calibration was to choose values to assign to the calibration parameters. The parameters adjusted during calibration of the GSSHA model were as follows: overland and channel roughness; retention (depression) storage; Green-Ampt infiltration parameters K_{sat} and

Ψ_f; groundwater hydraulic conductivity and porosity (K_{gw} and θ_{gw}); surface-groundwater interaction parameters K_{rb} and M_{rb}; channel node elevations; and initial soil moisture content.

In the second step of GSSHA model calibration, modeled data was compared to measured data to assess errors in peak flow rate, total runoff volume, and groundwater rise and drawdown. If the model was not accurately simulating these observed datasets, evaluated graphically and according to the criteria shown in section 4.1.4, the process continued to step three. The observed downstream flow rate was compared with modeled data from the first channel node downstream of I-59. The observed downstream and median groundwater table elevation was compared with modeled data from the solution cell closest to their physical locations.

The third step of GSSHA model calibration was to identify which parameters to adjust for better simulation accuracy. Some of these parameters are the same as for SWMM and will not be repeated here, including roughness coefficients and Green-Ampt infiltration parameters. One of the most important parameters in GSSHA for this work was the initial soil moisture content, and required the most consideration for each event simulated, since long-term simulations were not performed. The groundwater parameters K_{gw} and θ_{gw} was uniformly applied throughout the domain, and were adjusted primarily to attain the appropriate modeled data for the median groundwater table elevation, because the modeled data point was located further from the stream, and the propagation of the groundwater response affected that solution point more than others. Groundwater rise and drawdown at the downstream site, on the other hand, was more strongly tied to the groundwater interaction terms K_{rb} and M_{rb}, so these were identified when adjustments were required for that solution dataset.

The fourth step of model calibration, which was the consideration of interactions between multiple parameters, was more important for GSSHA than SWMM. This was because the computational time for GSSHA was much longer than SWMM, and it was infeasible to consider always changing one parameter at a time and repeating the process. Similar parameter interactions occur within GSSHA as SWMM, with the addition that increasing K_{rb} will secondarily increase the propagation of groundwater table variations associated with K_{gw}. After considering which parameters to adjust and the impact that those parameter adjustments will have on other parameters and solutions, the process is repeated by returning to step one.

The alternative pathway between step two and three for model calibration in GSSHA was performed when the error between modeled and measured data was relatively low, and the simulation of other rain events was performed with the existing calibration parameter set. Because GSSHA model simulations were performed for single events, this step was performed many times, often repetitively. For example, once the calibration parameter set for the high-intensity rain event of 9/12/2014 achieved low errors, the event on 11/16/2014 was run with the same parameters. Then steps one through four were performed until the adjustment of parameters yielded a modeled dataset close to the observed dataset. Then, the previously simulated 9/12/2014 event was simulated again with the newer calibrated parameter set and compared to measured data. This process continued, with multiple simulation events, until the model could not be improved by parameter adjustment any further.

4.1.3.3 Sensitivity Analysis

Sensitivity analysis is the identification of which parameters affect the model solution more than others. It was an especially important process for this work due to the complex nature

of the two hydrological models used. During the model setup of both SWMM and GSSHA, sensitivity analysis was performed before model calibration to determine which parameters would be focused on for adjustment to yield accurate solutions.

In this work, SWMM parameters that most largely affected the solution results were: depression storage, Green-Ampt hydraulic conductivity, A1, A2, B1, B2, overland and channel roughness, subcatchment width, and channel inlet offset (where applicable). GSSHA parameters affecting the simulation accuracy are similar: initial moisture, retention (depression) storage, Green-Ampt hydraulic conductivity, K_{gw} and θ_{gw}, K_{rb} and M_{rb}, overland and channel roughness, and channel elevation. Depression storage affects primarily the onset of surface runoff, as it reduces the overland depth in the depth-discharge equation for surface runoff. The hydraulic conductivity strongly affects the solution of surface runoff as larger values allow for more rapid infiltration into the subsurface, reducing surface runoff greatly. Overland and channel roughness affected the shape of the downstream hydrograph by spreading out the stream flow over time for high values of *n*, or by producing more rapid and larger peak runoff for low values of *n*.

There are some parameters unique to SWMM in regards to parameter sensitivity. The subcatchment width is tied to the overland roughness, as they have an inverse relationship in the depth-discharge equation for surface runoff. A smaller value for the width will allow the overland flow to remain on the surface for longer simulation time before discharging to the outlet point, which is can also be produced by a larger value of overland roughness. Large values of A1 and B1 led to rapid groundwater table rise, and reduced surface runoff; on the other hand, high values of A2 and B2 led to faster drawdown of the groundwater table and a more pronounced recession curve of the surface water hydrograph. These parameters are also pointed out by the user manuals (James et al., 2016) as parameters that greatly affect the solution results and

accuracy. One parameter that lead to large differences in the solution determined in the parameter sensitivity portion of this work that was not stated as clearly in the user manual was the channel inlet or outlet offset. By creating an offset, the user is able to effectively create a pool of water in the open channel simulation at one end of a channel conduit, which stores surface runoff and interacts with the aquifer solution. If this storage area exists in the open channel flow of the modeled area, as it does in the LCC in a few locations, then it should be recreated in the model. In adding this channel offset, groundwater interactions with the channel were better defined for a static elevation.

Parameters that greatly affected GSSHA simulation results are similar to SWMM parameters for equation sets that describe the same process or use the same fundamental equations to describe the flow of water through the domain. Initial moisture was by far the parameter that affected surface runoff the most, as larger values of initial moisture reduce the infiltration capacity of the soil, producing large amounts of surface runoff, and low values of initial moisture allow the soil to capture large volumes of precipitation. This was most pronounced in low-intensity rainfall simulations, where the rate of precipitation was closer to the rate of maximum infiltration rate. Additionally, the four parameters responsible for groundwater movement, K_{rb}, M_{rb}, K_{gw} and θ_{gw}, greatly affected groundwater results. K_{gw} and θ_{gw} affected primarily the groundwater results away from the stream channel, and the propagation of the bank storage effect. K_{rb} and M_{rb} produced more pronounced effects near the stream channels, but also the surrounding regions of the groundwater solution. As well, these latter two parameters affected to a small degree the channel flow, as very large values of K_{rb} reduced surface runoff by introducing surface water into the subsurface. Similar to the SWMM solution of surface runoff, editing the channel elevations produces in some regions adverse slopes, which retains water in

the channels. This allows the storage of surface runoff as well as stabilizes the connected groundwater solutions to a particular elevation, fixed by the elevation of the free surface in the channel. The determination of these parameters for simulation accuracy agrees with the user's manual (Downer and Ogden, 2002).

Some parameters did not affect the solution as much as the above mentioned parameters in the downstream flow rate and groundwater table elevations by the processes described here. This includes Green-Ampt suction head, impervious routing, hydraulic conductivity slope, and the choice of fully dynamic vs. diffusive wave approximation (in SWMM). In this work, parameters such as the hydraulic conductivity slope in SWMM were set as the values recommended in the user manual. Although the suction head did not affect the simulation accuracy as much as other parameters, it was still adjusted during calibration alongside the hydraulic conductivity in the Green-Ampt infiltration setup. This was performed primarily because soils that have a low hydraulic conductivity (such as clay) also have a larger suction head, and those that have high hydraulic conductivity (such as sand) have a smaller suction head. In calibration, when the hydraulic conductivity was reduced, the suction head was increased in proportion with published values, and vice versa.

One aspect of the GSSHA simulation that greatly affected the simulation accuracy was an overland backwater option in channel routing. In application, this option simulates the effect of a floodplain on surface water routing during flood events. However, during this work, this option created unrealistic ponding on the overland area, and water did not return to the channel. After multiple unsuccessful attempts at resolving this issue, this option was turned off for all simulations.

4.1.4 Criteria for Calibration and Validation Assessment

As introduced earlier, four criteria were selected for calibration and error analysis: peak flow rate, total runoff volume, event groundwater table increase, and post-event groundwater table drawdown. Event groundwater table increase was calculated as:

$$\Delta H = H_{max} - H_{min} \quad \text{(Eq. 4.13)}$$

Where ΔH is the groundwater head increase (m), H_{max} is the maximum measured or reported head (m), and H_{min} is the minimum measured or reported head (m) during the time interval shown, which corresponds to the storm event response. Error analysis in this work follows the recommendations of the ASCE task committee (ASCE, 1993; and references therein), particularly those recommended for discrete event simulation.

Following the ASCE (1993) notation, the peak flow rate and groundwater head increase errors for SWMM and GSSHA were evaluated as follows:

$$PEP = \frac{Q_{ps} - Q_{pm}}{Q_m} \quad \text{(Eq. 4.14)}$$

$$R^2 = 1 - \frac{\sum_{i=1}^{n}[Q_m(t) - Q_s(t)]^2}{\sum_{i=1}^{n}[Q_m(t) - Q_{ave}]^2} \quad \text{(Eq. 4.15)}$$

$$TSAR = \sum_{i=1}^{n}[Q_m(t) - Q_s(t)] \quad \text{(Eq. 4.16)}$$

$$G = \sum_{i=1}^{n}[Q_m(t) - Q_s(t)]^2 \quad \text{(Eq. 4.17)}$$

Where *PEP* is the percent error of peak flow rate, Q_{ps} is the simulated peak flow rate, Q_{pm} is the measured peak flow rate. R^2 is the Nash-Sutcliffe coefficient, $Q_m(t)$ is the measured flow rate at

time *t*, $Q_s(t)$ is the simulated flow rate at time *t*, Q_{ave} is the average yearly flow rate (m^3/s for all flow rates), and n is the number of data points in measurement and simulation. *TSAR* is the total sum of absolute residuals of flow rates. *G* is the sum of squares of the flow rate residuals for hydrograph shape assessment proposed by the ASCE task committee. A special case of this criteria, *G*, was used to evaluate the drawdown of groundwater modeled:

$$G_{gw} = \frac{\sum_{i=1}^{n}[H_m(t) - H_s(t)]^2}{N} \quad \text{(Eq. 4.18)}$$

Where G_{gw} is the drawdown curve error metric, $H_m(t)$ and $H_s(t)$is the measured and simulated, respectively, groundwater elevation (m) at each time interval, and *N* is total the number of measurements involved in the error calculation. This addition of dividing the sum of squares by the total number of measurements was added because each event discussed has a different time scale of groundwater response, and this addition normalizes the error metric.

4.2 Results

4.2.1 Modeled and Measured Data

Figure 4.5 shows streamflow and rainfall measured for one year upstream and downstream of I-59. Rainfall data was missing for March 26th through May 7th 2015 due to sensor malfunction. Groundwater table elevations at three sites were measured and are shown in Figure 4.6. Groundwater data in the interstate median is missing during some portions of September and October, 2014, because the groundwater table was below the observation well. Timing of groundwater head variations suggests that the groundwater table at the upstream and downstream sections was strongly tied to the stream head. The groundwater levels in the interstate median, however, increased before the stream during a rain event, which indicates that groundwater levels in the median were more strongly tied to infiltration of stormwater.

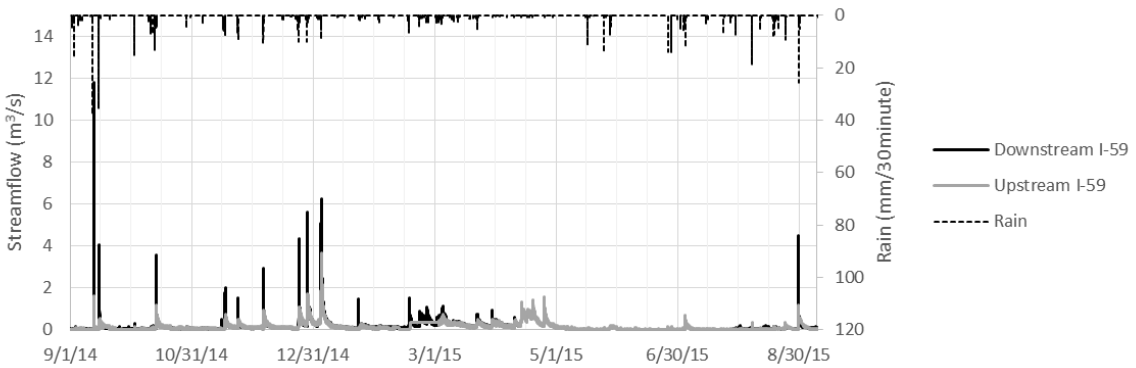

Figure 4.5. Rainfall and streamflow at the upstream and downstream stations for one year of the study.

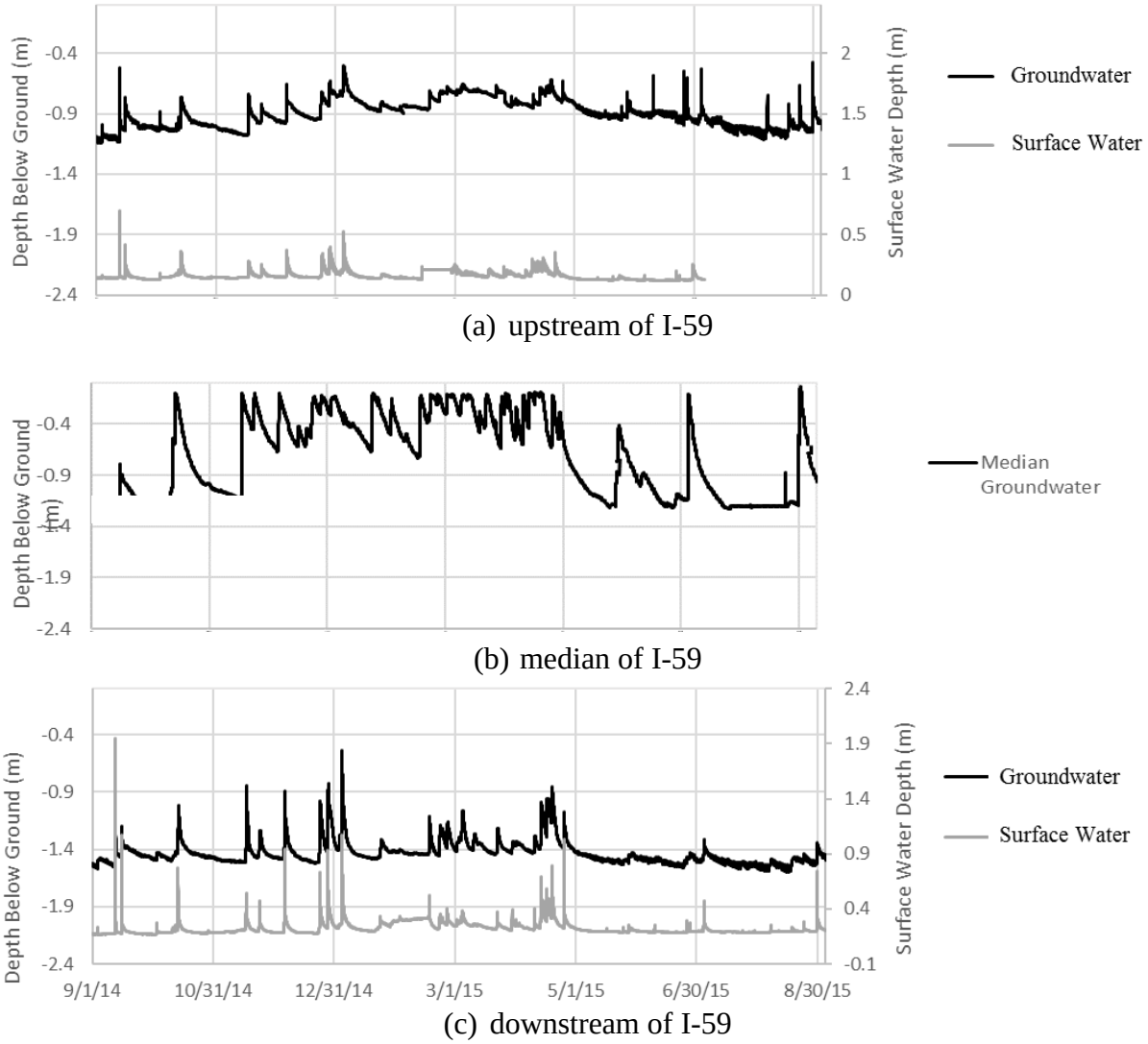

(a) upstream of I-59

(b) median of I-59

(c) downstream of I-59

Figure 4.6. Groundwater table and surface water head at the upstream, median, and downstream sites of the main brain of the LCC as it crosses over I-59 (see Figure 4.1 for locations).

The difference between these sites may also be due to proximity of the wells to the stream channel. The upstream and downstream groundwater monitoring wells were located 5 m from the stream margins, whereas the median groundwater monitoring well was located further away, 20 m from the stream.

Throughout the year at the research location some rain events produce high levels of surface runoff through the channels (i.e., 09/12/14). Other rainfall events produce little or no measured runoff, and were likely captured by infiltration, evaporation, or other sources of abstraction (i.e., 10/13/14). Figure 4.7 contains four of these events showing more clearly the measured streamflow and rainfall distribution, as well as modeled data from the calibration dataset. These hydrographs show that both SWMM and GSSHA are capable of qualitatively reproducing surface runoff rates for medium and strong rain events. The measured upstream flow rates are included in each hydrograph because this data was used as an input upstream boundary condition at that point in the channel. This was a simplification, in that there may exist effects of groundwater fluctuations, which were neglected in the modeled boundary condition at the upstream site. However, modeled results compare relatively well with measured streamflow rates, so it was assumed that this approach was a reasonable representation.

Groundwater levels in the median and downstream of the roadway for the calibration events previously discussed are shown in Figure 4.8. Upstream groundwater levels are not presented here because the measured groundwater levels correspond to an area outside of the boundaries of the numerical model setup; rather, groundwater elevations are compared for both the median of I-59 and the location downstream of the roadway. Also, measured data was compared against the modeled data from SWMM and GSSHA at the representative locations.

One aspect of the groundwater table that stands out is the complexity of groundwater within the interstate median. The groundwater table was below the observation well during the event of 9/12/14, and rises to a measurable level during the 9/15/14 event. The elevation of the groundwater table before that rain event is unknown. Thus, during hot and dry periods, like that experienced in early September, the groundwater table can be much lower than other times of the year in the roadway median. Compare this to the downstream location, which does not vary as much seasonally, although it was only 75 m away from the median observation well. During the summer of 2014, there were no significantly large storms to produce any runoff up to 2 months before 9/12/14. The most recent small rain event was 10 days before this event, producing 16 mm of rain with no measurable surface runoff or groundwater variation.

The late fall, on the other hand, can be a very wet period in this location. During low intensity rain events, such as the ones shown for 10/13/14 or 11/16/14, it was observed that significant rises in the groundwater table led to surface soil saturation lasting for days after the event. This was due to the large volume of rain, up to 85 mm on 11/16/14, distributed over a longer period with a maximum rate of 12 mm / 30 minutes. During these large volume, low intensity events, the soil was capable of infiltrating larger fractions of total precipitation and retaining it for long periods of time, particularly within the interstate median. Attempts to model this groundwater response were unsuccessful, in part because neither program can precisely model the vadose zone and capillary pressure forces using the Green-Ampt equation. It is speculated that if Richard's infiltration equation were used, perhaps this feature could be better modeled with GSSHA, but that approach was not attempted since SWMM does not have this feature, and a direct model comparison would be compromised.

Measured groundwater table levels near the stream indicate that the natural process of stream bank storage was an important hydrological process in this location during and after rain events. Since groundwater levels were close to the surface at this location, exchange between surface water and groundwater occurred continuously. The ground surface elevations were 224.9 and 225.1 m for the median and downstream sites, respectively. The process of bank storage occurs when stream or river levels increase above the head of groundwater, and flow occurs towards the aquifer. When the stream or river levels decrease below the groundwater levels, flow occurs towards the channel. Thus, during high flows associated with rain events, water may be temporarily stored in the near-stream aquifer leading to lengthy flow recession periods (for more detail, see Hantush et al., 2011).

In addition to bank storage, there is a complicated relationship between rainfall and groundwater levels within the median of the interstate. For some rain events, in conditions where rain events occurred 1 to 3 days beforehand, rainfall conveyed to the median created a large increase in groundwater head. For example, the data for events on 10/14/2014 and 11/16/2014 show an increase in groundwater head up to the ground surface (224.9 m) that preceded stream level rise. Additionally, soil moisture was retained in this area much longer than the other two sites of this study. Since this setting violates the assumptions of the simplified Green-Ampt equation, there is severe difficulties in attempting to represent these conditions at the interstate median with the developed models.

In addition to the four events used in calibration discussed above, SWMM and GSSHA were run for a group of rain events to assess the validation of the model. These events are shown in Figure 4.9, from 7/23/13, 8/1/13, 8/4/13, and 4/6/14 from the previous year of data measurement. During this time, the groundwater observation wells were not yet installed; there

was no observed data to compare the groundwater simulations for these events. These events show comparable surface runoff rates to the observed data, though the models produce the downstream runoff earlier than the measured data indicates.

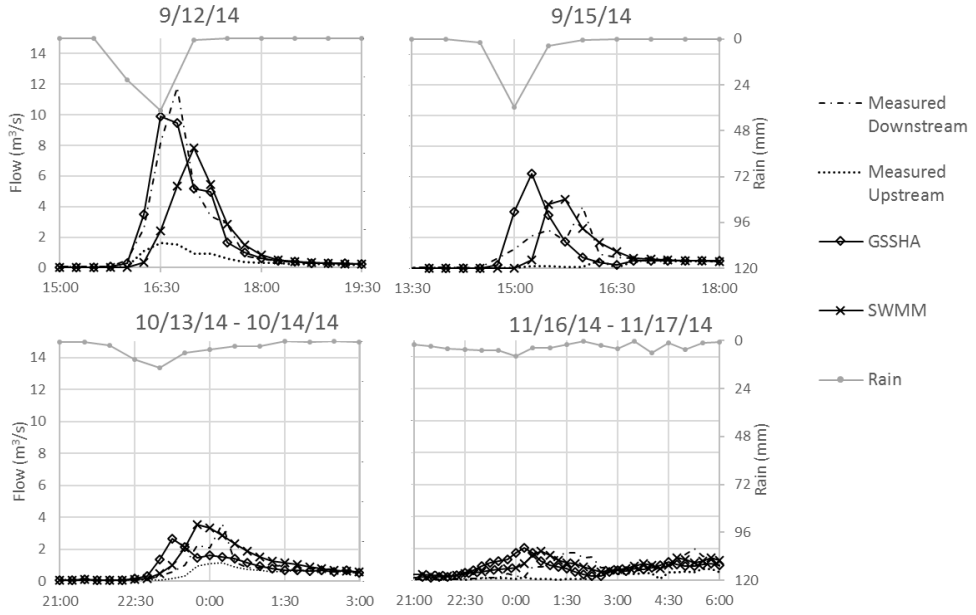

Figure 4.7. Stream flow hydrographs of selected rain events, with measured and modeled results.

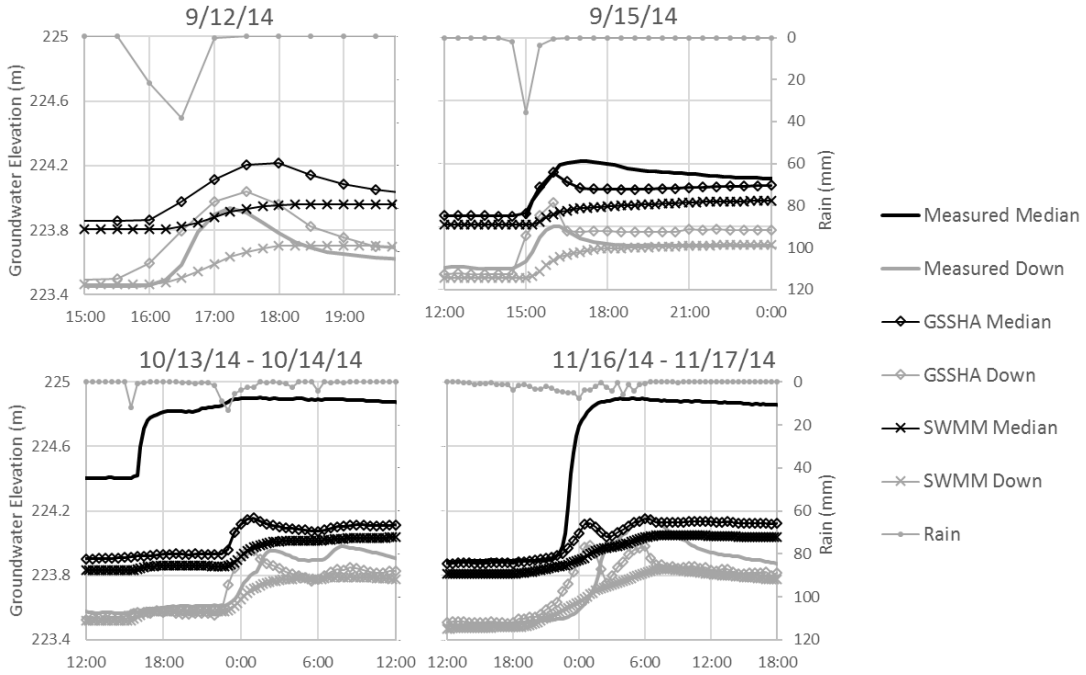

Figure 4.8. Groundwater measurements and modeled data in the interstate median and downstream of the roadway.

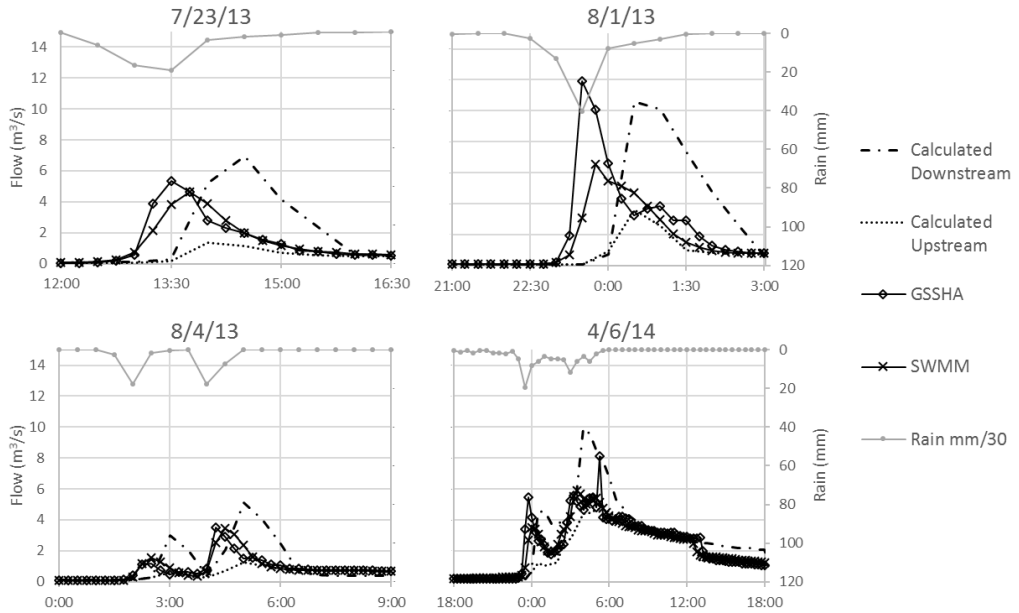

(a) modeled and measured stream flow results

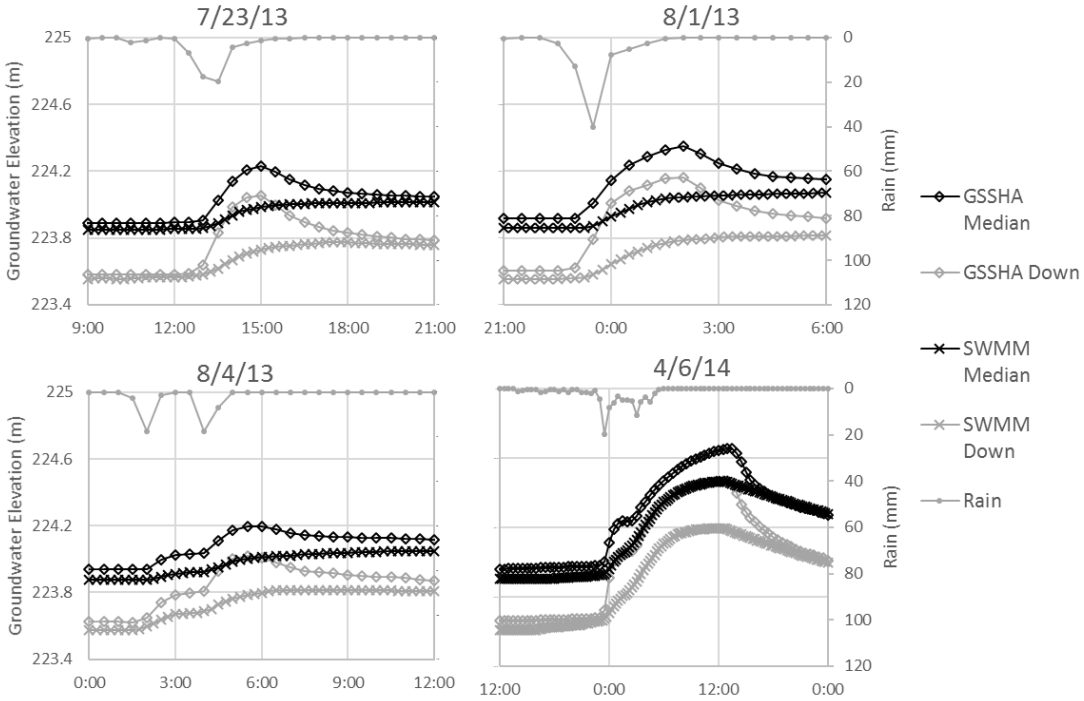

(b) modeled groundwater results

Figure 4.9. Modeled and measured data for the validation events.

4.2.2 Calibration and Validation Assessment

Error analysis of the calibrated SWMM and GSSHA models was conducted to determine how well the modeled data compared with measured data. Table 4.5 shows the measured and simulated data for the selected four storm events presented in this paper, which constitute the calibration dataset. Table 4.6 shows the error analysis statistics, including composite statistics for all 4 events. These composites are the total sum of each event per model for the *G*, *TSAR*, and G_{gw} error statistics, or the average value for each model of the *PEP*, R^2, and *PEH* error statistics.

Table 4.5. Measured and simulated streamflow and groundwater data from calibration set.

		Peak Flow Rate (m^3/s)	Total Flow Volume (m^3)	Head Increase Median (m)	Head Increase Down. (m)
9/12/2014	Measured	11.81	34,222	-	0.49
	GSSHA	9.90	34,771	0.36	0.56
	SWMM	7.86	25,864	0.39	0.24
9/15/2014	Measured	4.05	16,403	0.37	0.27
	GSSHA	6.19	17,759	0.28	0.45
	SWMM	4.51	16,270	0.16	0.22
10/14/2014	Measured	3.59	17,644	0.50	0.41
	GSSHA	2.65	18,741	0.28	0.48
	SWMM	3.54	24,535	0.20	0.27
11/16/2014	Measured	1.99	33,824	1.02	0.67
	GSSHA	1.75	26,558	0.28	0.51
	SWMM	2.66	28,797	0.43	0.37

For each event shown, data in the error analysis includes the total event time shown in each graph from Figures 4.6 and 4.7 (i.e., for the event on 9/15/14 flow and volume data are from 13:30 to 18:00 and groundwater data are from 12:00 to 24:00). This was done to focus on event based statistics that are relevant to the criteria measured. Timing of the surface runoff hydrograph is one aspect addressed in ASCE (1993). It is recommended to use a time-shift to reduce the error calculations, however the committee report urged that this be justified. It is clear from the hydrographs and groundwater figures above that the simulated response was not always

coincident with the measured watershed response. However, the cause for this discrepancy was not known by the author, and no effort to reduce errors by time-shifting the data was done.

Due to the timing differences in the modeled and measured hydrographs, the *G* and R^2 error metrics from Tables 4.5 and 4.6 indicate a worse fit than if the data were time-shifted. The *PEP* and *TSAR* error metrics from the validation dataset are in a similar range as the calibration data for these events; these two error metrics are not as time-dependent as the others. That these error metrics are similar to the calibration dataset indicates that the models are representing the peak runoff and shape of the hydrograph of these validation events as well as the calibration set. It is clear, however, that the calibrated parameters and processes used in this study do not represent as well the timing of surface runoff, and coincidently the groundwater table response.

Since the infiltration parameters are the same for both of these models, it is expected that SWMM and GSSHA produce approximately the same amount of overland runoff, even though the two programs implement the governing equations differently. Comparing the peak runoff rates, total runoff volumes and groundwater table elevation changes from Tables 4.4 and 4.6, the two models produce different results for these calculations. Both models represented peak flow rates reasonably well, although the variations seem significant. The total flow volumes for these events were in general better represented by GSSHA.

Groundwater table elevation change for the median site had much larger errors from both models (*PEH* and G_{gw}) than the downstream site. Errors are not presented for the median on 9/12/2014 because the groundwater table was below the observation well at that time, and remained below it until 15:00 on 9/15/2014.The high variability of groundwater elevation in the interstate median was not likely tied to the stream-groundwater interactions primarily modeled

here. The downstream groundwater table elevations were much better represented by this interaction, and errors were much lower for both models.

Table 4.6. Error analysis of streamflow and groundwater data.

Dates	Model	Channel Flow Rate Error				Groundwater Error			
		PEP[1]	R^2 [2]	***G***[3] (m^3/s)	***TSAR***[4] (m^3/s)	***PEH***[5] Median	PEH[5] Down.	G_{gw}[6] Median	G_{gw}[6] Down.
9/12/2014	GSSHA	-16.2%	0.95	13.1	-0.61	-	15.6%	-	0.0116
	SWMM	-33.4%	0.62	91.3	9.29	-	-50.6%	-	0.0162
9/15/2014	GSSHA	53.0%	-0.12	35.3	-1.92	-24.3%	65.8%	0.0077	0.0074
	SWMM	11.5%	0.42	17.3	-0.26	-54.9%	-19.6%	0.0354	0.0066
10/14/2014	GSSHA	-26.2%	-0.16	12.1	-1.22	-43.3%	15.0%	0.6017	0.0085
	SWMM	-1.2%	0.67	8.5	-7.66	-59.2%	-34.4%	0.7407	0.0120
11/16/2014	GSSHA	-11.9%	0.24	18.6	-3.92	-72.3%	-24.3%	0.3537	0.0206
	SWMM	33.8%	0.68	7.7	-4.11	-58.3%	-45.3%	0.4529	0.0249
Total OR Average	GSSHA	-0.3%	0.23	79.1[7]	-7.67	-46.6%	18.0%	0.9632	0.0481
	SWMM	2.7%	0.60	124.8[7]	-2.75	-57.5%	-37.5%	1.2290	0.0597

Note: [1]*PEP* = Percent Error Peak flow; [2]R^2 = Nash-Sutcliffe coefficient; [3]*G* = sum of squares of residuals of streamflow; [4]*TSAR* = Total Sum of Absolute Residuals of streamflow; [6]*PEH* = Percent Error of groundwater Head; G_{gw} = sum of squares of residuals of groundwater head. *PEP*, R^2, and *PEH* are averaged on the bottom rows; *G*, *TSAR*, and G_{gw} are totaled on the bottom rows. [7]When *G* is summed, it becomes the *TSSR* = Total Sum of Squared Residuals.

Table 4.7. Groundwater and streamflow data, with error analysis of streamflow data for validation events.

Dates	Model	Peak Flow Rate (m^3/s)	Total Flow Volume (m^3)	Head Increase Median (m)	Head Increase Down. (m)	***PEP***	R^2	***G*** (m^3/s)	***TSAR*** (m^3/s)
7/23/2013	Measured	7.27	36,935	-	-				
	GSSHA	5.36	26,954	0.36	0.50	-26.3%	0.17	79.6	-0.81
	SWMM	4.65	26,038	0.16	0.23	-36.1%	0.30	66.6	-2.18
8/1/2013	Measured	11.67	70,663	-	-				
	GSSHA	11.90	53,544	0.48	0.61	2.0%	-0.01	335.0	-4.87
	SWMM	6.52	38,621	0.23	0.28	-44.1%	0.25	249.2	-6.17
8/4/2013	Measured	5.11	22,219	-	-				
	GSSHA	3.49	17,823	0.32	0.47	-31.8%	0.40	35.7	4.88
	SWMM	3.44	18,607	0.18	0.23	-32.6%	0.42	34.5	4.01
4/7/2014	Measured	9.93	131,793	-	-				
	GSSHA	6.64	104,993	0.78	0.92	-34.9%	0.82	125.6	29.78
	SWMM	5.77	101,885	0.90	0.59	-41.8%	0.85	105.3	33.24
Total or Average					**GSSHA**	**-22.7%**	**0.35**	**575.9**	**28.99**
					SWMM	**-38.7%**	**0.46**	**455.7**	**28.90**

SWMM consistently modeled a groundwater head increase lower than measured data; this is primarily because SWMM calculates a uniform water table depth for each subcatchment. Modeled GSSHA groundwater head change had smaller errors for 3 out of the 4 events shown here, but the G_{gw} errors for the downstream locations were similar between SWMM and GSSHA. This indicates that in the context of this study, both models represent the longer time-scale drawdown of groundwater in response to a storm event within a similar accuracy. However, the GSSHA simulation reproduces more accurately the initial change in groundwater head than SWMM. In addition to the error analysis defined above, mass balance calculations for event based precipitation, infiltration loss, and surface runoff are presented in Table 4.8. The ratio of rainfall to infiltration indicates that both models are consistent with one another in the overland processes.

Table 4.8. Mass balance summary of rainfall, infiltration, and runoff volumes for both SWMM and GSSHA calibration dataset.

Dates	Model	Total Precipitation (m^3)	Infiltration Loss (m^3)	Surface Runoff (m^3)	Rainfall / Infiltration
9/12/14 to 9/15/14	SWMM	89,564	48,003	40,822	0.54
	GSSHA	89,564	43,891	45,617	0.49
10/13/14 to 10/14/14	SWMM	53,782	43,342	9,778	0.81
	GSSHA	53,783	40,813	12,942	0.76
11/16/14 to 11/17/14	SWMM	74,228	51,745	22,185	0.70
	GSSHA	74,229	48,316	25,874	0.65

SWMM and GSSHA can be applied to model situations where bank storage significantly affects groundwater and stream levels. However, the formulation of the groundwater representation for these two models is very different, and is a key focus of the next section.

4.2.3 Evaluating Effects of Groundwater Formulation between SWMM & GSSHA

One of the most distinct differences between SWMM and GSSHA noticed in the present work was the difference in the representation of groundwater. In SWMM, the flow between the groundwater and surface water is functionally defined by the depth of the surface water versus

the elevation of the groundwater (Eq. 4.11). Comparing the results from measured data and SWMM modeled data for groundwater near the stream boundary is relatively difficult due to this averaged groundwater elevation. The measured data represents a known groundwater elevation at a specific point, whereas the SWMM solution is an average over the whole subcatchment. Thus, attempting to calibrate the groundwater-surface water interaction equation to match the observed data may lead to an erroneous representation of the average groundwater surface elevation in this situation.

In GSSHA, the propagation of a locally increased water table can be seen and felt at multiple locations due to the discretization of the model. This would be the case at the boundary of a stream or river. Comparison between the elevations of the groundwater surface in measured data vs. modeled data can be done by specifying a cell that is in the location of the measured data. Resulting groundwater elevations from these calculations are represented in Figure 4.10.

During the rain event on 10/13 to 10/14/2014 (61.5 mm total precipitation, max intensity of 19 mm/hr), stream levels rose, as shown in Figure 4.10(c), from 0.2 to 0.8 m and the falling limb of the hydrograph had a typical recession curve. During that event, the local groundwater table rose from 223.6 to 224 m, a rise of 0.4 m, near the stream bank boundary. Modeled results from SWMM and GSSHA were of a similar magnitude and have a similar duration of response after calibration. The modeled data point (in GSSHA) closest to the measured data was the cell 15 m from the center of the stream. Figure 4.10(a) shows the variation of the groundwater surface at points 0, 15, 30, and 45 m from the center of the stream at the downstream location. Figure 4.10(b) shows the solution of the SWMM groundwater table for the corresponding subcatchment.

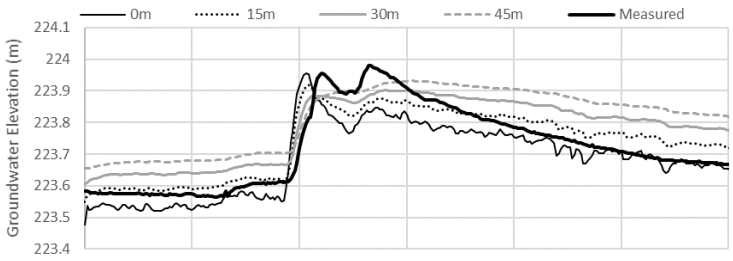

(a) groundwater measurements vs. GSSHA modeled results

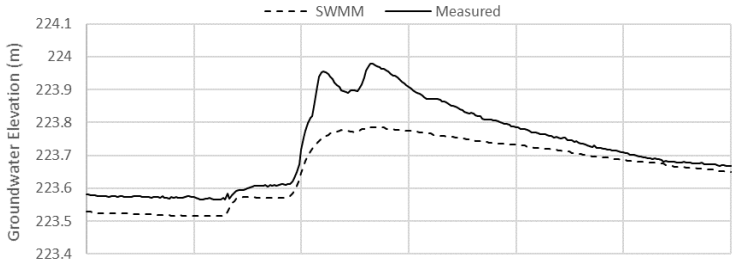

(b) groundwater measurements vs. SWMM modeled results

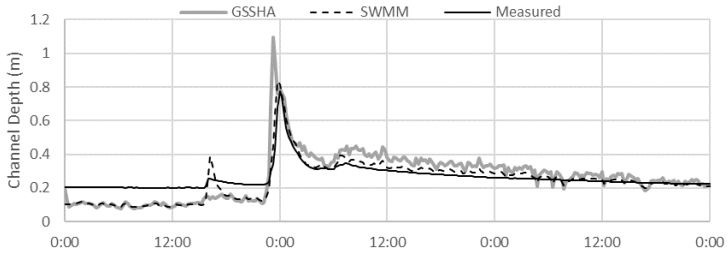

(c) measured stream depths vs. both SWMM and GSSHA results

Figure 4.10. Groundwater results from the downstream site location for 10/13 to 10/16.

The differences in groundwater modeling are significant in respect to the local variations occurring due to interactions with the stream. Both SWMM and GSSHA model the stream level rise occurring during the rain event previously mentioned fairly well. The groundwater levels in the surrounding region increased in response to the stream head, as seen in the measured data. However, the groundwater table further from the stream did not usually respond as quickly or as much as at near-stream locations. Therefore, the average groundwater table elevation fluctuation should be less than the near-stream well measurements presented here. This is the approach SWMM uses to model the groundwater, as the spatial average elevation of the water table. Calibration of the groundwater-interaction equation parameters should reflect this difference.

However, this approach of SWMM can be considered a simplified approximation of the groundwater table, which would be more applicable if the water table were relatively flat, with very little variation within and between subcatchments. In some situations, the water table should vary considerably within subcatchments, such as local variations at the stream bank interface or changes created by discontinuities in grade elevation (e.g. road medians). An advantage GSSHA offers is the ability to consider a groundwater table with varying elevations at each point in the solution domain, and interactions between neighboring cells. As is the case in Figure 4.10, the groundwater response to sudden rise of stream level can be modeled to show rapid and large variations near the stream, and a delay with increasing distance from the stream.

In this case, GSSHA offers a more realistic solution for the groundwater table than the SWMM solution, but the computational requirements for GSSHA are more intense than SWMM. For the spatial domain and setup discussed in this paper, SWMM ran calculations for an entire year of simulation in approximately 5 minutes, whereas GSSHA ran calculations for 1 day of simulation in about 5 minutes. In situations where this variation in the groundwater table is not a significant portion of the hydrological system, the reduced computational time of SWMM may be of more benefit for the hydrologic modeler.

4.2.4 Impact of Roadway Imperviousness and Soil Compaction

One of the benefits of using SWMM over GSSHA is the reduced computational time, and thus it can be run for much longer simulation times. SWMM is commonly used to simulate pre- and post-construction scenarios, which would often include at least a year of simulation to capture the varying effects of seasonality trends in rainfall and evapotranspiration. To quantify the impact of I-59 on the LCC, a year of simulations for pre- and post-construction scenarios of I-59

was run in SWMM. Due to data and computational requirements, this was not feasible with GSSHA. The calibrated model, as setup and discussed in section 4.1.3 and 4.2.2, was considered the post-construction (or current) conditions of the LCC watershed. The pre-construction model was developed by changing the model parameters of the roadway area to the calibrated values from the forested regions. The following parameters were altered, and were equal to the forested land use values in Table 4.2 and 4.3: Manning's overland roughness (not channel); depression storage; and infiltration parameters (K_{sat} and Ψ_f). Also, the impervious area was reduced to 5%. Groundwater and channel routing parameters were unchanged. Figure 4.11(a) shows the SWMM results at the downstream site for streamflow under the pre- and post-construction scenarios.

For the pre-construction scenario, the majority of runoff events would have lower peak runoff rates than the post-construction scenario. Figure 4.11(b) shows the contributions of the roadway relative to pre-construction estimates, created by subtracting the pre-construction runoff estimate from the post-construction runoff. This results in the absolute difference in runoff from the two conditions, and was considered in this work the additional runoff associated with the presence of the roadway. Table 4.9 shows the peak runoff for both scenarios for the majority of significant events shown in Figure 4.11. The absolute difference in this table is the same as defined above; the relative difference is the absolute difference divided by the pre-construction estimate. Thus this value is the increase in runoff relative to pre-construction estimates.

Table 4.10 shows the total volume of stream water passing through the downstream site for the year from 9/1/2014 – 9/1/2015. As Table 4.10 shows, the total volume of streamflow that could be attributed to the presence of I-59 is 88,700 m^3 for the year of estimations shown here, a 1.8% increase in total flow volume. The upstream inflow volumes are shown as well, because this source contributed the majority of streamflow volume. Although these pre- and post-

construction estimates are the modeled results from SWMM calculations, they provide a framework for understanding the contributions of the roadway. Looking at this specific crossing of the LCC over a stretch of I-59 about 1.4 km long, the overall increase in stormwater volume was only 1.8% (88,700 m^3). This is low, especially when compared to stormwater runoff volumes from other areas.

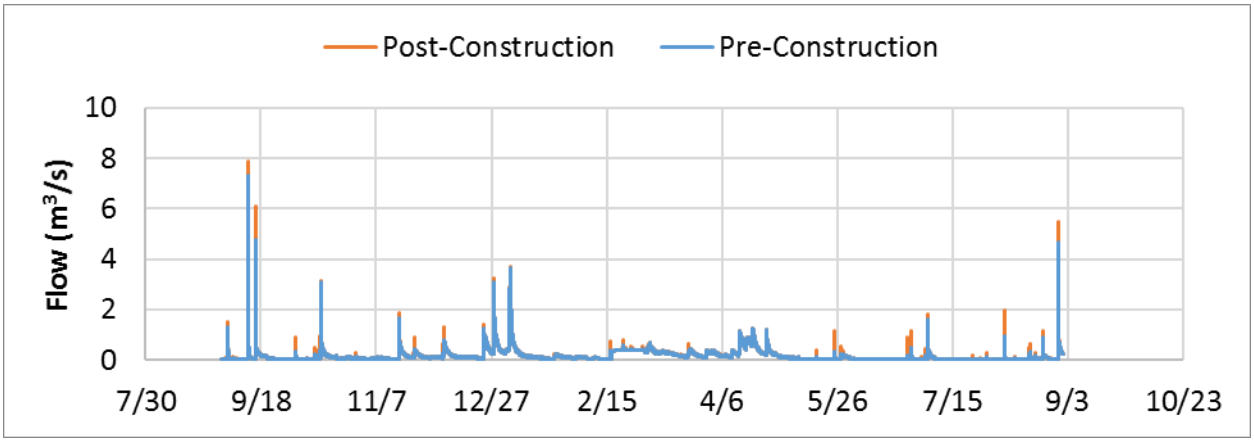

(a) pre- and post-construction results shown together.

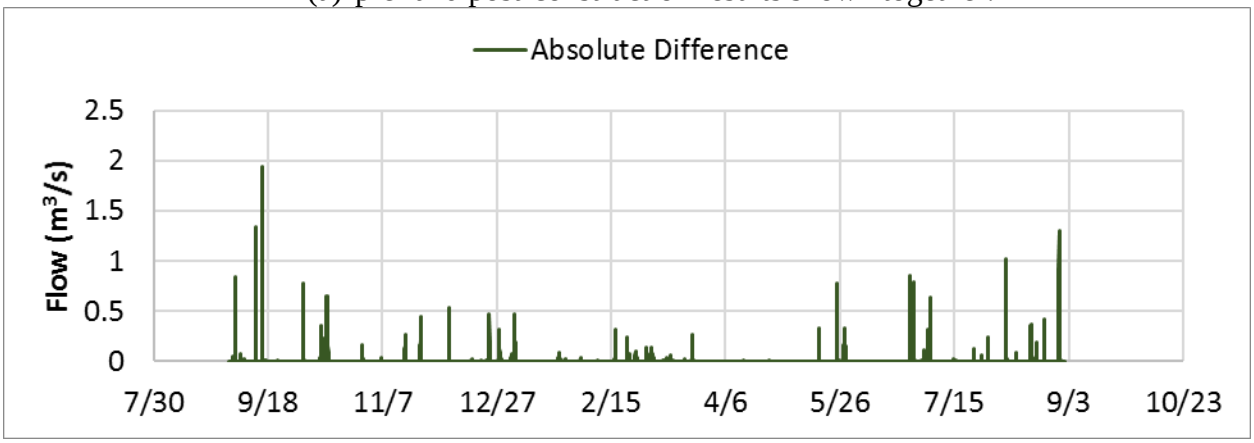

(b) contributions of the presence of the roadway

Figure 4.11 SWMM results of pre- and post-construction streamflow at the downstream location.

Table 4.9 Peak flow estimates for pre- and post-construction scenarios.

Date	Peak Flow Post-Construction (m^3/s)	Peak flow Pre-Construction (m^3/s)	Absolute difference	Relative Difference	Max Measured Rain Intensity (mm/hr)
9/3/2014	1.50	1.32	0.182	13.8%	18.8
9/12/2014	7.87	7.31	0.559	7.7%	59.4
9/15/2014	6.10	4.75	1.341	28.2%	39.4
10/3/2014	0.91	0.35	0.562	160.6%	21.6
10/14/2014	3.14	3.10	0.047	1.5%	21.8
11/17/2014	1.87	1.68	0.197	11.7%	12.7
11/23/2014	0.90	0.45	0.452	100.8%	7.6
12/6/2014	1.31	0.82	0.492	60.3%	18.5
12/23/2014	1.43	1.25	0.174	13.9%	13.7
12/28/2014	3.25	3.08	0.175	5.7%	17.0
1/4/2015	3.71	3.65	0.060	1.6%	15.0
2/16/2015	0.73	0.41	0.317	76.5%	11.9
2/21/2015	0.81	0.57	0.235	41.0%	8.1
3/23/2015	0.62	0.36	0.259	71.5%	8.4
5/16/2015	1.14	1.14	0.003	0.2%	0.5
5/24/2015	1.21	1.21	0.001	0.1%	0.5
6/25/2015	0.31	0.11	0.204	185.3%	11.9
7/4/2015	1.14	0.36	0.784	218.6%	17.0
8/6/2015	0.92	0.17	0.747	432.6%	18.3
8/17/2015	1.69	1.62	0.069	4.2%	17.3
8/23/2015	1.98	0.95	1.026	108.0%	24.4
8/29/2015	0.64	0.32	0.324	101.6%	8.1

Table 4.10. Total streamflow volume for year of simulations in SWMM.

	Post-Construction	Pre-Construction	Upstream Inflow
Total Volume (m^3)	4.91×10^6	4.82×10^6	4.78×10^6
Downstream – Upstream (m^3)	1.25×10^5	3.65×10^4	
Difference between Scenarios (m^3)	8.87×10^4		

4.2.5 Continuous Simulations with SWMM of 1st Year of Measurement

The runoff events and data discussed in section 4.2.1 was used as described earlier to formulate and calibrate hydrological models of the LCC using SWMM and GSSHA. That period was from 09/01/14 – 11/31/14, which was focused on because the quality of data for stream flow measurements was better, due to the installation of ISCO area-velocity sensors, and there were continuous groundwater measurements during that time as well. Stream depth was recorded with HOBO® pressure transducers for both the upstream and downstream locations continuously since 04/11/13, as introduced in Chapter 3. Figure 3.3 shows an earlier developed head-discharge curve, created from stream head and velocity measurements, and is accurate for low-flow events. The primary purpose for the installation of the area-velocity meters was to characterize high flow events, which were not well represented with that earlier head-discharge curve.

Compiling the data from the area-velocity sensors, and creating a functional relationship between the reported head and discharge from the instrument yielded the head-discharge curves shown in Figure 4.12. These two curves, combined with those previously mentioned (repeated in Figure 4.12 as well), were used with measured stream head data to calculate stream flow rates for low and high intensity events.

For events with a stream height recorded higher than 0.6 m, the equation from Figure 4.12 was used for both upstream and downstream; stream heights less than 0.6 m use the equation from Figure 3.3. This was done to ensure quality of data, since using the equation derived from the area-velocity sensor (Figure 4.12) yielded base flow rates that were 10x larger than measured values. Thus, this was used only for measurements of high stream head levels. The calculated stream flow rates are shown in Figure 4.13 for the measurement period 4/11/13 – 7/24/14.

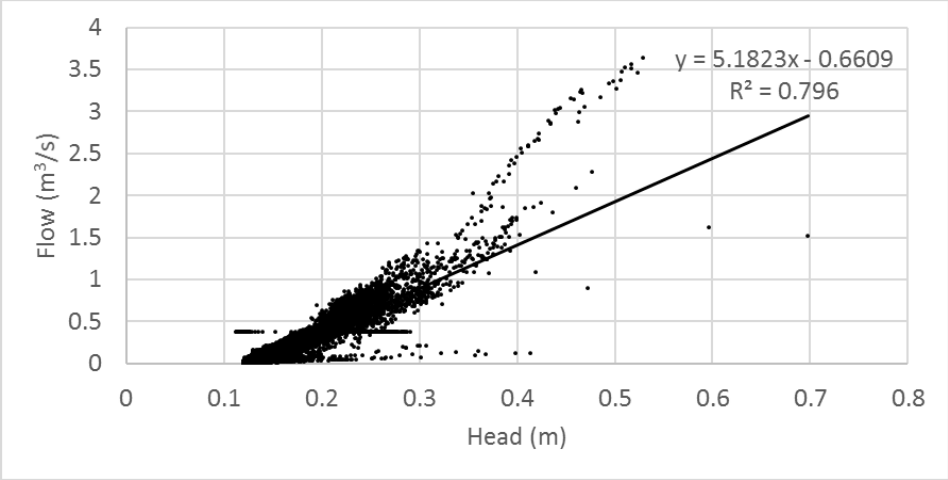

(a) upstream

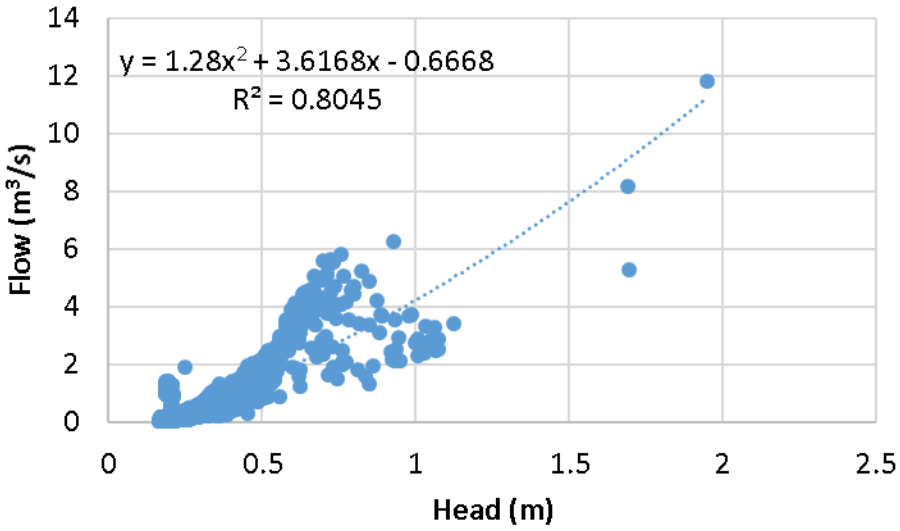

(b) downstream

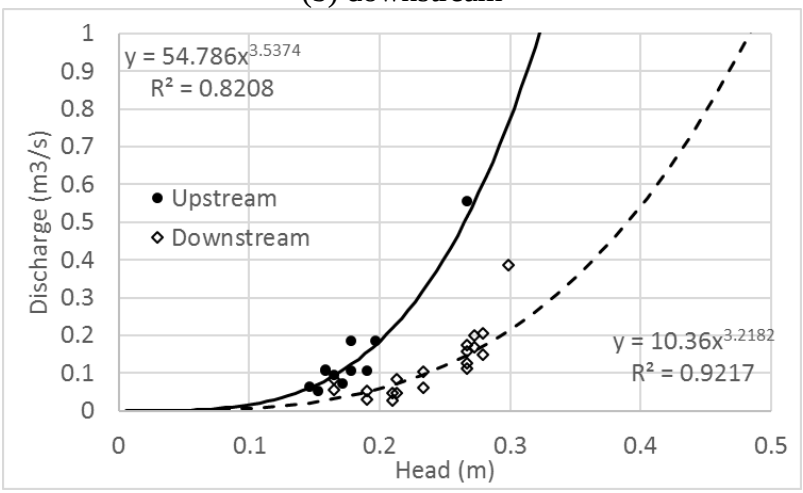

(c) low flow events (repeated from Figure 3.3)

Figure 4.12 Head-discharge curves from area-velocity meter measurements.

As mentioned previously, the SWMM model setup was capable of running long-term simulations with limited computational requirements. Using the same procedures as discussed above, SWMM was run for the simulation period 4/11/13 – 7/24/14, and results are shown in Figure 4.14 for stream flow and Figure 4.15 for groundwater levels in the median and downstream location. A secondary benefit of using long term simulations is in considering any discrepancies between the measured rainfall and stream flow calculations.

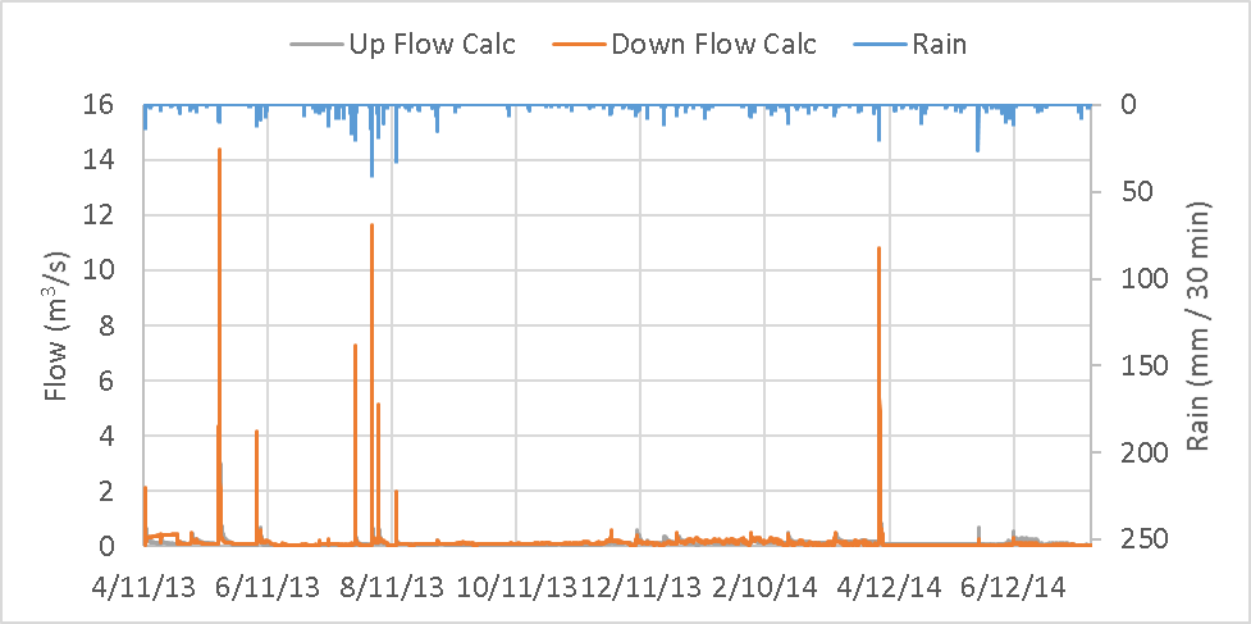

Figure 4.13 Calculated flow rates for the upstream and downstream locations for earlier measurement period.

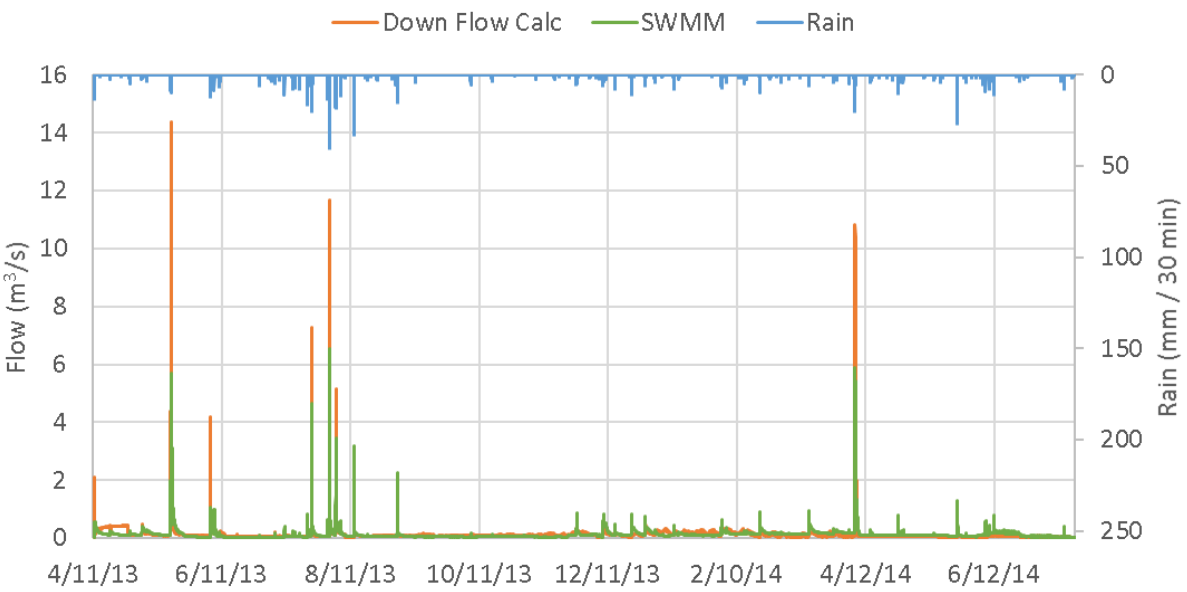

Figure 4.14 Downstream calculated flow rates and SWMM modeled data.

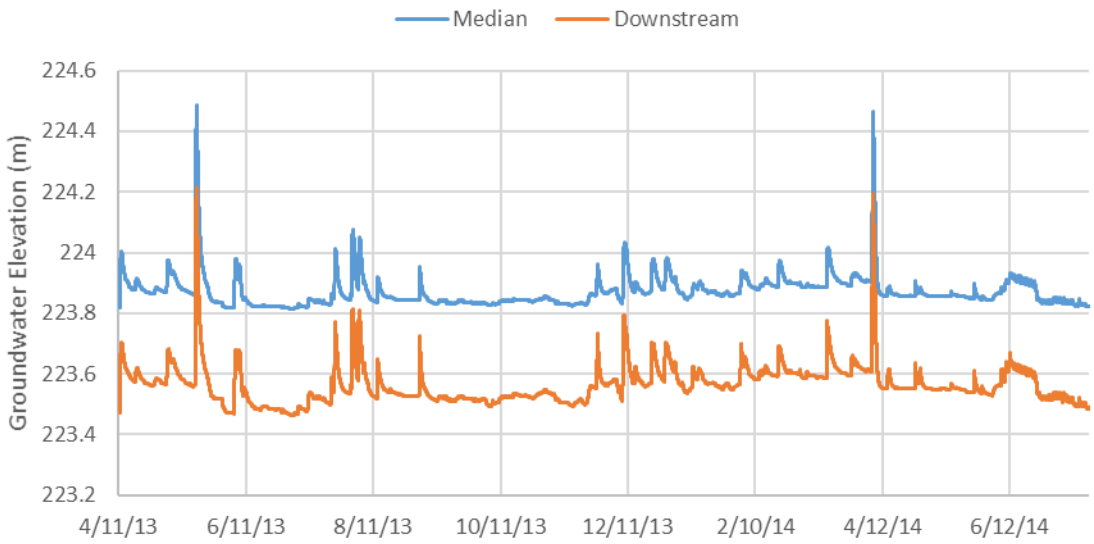

Figure 4.15 Modeled groundwater table elevation for the median and downstream locations.

For most events, there was a general agreement between the timing and intensity of measured rainfall and modeled runoff events. Three events do not correlate well at this larger time scale approach: 5/18/13; 6/5/13; and 9/2/13. The first two, from the months of May and June, do not yield downstream flow rates from the rainfall-driven SWMM model much larger than the upstream inflow-hydrograph boundary condition. There was not enough rain as an input

parameter to generate a comparable runoff in simulations of the LCC. The third event, in the 9th month, has significantly high rainfall measured to produce up to 2.2 m^3/s streamflow downstream in the SWMM simulation, however none was measured either upstream or downstream above baseflow conditions. Because the SWMM model consistently reproduces runoff of a similar magnitude for the majority of events, these three mentioned disparities between the measured and simulated runoff results is most likely attributed to spatial differences in rainfall distribution.

The simulated data here shows that the calculated head-discharge curve agreed well with simulated stream flows with SWMM, in particular when there was certainty that the runoff-generating rain event was captured with the deployed rain gauge. Additionally, the model continued to perform well in simulating the bank storage effect, lending insight into the behavior of the groundwater table elevation in rain events before observation wells were installed. Long term simulations with SWMM also add the ability to consider the variations throughout the season with limited computational requirements.

4.2.6 Impact of Discretization in GSSHA

As discussed in previous sections, due to the setup of the GSSHA model of the LCC, long-term simulations were not feasible due to computational requirements associated with the discretization chosen in this study. In order to characterize the small features of the roadway, including drainage features, a small grid size (5 m) was chosen for this research. As is the case with all hydrological models, GSSHA results should vary with discretization choices. To demonstrate this, and test the hydrological response to multiple cell size choices in GSSHA, 2 additional models were set up with cell sizes of 10 m and 20 m, in addition to the original 5 m

setup. Figure 4.16 shows the familiar I-59 crossing of the main branch of the LCC, with the original 5 m cell discretized domain of GSSHA. Three squares are shown filled in, a black square of 5 m x 5 m, a blue square of 10 m x 10 m, and a green square of 20 m x 20 m. This figure shows that by increasing the cell size by a factor of 2x, the number of cells for calculations and solutions reduces by 4x.

In addition to reducing the number of calculations and solutions, increasing the size of computational cells in GSSHA affects the characterization of the roadway and groundwater solution. This is demonstrated in Figure 4.17, where the discretized solution domain is shown in the 5 m, 10 m, and 20 m models with the image of the roadway, land use designation, and stream-groundwater interaction cells. The groundwater observation wells are shown as light-grey circles, and the road surface is represented as red squares in the land use images of Figure 4.17 B, E, and H. Inspection of Figure 4.17 shows that the 10 m cell size maintains a continual representation of the road surface, and brings the location of the cell representing the observed data nearer to the boundary of the groundwater-surface water interaction cells. The 20 m cell size no longer represented the roadway continuously, and the groundwater-surface water interaction area was grossly exaggerated. The 5 m model was converted to 10 m and 20 m grid size models using the grid-grid conversion feature within WMS, as opposed to starting the model from scratch at the 10 m and 20 m resolution. This latter option would have inevitably introduced additional discrepancies between the three models.

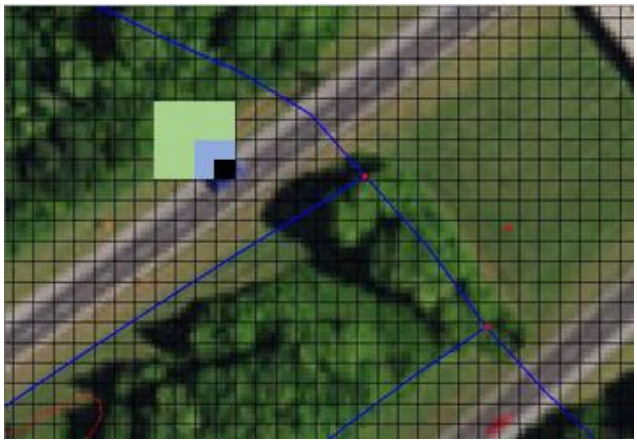

Figure 4.16 Image of I-59 and multiple cell size shown in black, blue, and green for 5 m, 10 m, and 20 m cell size, respectively. Image from ESRI (2016).

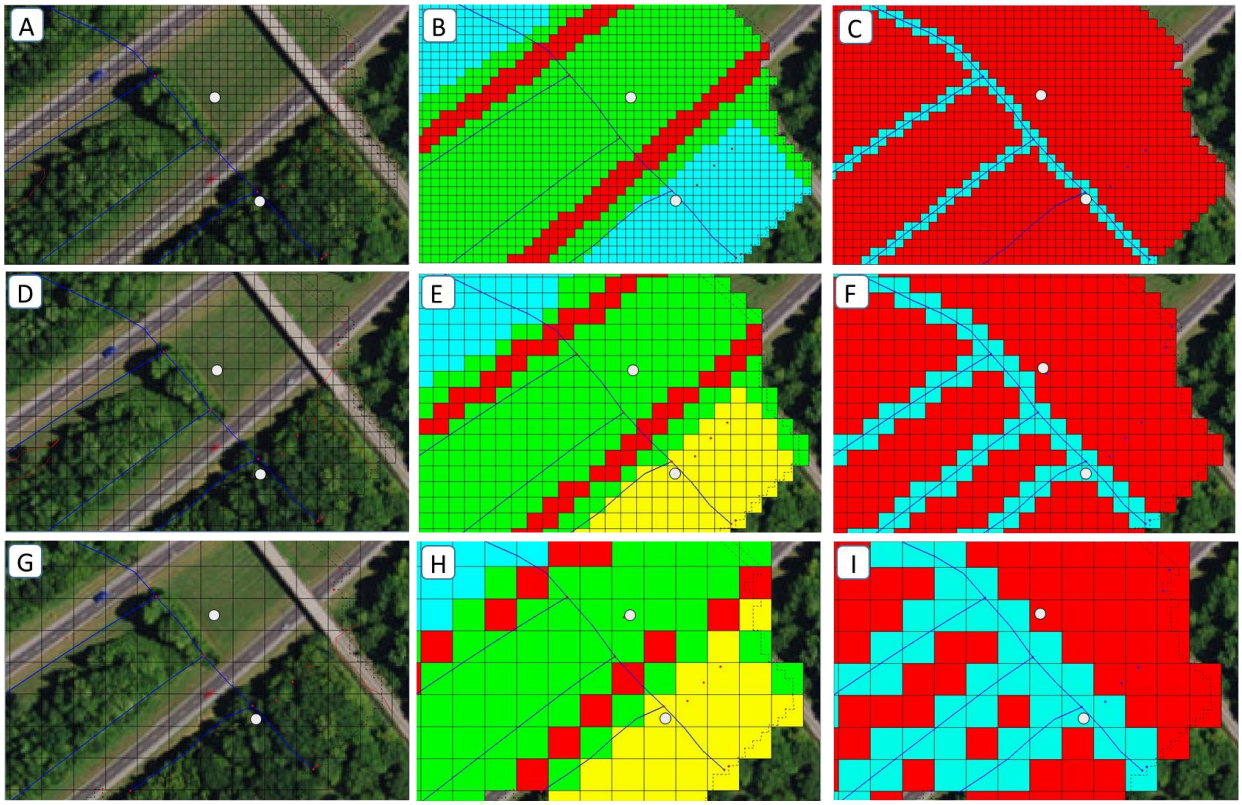

Figure 4.17 Image of the roadway, land use designation, and stream-groundwater interaction cells in GSSHA for 5 m, 10 m, and 20 m cell sizes. Background image from ESRI (2016).

For the three different setups discussed, the 4 events discussed in section 4.2.1 above were run with the same calibrated parameters, only changing the discretized cell size. The results for all three models are shown in the downstream hydrograph in Figure 4.18. For all four events, as the cell size increases, the peak flow decreased by as much as 2 m^3/s. The stream flow rate is

approximately equal for the 10m and 20m setup for the lower intensity events of 10/13/14 and 11/16/14.

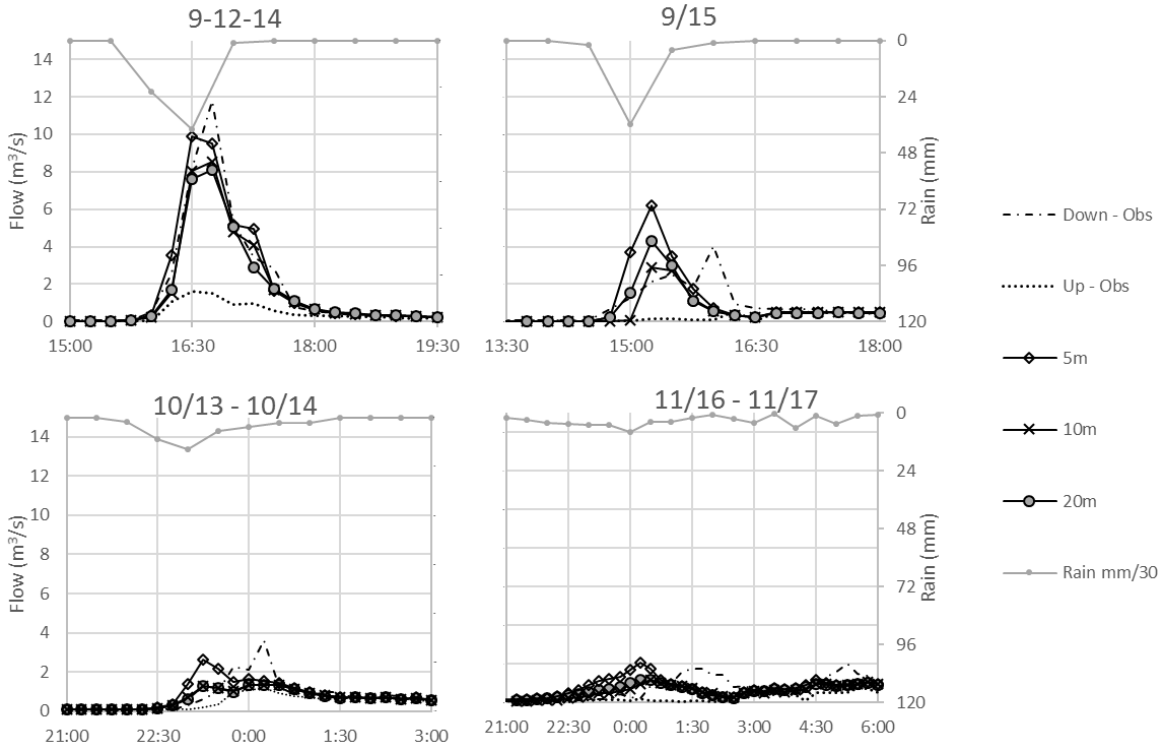

Figure 4.18 Downstream hydrographs for the 5m, 10m, and 20m GSSHA discretization.

There are a few possible reasons why the stream flow rates for the events modeled here are lower with larger cell size. The first is that the calibrated parameters for the overland and infiltration processes were cell size specific. It's not likely that the infiltration parameters should change according to cell size, unless the changed grid also greatly changes the overall area that each land use contributes. A likely candidate for required adjustment is the manning's overland roughness parameter. This is due to the variation in flow paths evident in smaller discretization and obscured in larger discretization. The second potential reason for variation is that some variables in the calculation set have been averaged or altered by reducing the number of cells. This includes the slope between adjacent cells and the depth of water accumulating on the surface. The third reason, and most likely candidate, for variations is the groundwater-surface

water interaction cells have grown larger (as seen in Figure 4.17 F and I) and allow for more rapid interaction between these two domains.

Figure 4.19 shows the solutions for downstream and median locations of the groundwater domain. As with stream flow, the difference in groundwater solutions for the three discretization sizes was most pronounced during the high intensity events of September. The difference mainly seen in the solutions was the increased response of groundwater table elevation for the larger cell sizes. Thus for the same calibrated parameters, the larger cell size introduces larger errors in the solution.

Inspection of the groundwater-surface water interaction equation in GSSHA [EQ-4.12] would indicate that most variables are not dependent on the cell size. However, the groundwater flow, *f*, is the flow per unit area (m/s); when multiplied by the surface area of the cell and then implemented into the groundwater equation [EQ-4.10] as $W(x,y,t)$, that source term (W) is increased proportionally with the cell size. Thus for the 10 m and 20 m cell sizes, W increases 4 and 16 times from the 5 m equation set. Because of this, it should be noted that the groundwater interaction and calibration parameters are highly dependent on cell size.

Additionally, if a stream or river is substantially smaller than the cell size, as was the case here, this representation would overestimate the amount of surface area receiving direct groundwater-surface water interactions. In this case, the stream was approximately 5 m wide, thus a 5 m cell size would closely approximate the area of groundwater interaction. If the variables in the groundwater interaction equation were essentially calibration parameters, as is the case with the SWMM equation, then they could be adjusted in calibration to match measured field data. However, they are physically meaningful parameters (hydraulic conductivity and stream bed sediment thickness), and should not exceed established values; nor should they

change with grid size, technically. Thus, it is important to consider the width of a channel in selecting grid cell size.

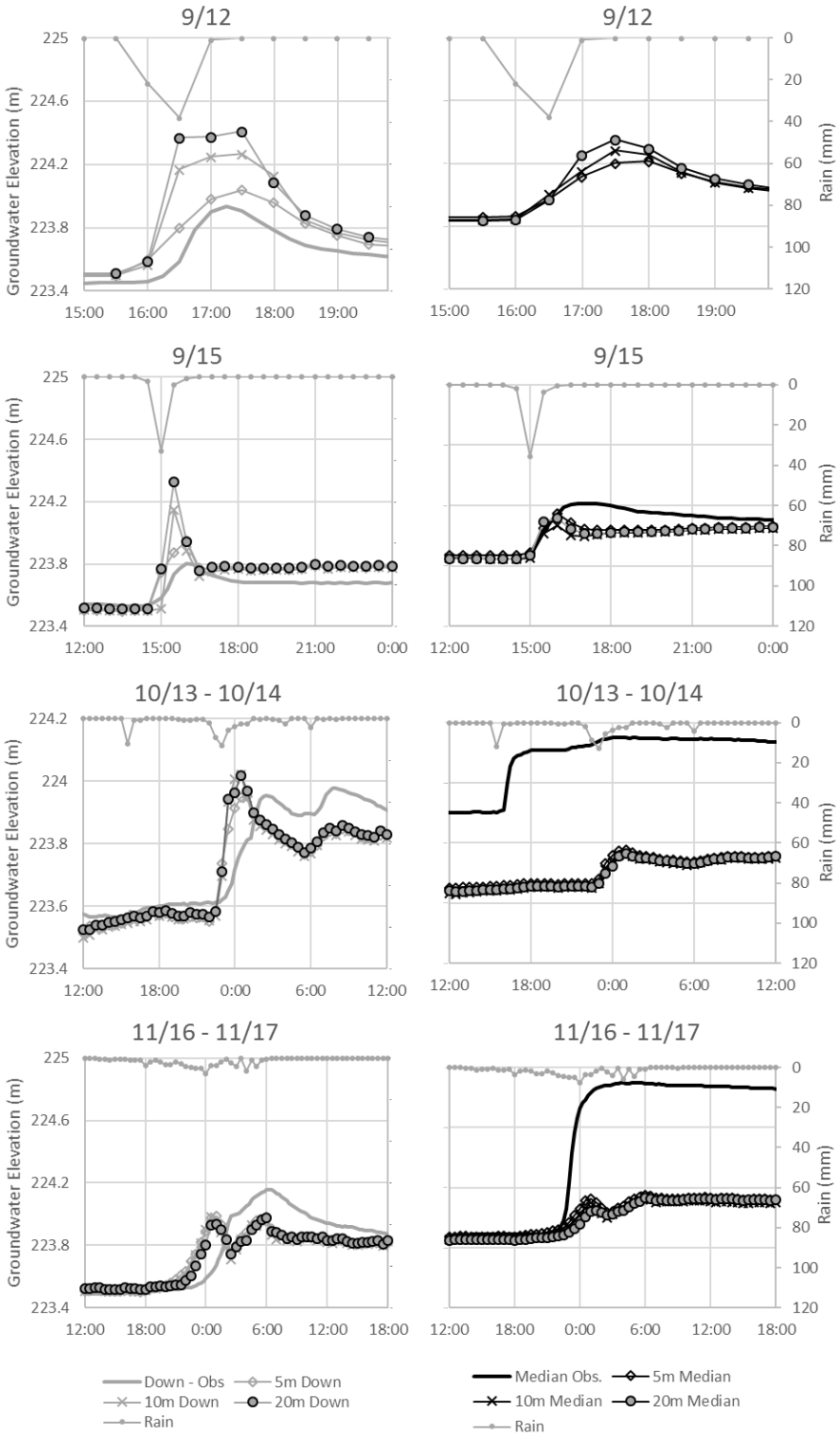

Figure 4.19 Groundwater solution for the 5m, 10m, and 20m GSSHA discretization.

4.3 Conclusions

This chapter discusses hydrological modeling of stormwater runoff and groundwater table fluctuations across I-59 in central Alabama using two models: SWMM and GSSHA. Field data showed a complex relationship between rain events and the measured groundwater table and streamflow within the median of the interstate and downstream of the roadway. In particular, the interstate median retained moisture from rain events during the frequent, low-intensity events of the winter. During the work presented herein, some key differences between SWMM and GSSHA were explored. Surface water stream flow, volume of infiltrated precipitation, and surface runoff were comparable between both models and measured data after model calibration. This demonstrated the similarities in overland simulation and infiltration processes between the two programs, though the specific implementation of the governing equations differs.

In general, GSSHA reproduced the observed groundwater table variation more closely than SWMM. For the downstream site, GSSHA data had an overall 18% error for the PEH statistic, while SWMM data had an overall -38% error. Additionally, the G_{gw} statistic was 0.0481 and 0.0597 for GSSHA and SWMM, respectively. In situations where the groundwater table has a large variation spatially and responds to storm events very quickly, as seen in roadways as discussed in this work, a spatially-discrete 2-dimensional model like GSSHA will likely represent the groundwater table more accurately. Surface-groundwater interactions with channel flow have a similar form and both programs are capable of reproducing the stream bank storage occurring in this study location. SWMM would be preferred if several long-term simulations are planned in stormwater management studies. If data and computational requirements are not a limiting factor or limited numbers of extended period simulations are envisioned, GSSHA offers a similar overland scheme with a more realistic and robust groundwater component. Current

SWMM users may find this feature helpful in settings that have dynamic groundwater environments.

Some aspects of rainfall-driven hydrological responses were not entirely successfully represented in either models by the author. In particular, attempts to represent the shallow groundwater table of the interstate median was unsuccessful using the simplified Green-Ampt equation, and uniform groundwater parameters. It was speculated that the interstate median subsurface had a different response to rain events and groundwater table rise than the areas outside of the roadway. Future work on interstate stormwater runoff should focus on this aspect of interstate drainage.

Taking advantage of the reduced computational time of SWMM, a year of rain events was run with both pre- and post-construction parameters. Calculated peak flow estimates indicate that up to 1.34 m^3/s could be attributed to the presence of the roadway in some large rainfall events (9/15/14) or in some cases between 60 to 200% increase during lower intensity events (see Table 4.9 for detail). However, the total volume of stormwater, rather than peak flow rate, has received increasing attention for stormwater management in highway environments (Strecker et al., 2014). When including the inflow from upstream of I-59, the additional volume indicated in this work from the roadway was only 1.8% of the total flow through the channel. These estimates support the need for volume reduction approaches in stormwater management, which must include an assessment of groundwater conditions as many of these approaches typically use high-infiltration structures.

Additional insights were gained through the modeling approaches used in this work. Comparing a year of rainfall-runoff simulations in SWMM indicated that, even in this small watershed, rainfall spatial heterogeneity can yield inaccurate modeling results. This is a

commonly recognized phenomenon, which should be considered in interpretations of modeling results. Additionally, though GSSHA is often used with cell sizes of 30 m or more, there is a significant difference in results between cell sizes of 5 m and 10 m or 20 m when using the same model parameters. This was largely due to the difference between channel width and cell size, and the groundwater-surface water interaction equation.

This work also pointed to new research questions that could be the focus of future work in stormwater runoff modeling. Stream bank storage was a significant hydrological process in the streamflow and groundwater components of this system, but it is not known to what extent roadway ditches and other drainage features offer stream bank storage. Also, measured data showed that during wet periods the groundwater saturated the median, which would allow for no infiltration during subsequent rain events. With the growth of using infiltration-based BMPs, it is essential to accurately assess the location of the groundwater table for proper design of roadway drainage structures. Future work could determine a way to better represent the dynamics of runoff generation on saturated soils of roadway medians during wet periods.

Chapter 5 – A Procedure for Resolving Thermal Artifacts in Pressure Transducers

5.1 Background

Despite the abundant and widespread use of pressure transducers to measure stream height and groundwater table elevations, few users are aware of thermal artifacts in pressure data, which cause artificial fluctuations in stream and groundwater data. Although some researchers have identified the presence of these thermal artifacts, a standardized procedure for mitigating thermal artifacts in sampled data has not been presented in the literature. If it is determined that errors associated with temperature effects exist in a particular sensor or deployment, the only recommendation at this time by researchers is to deploy the instruments in conditions that reduce temperature fluctuations as much as possible (Cuevas et al., 2010). While this is valid, such recommendations do little to address the errors in already collected data, which may be of crucial importance in many applications.

In essence, there is no guideline on how to rectify erroneous data as a result of thermal artifacts that has already been collected. For now, researchers must: 1) be content with data even though it not representative of the true values; 2) attempt to average the fluctuations, which would eliminate an evapotranspiration response and introduce a guessing element in the results; and 3) use a daily time-step in any calculations, thus ignoring the fluctuations that occur within 24-hour cycles. The recent growth in time-sensitive watershed modeling tools has been aided by increasingly accurate instruments for model calibration/validation. In an effort to continue forward, it is imperative to determine a way to reduce this thermal artifact signal from existing and future pressure transducer datasets.

5.2 Methods

To evaluate and connect effects of temperature variation on reported pressure readings, a number of experiments were performed along with data analysis. The presented methodology follows three steps. First, laboratory experiments were set up to derive temperature-based pressure head variations for multiple sensors. Second, data analysis was performed to derive an equation relating temperature readings to reported pressure head variations. Third, this equation was applied to existing data to assess the quality of the pressure rectifying procedure.

Applying a method similar to Liu and Higgins (2015), pressure transducers were placed in a bucket with static volume of water. Multiple experiments were performed in a laboratory that consisted of changing the water temperature. One sensor was used to report barometric pressure within the laboratory, which had a regulated air temperature via air conditioning (this sensor was outside of the bucket). In field settings, both sensors will experience temperature variations; in that case, evaluation and correction of temperature variations should be applied for both sensors. For brevity, only select data is shown and discussed in the present work. These experiments were simple since the goal was to provide a straightforward and easy to reproduce pathway for analysis and rectification of faulty sensors and data. Sensors (pressure transducers) used in this project are Onset® HOBO® U20L-01, and U20-001-01. The U20L-01 model was used as a barometric sensor; all others (those experiencing temperature fluctuation in this experiment) were model U20-001-01 sensors. As specified in the user's manual (Onset, 2014) for these sensors, the water depth measurement has a typical error of ±0.46 cm and a maximum barometric pressure error of 1.20 kPa. The pressure error is described as including the effects of sensor drift, temperature variations, and hysteresis-induced errors. The water height error is specified as representative of the expected errors in a stable temperature environment and

accurate barometric pressure data. The operation range for temperature measurements is from -20 to 50 °C with an accuracy of ±0.37 °C and resolution of 0.1 °C.

5.2.1 Laboratory Experiments

Previous workers have observed how temperature affects pressure transducer readings in various ways, including using an oven or heater (Cuevas et al., 2010), solar radiation (Liu and Higgins, 2015), or natural temperature changes (McLaughlin and Cohen, 2011). In this study, analyses were performed on pressure transducers where temperatures were changed in a controlled laboratory setting. This was performed using two buckets: An 18.9 L bucket was connected to a water supply where hot water, room temperature water, or ice was added to change the temperature; a smaller, 7.6 L bucket was placed inside of the 18.9 L bucket with a fixed amount of water by volume and the sensors were placed inside it, as seen in Figure 5.1. This setup was used to allow conductive heat transfer to affect the internal bucket temperature in a slow, controlled way. By increasing or decreasing temperature in the external, 18.9 L bucket, the sensors would slowly experience a temperature change as opposed to directly adding hot or cold water to the internal 7.6 L bucket.

Experiments began by filling both buckets with cold water (approximately 4 °C), then turning on all pressure transducers and placing them inside the internal bucket. The height of water in the bucket was measured with a ruler, which is used during barometric compensation and data analysis and is indicated later as H_T. After allowing the sensors to reach equilibrium with the water temperature, which took about 30 minutes, the water in the external bucket was heated. This was accomplished by turning on the water supply with an attached tube to direct flow into the external bucket (without disturbing the internal one). First, room temperature (20 °C) water was added at a continual and slow rate (0.5 L/min for 1-2 hours) to smoothly increase

the temperature. Then hot water (38 °C) was added for another 2 hours. When the internal bucket reached approximate equilibrium with the external one (temperature difference less than 0.5 °C, monitored through thermometers), room temperature water (20 °C) was slowly added (about 0.5 L/min) to cool the sensors for about 2 hours, then ice (less than 1 L) or cold water (4 °C). Following this protocol, the experiment was repeated (10-15 times) in order to achieve a smooth temperature transition as recorded by pressure transducers. Laboratory experiments were performed indoors over a period of 8-10 hours, with sampling rates at 1 minute intervals.

The above procedure was found to best mitigate issues related to rapid temperature changes during the experiments. As specified by the device's user manual, these sensors experience additional errors if the temperature is changed rapidly. This was noticed in this experiment as well, and was most problematic at the moment that the experimenter attempted to change the temperature. The addition of too much cold/hot water at one time can cause additional errors at a temperature gradient above 0.2 °C/min. This high temperature gradient produced artificial changes in the pressure that is both difficult to quantify and is not typically seen in real applications of these sensors.

Figure 5.1. External and internal bucket configuration for laboratory experiment.

5.2.2 Data Analysis of Temperature Dependency

Figures 5.2 and 5.3 show the results of one laboratory experiment where the water temperature was changed in variations between 10 to 37.7 °C over the course of approximately 8 hours. The temperature change imposed on the external bucket and recorded by the sensors is shown in Table 5.1. Six pressure transducers were used in this experiment, five experiencing changing temperatures under a constant water head, and one recording only atmospheric pressure with a nearly constant temperature (air conditioning). A relatively long time period is required for this experiment (at least 2 hours for each 20 °C change), in order to reduce inaccuracies (additional errors) associated with rapid temperature fluctuations. Two graphs show the pressure head fluctuations after barometric compensation. Figure 5.2 shows the pressure variation for three sensors (labeled A, C, and E), which show similar fluctuations. These three sensors could be considered as operating within an acceptable range, fluctuating less than 2.25 cm in total over the temperature range of this experiment. Despite being considered within an acceptable range, such

pressure head fluctuations are more than twice the magnitude of the error associated with the instrument, ±0.46 cm. Figure 5.3 shows the pressure variations for three sensors: two sensors (labeled B and D) producing fluctuations much larger than those in the previous figure, and one of the sensors (C) from the previous figure for comparison. Though Figures 5.2 and 5.3 contain data points from the initial start of the experiment, data during this equilibrium stage is not used in this work's data analysis due to rapid nature of temperature change experienced.

Table 5.1. Temperatures experienced in the laboratory experiment

Time	Sensor T (°C)	External Bucket T (°C)
9:22 AM	18.1	9.4
9:31 AM	9.5	9.4
11:00 AM	20.1	21.1
12:10 PM	34.8	35.0
1:45 PM	27.3	26.7
2:20 PM	18.6	18.3
3:45 PM	35.7	36.7
5:15 PM	10.6	10.0

.

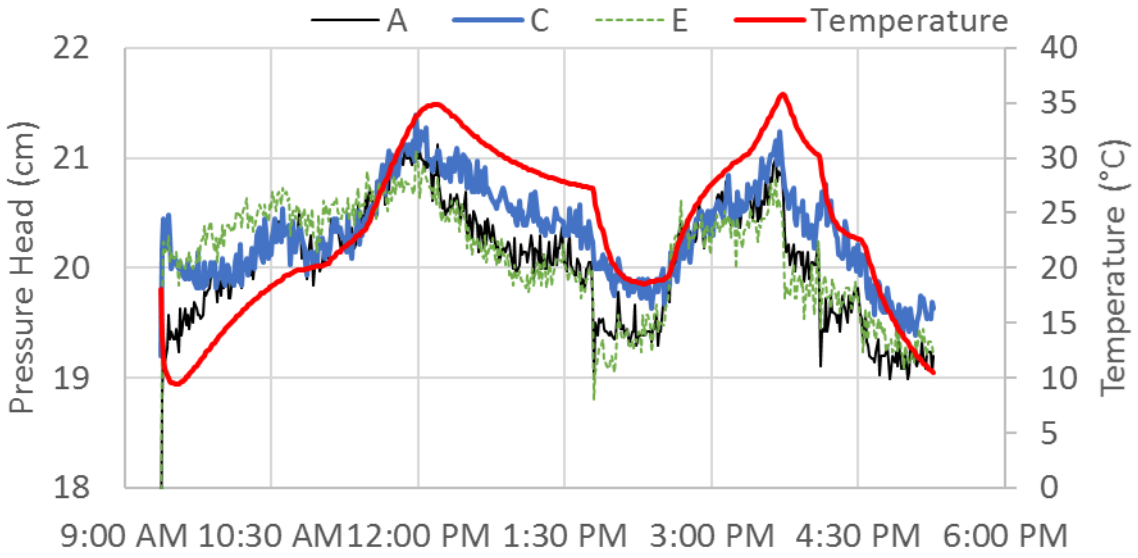

Figure 5.2. Pressure variations according to sensor temperature.

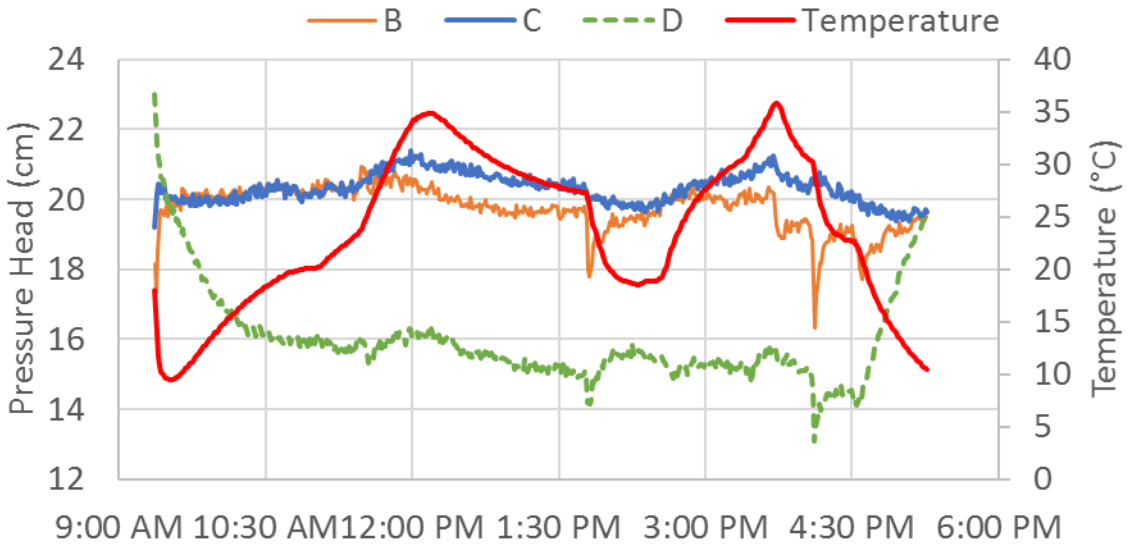

Figure 5.3. Pressure variations according to sensor temperature, including sensor C from the previous figure for comparison.

There are a variety of responses that pressure transducers report with variation in temperature. Some sensors present relatively small error ranges (like A, C, and E from Figure 5.2) and may report variations of pressure head that have a linear relationship with temperature. This linear dependence is readily seen in Figure 5.2. As temperature increases or decreases, so does the reported water head. Trendlines expressing the linear relationship between temperature and reported pressure head, as exemplified in Figure 4, can be determined as shown in Equation 5.1:

$$H_L = C_T * T_L + K \quad \text{(Eq. 5.1)}$$

Where H_L is the reported pressure head from the pressure transducer (cm) in the laboratory experiment, C_T is the coefficient of temperature slope (cm/°C) determined by fitting a linear regression against the pressure head, T_L is the reported temperature from the pressure transducer (°C) in the laboratory experiment. In Equation 5.1, K is simply the y-intercept, the pressure head that would be reported if the temperature were zero. This parameter is only useful as a calibration variable in this equation, not as a meaningful instrument parameter. Equation 5.1 can

be found using linear regression analysis of any statistical software package or spreadsheet program, or by following the procedure for determining the least-squares fit or linear regression (see for instance Taylor, 1982). During this linear regression analysis, the residuals should be analyzed to ensure a normal distribution of the data. For the data shown in this study, residuals were distributed normally around the linear regression equation shown.

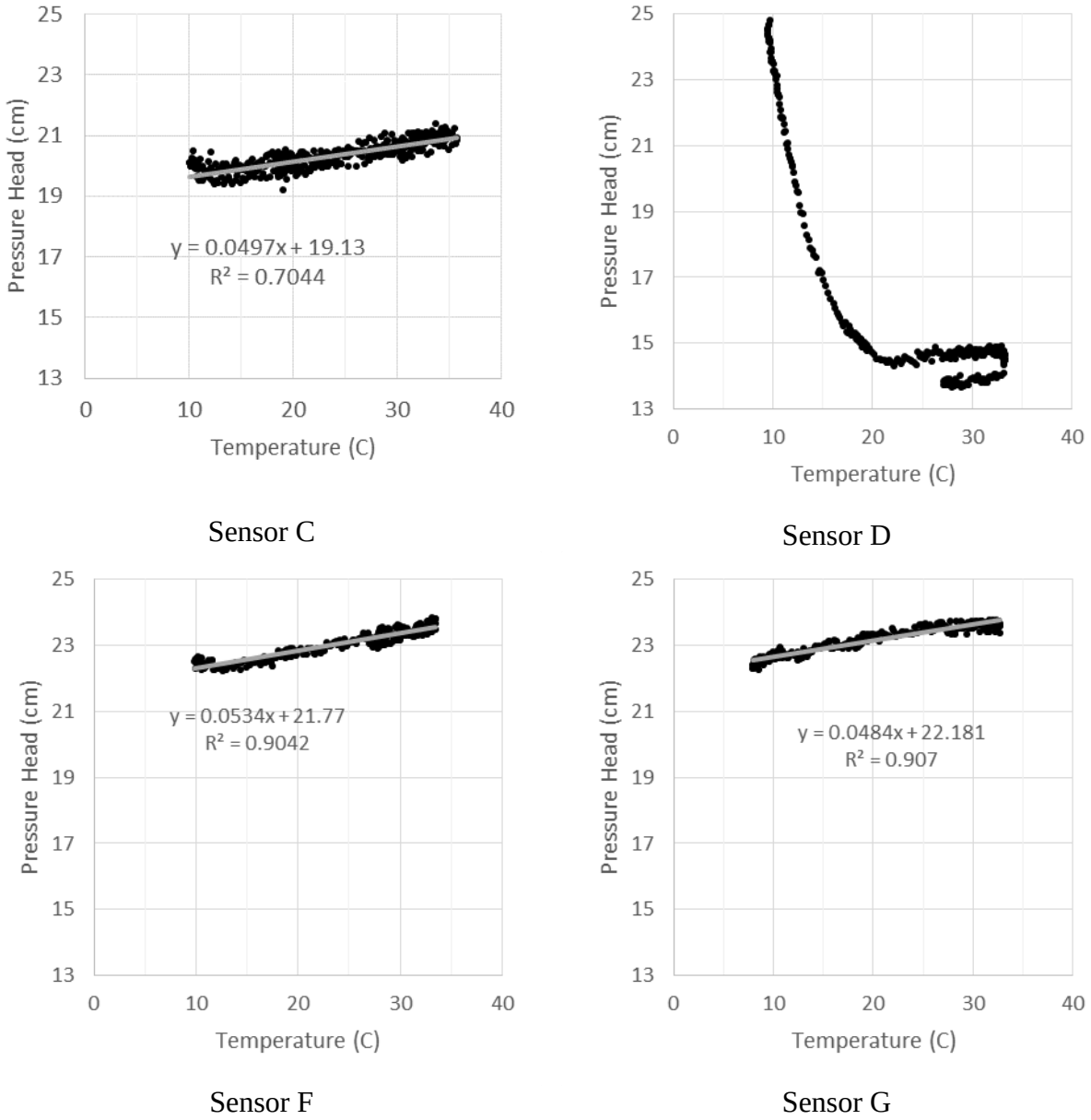

Figure 5.4. Four sensors showing temperature dependency on pressure head readings.

In addition to the parameters mentioned above, the temperature correlating to the true pressure head must be determined. This can be done by rearranging EQ-5.1 as follows:

$$T_i = \frac{H_T - K}{C_T} \quad \text{(Eq. 5.2)}$$

In Equation 2, T_i is the experimental temperature (°C) where the pressure head reported is equal to the true pressure head. H_T is the measured pressure head (cm), K and C_T are the same variables defined in the previous equation.

Figure 5.4 shows four datasets for different sensors (C, D, F, and G) following the experimental procedures previously mentioned, and the linear-regression line as discussed for EQ-5.1. In Figure 5.4, sensor C data was from the previous experiment shown in Figures 5.2 and 5.3. Data for sensors D, F and G were from a different experimental dataset, although the abovementioned standard procedure was followed. Two sensors, F and G were not included in the previously mentioned dataset. It is clear that sensors C, F, and G all have a linear relationship with temperature (over the range of the experiment), and the trend line is plotted against the data. Sensor D, however, had a more complicated relationship that varies over the range of temperatures experienced in this experiment. Additionally, the overall pressure head variation was 500% larger for this sensor than in the others shown here. Sensors C, F, and G shown in Figures 5.4(a), 5.4(c), and 5.4(d) respectively, varied 1-2 cm, which was close to the expected error range. On the other hand, sensor D in Figure 5.4(b), varied more than 10 cm, an exceptionally large variation.

Large fluctuations in pressure reported by sensor D were observed at temperatures less than approximately 20 °C. For sensors experiencing these types of errors, it may be most useful to calculate two sets of variables: (1) a set for a lower temperature range, and (2) a set for a higher temperature range. Then, depending on the temperature experienced in the field, the

appropriate corrections can be applied for each data point. An approach for this type of problem is presented in section 5.3. Though the example shown there is straightforward, additional errors may be introduced where two equations are required, especially when temperatures experienced are near the intersection of the two lines. While each sensor may produce varying pressure head variations according to temperature, a standard procedure is needed to reduce these errors.

5.2.3 Rectifying Data by Reducing Temperature Dependency

Having defined the specific relationship of erroneous pressure head variations caused by temperature changes, it becomes possible to rectify data by removing thermal artifacts. The temperature dependency defined by Equations 1 and 2 can be used to adjust the pressure readings according to the recorded temperature. The following equation can be used:

$$H_{L,R} = H_L - C_T * (T_L - T_i) \quad \text{(Eq. 5.3)}$$

In this equation, $H_{L,R}$ is the rectified pressure head (cm) for the laboratory data.

This method was followed for sensor C in the above described experiment (shown Figures 5.2, 5.3, and 5.4). Figure 5.5 shows the reported pressure head plotted as a function of temperature for sensor C. Table 5.2 shows the variables that were found from Equations 1 and 2 for sensor C. The variables T_i and H_T are also indicated on Figure 5.5(a). Figures 5.5(a) and 5.5(b) include the actual pressure head (19.81 cm) represented by a dashed line, and bracketed by two solid lines representing the error (±0.46 cm) of the sensor.

After correcting each data point for the temperature based fluctuations, there was no additional variation over the temperature range in this experiment, as shown in Figure 5.5(b). In Figure 5.6, it is seen that the sensor reported pressure readings (water heights) inflated with temperature change. After the correction, this fluctuation was resolved to within the specified

error range for the instrument. The L2 error estimates (an Lp-norm defined by Wesseling, 2009) was used to determine the improvement of data calculations:

$$L_2 = \frac{\sum_{i=1}^{n}(H_i - H_T)^2}{N} \quad \text{(Eq. 5.4)}$$

Where H_i is the reported head (cm), H_r, at each time, H_T is the true (or measured) head (cm), and N is the total number of data points. Using this equation, the error of this dataset was reduced from 0.66 to 0.23 for the experimental and temperature corrected data, respectively.

Table 5.2. Values for Sensor C from Equation 5.1 and 5.2

H_r (true)	19.812
C_T	0.0497
T_i	13.72
K	19.13

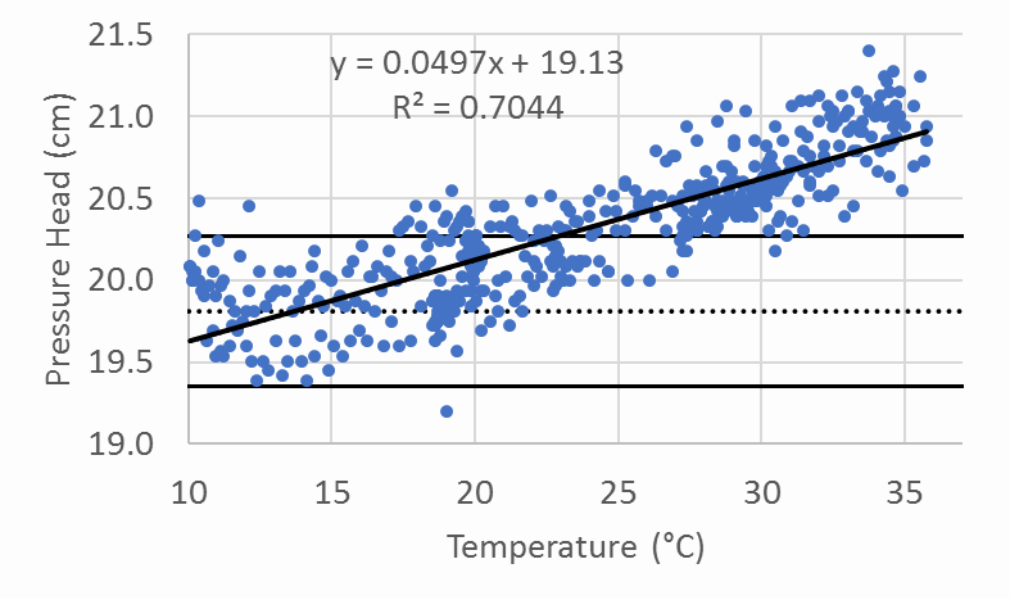

(a) Experimental Data

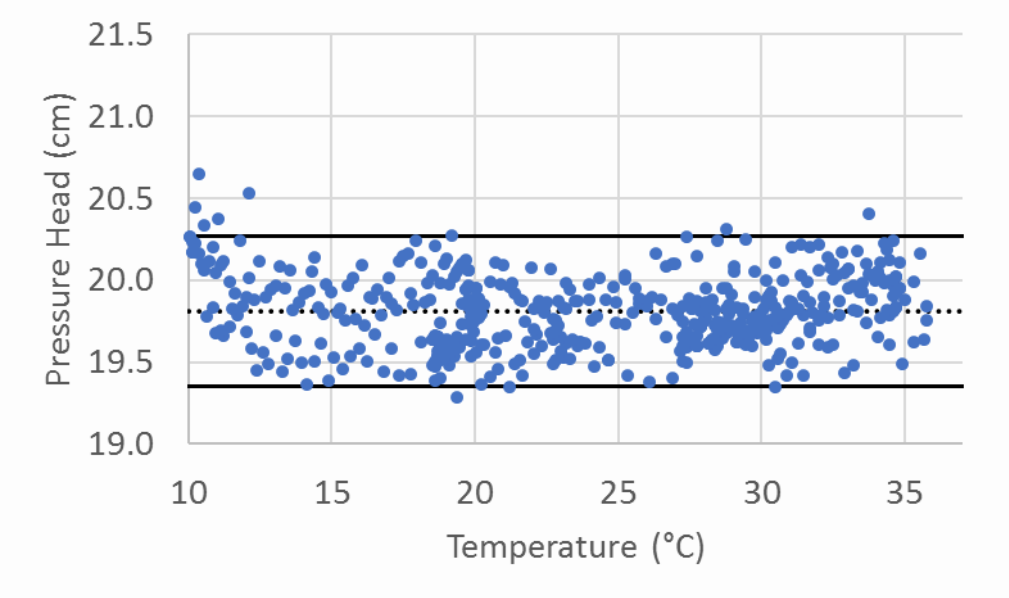

(b) Temperature Corrected Experimental Data

Note: the dotted line represents the known pressure head (19.81 cm), bracketed by two solid lines representing the error range of the sensor, ±0.46 cm.

Figure 5.5. Raw and corrected data for pressure transducer "C".

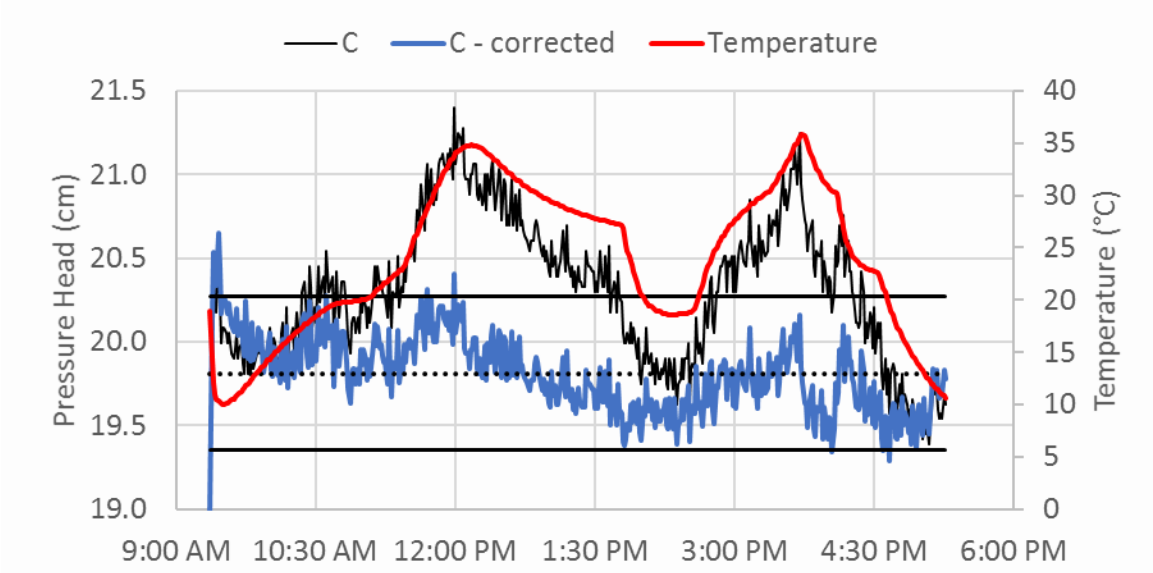

Note: The time series of this sensor over all temperature fluctuations experienced in the experiment. Before correction, the sensor reports pressure readings (water height) inflated with temperature change. After the correction, this fluctuation is reduced and is within the error range of the sensor.

Figure 5.6. Sensor C Corrected for Temperature Fluctuations

5.3 Results and Discussion – Applying Approach to Collected Field Data

One benefit of performing laboratory experiments on pressure transducers is in correcting erroneous field data measured by faulty sensors as a result of temperature fluctuation. Consider the hydrograph shown in Figure 5.7 from the LCC, where two different sensors yielded pressure-head data during a 3-week period. The hydrograph shows three prominent rain events seen in the "accurate data". One sensor ("erroneous data") yielded data fluctuating on a daily cycle with relatively large amplitudes, nearly 15% of the total stream height for the period. These variations were so strongly affected by temperature variations that the runoff events were masked by this error. In this figure, the daily maximum reported pressure head for this sensor fluctuated in an inverse relationship with the stream temperature, which fluctuated from approximately 16.8-20.6 °C during this time period. For example, on 6/17 the maximum pressure head (23.74 cm) occurred at 4:30 during the time when the stream was at a minimum temperature of 17.38 °C.

The minimum pressure head (20.03 cm) occurred at 17:00 during the maximum stream temperature of 20.23 °C.

The other pressure head sensor ("accurate data") shows a drawdown curve from a previous rain event, and a few other peaks associated with subsequent rain events. Knowing that the "accurate data" line came from a new ventilated sensor yielding more accurate data, which was backed up by field measurements of stream depth, and hypothesizing that the faulty sensor yielding the "erroneous data" had issues with thermal artifacts, the faulty sensor was replaced and brought to the laboratory for testing as discussed above.

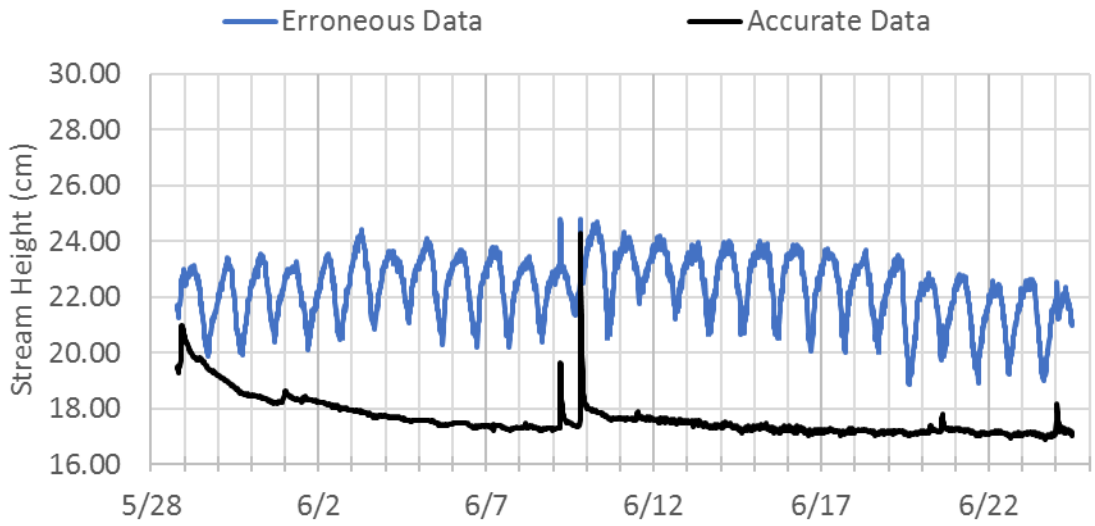

Note: This hydrograph of a monitored watershed shows three prominent rain events seen in the true hydrograph. The faulty sensor (pressure transducer) is showing daily cycles of stream height that are so strongly affected by temperature variations that the runoff events are masked by this error.

Figure 5.7. Two different measured hydrographs from two different sensors.

Following the steps detailed above for the laboratory experiment, a temperature-based pressure variation was found for the faulty sensor. This relationship is shown in Figure 5.8. For the faulty sensor, there is little variation in the pressure readings above approximately 20 °C, but there is high variation for temperatures below 20 °C. Therefore, an equation for the lower temperature range is the only correction required for this sensor. The variables for Equations 5.1

to 5.2 for this sensor are as follows: C_T = -1.6476, T_i = 20.698 °C, H_T = 19.812 cm, K = 53.914 cm. These variables were used to correct the dataset for the temperature variation experienced by the faulty in-stream sensor with the following equation:

$$H_{F,R} = H_F - C_T * (T_F - T_i) \quad \text{(Eq. 5.5)}$$

In equation 5, $H_{F,R}$ is the rectified pressure head (cm), H_F is the reported pressure head (cm), and T_F is the reported temperature (°C) for the field data.

The results of this correction are shown in Figure 5.9; these results are using only data determined from the temperature experiment and pressure data given from the utility software from ONSET. The peak head for the corrected data was 24.49 cm, compared to the accurate data peak of 24.29 cm. Following this correction, the L2 norm error was reduced from 4.84 for the original data to 0.93 for the corrected data (an 81% reduction). This is substantial, particularly because the "true" hydrology of the stream is now partially rectified. Before the data correction, the drawdown curve of the previous event was unseen, and 2 rain events on 6/9 were seen but look no more significant than the daily fluctuations of stream head. Any modeling of this watershed using such data would require high levels of evapotranspiration as well as nearly perfect infiltration and loss to groundwater of most rainfall (which is not reflective of the true hydrology). After correcting the data due to temperature errors of the in-stream sensor, these hydrological events are seen.

As Figure 5.9 shows, there were still daily fluctuations in the corrected data. These fluctuations were thought to be due to a similar temperature-induced error from the barometric sensor. The same experimental procedure was attempted for this sensor, and the temperature vs. pressure head relationship is shown in Figure 5.10. This data shows a relatively constant pressure head over the temperature range of the experiment. While other sensors in this paper yielded data

with a linear regression fit of 70% or more, this sensor yielded a linear regression fit of less than 28%. Thus, the fluctuations that exist in "corrected data" of Figure 5.9 could not be resolved any further without introducing additional errors.

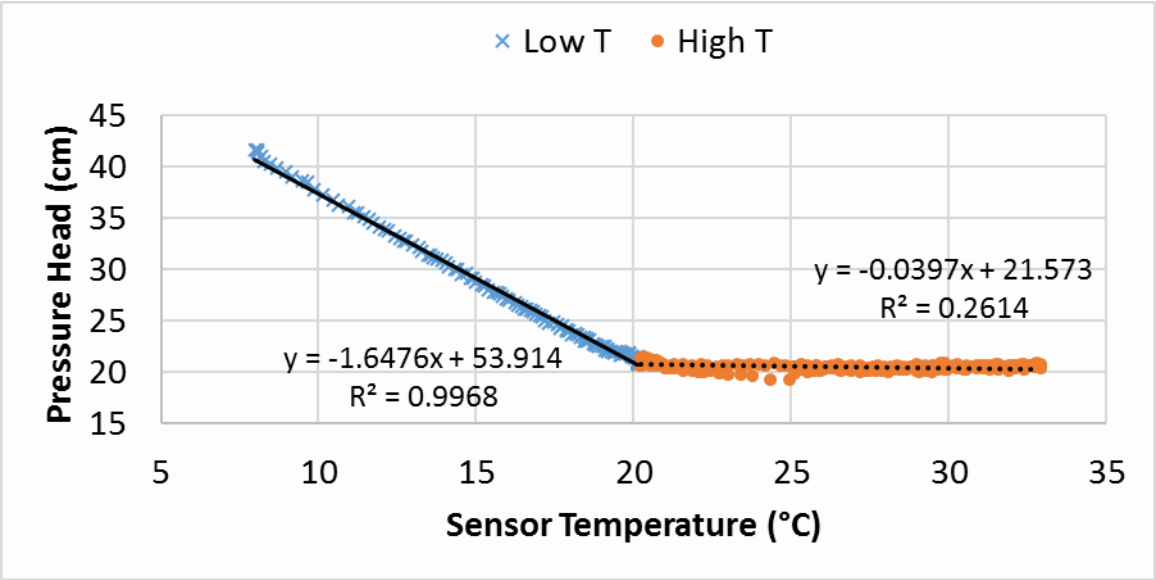

Figure 5.8. Results of lab experiment for the sensor retrieved from the field.

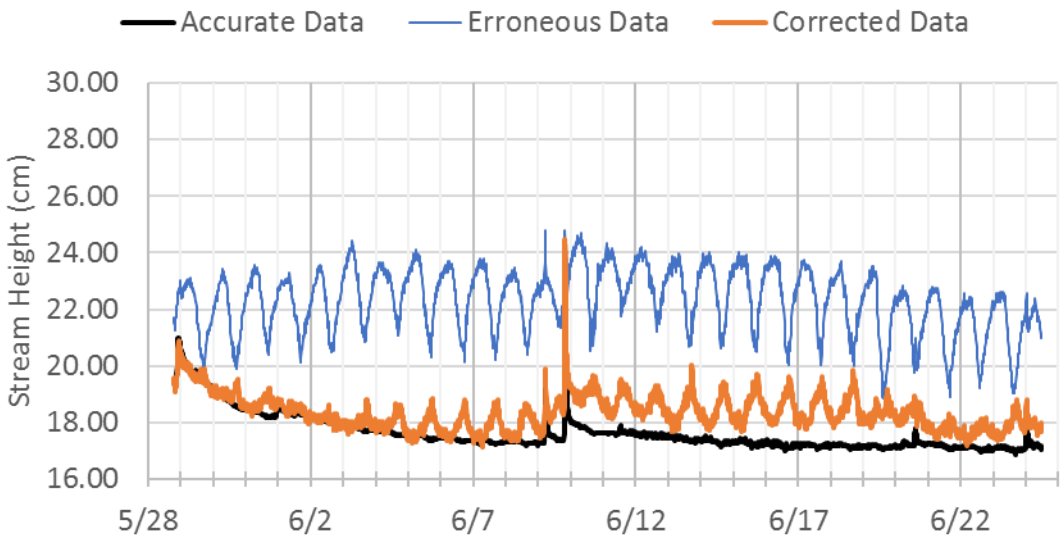

Figure 5.9. Hydrograph of the monitored watershed after temperature corrections.

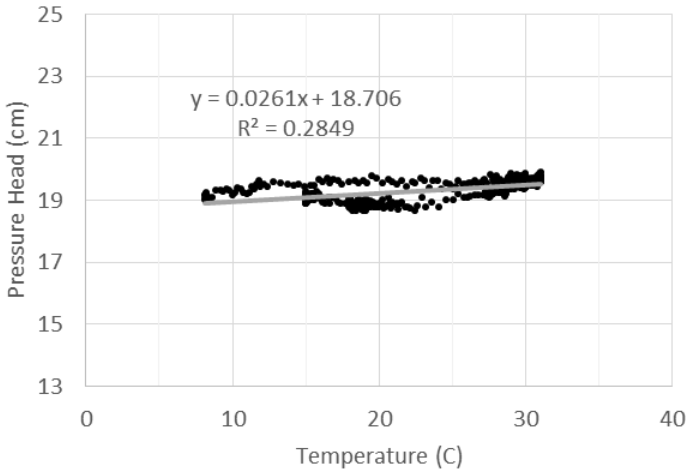

Figure 5.10. Barometric sensor pressure variations according to temperature.

The process described herein should be straightforward in nature, so that it can be applied by practitioners deploying these sensors in the field. It was not attempted to consider the complex nature of electronic signals that exist in data (such as that discussed by Freeman, 2004) in order to produce more reliable data. To better portray the process of removing temperature errors from pressure transducer data, a flowchart is shown in Figure 5.11 of the basic steps described in this work. This flowchart could be consulted for repetitions of the experiment and data analyses once the details of the process are understood.

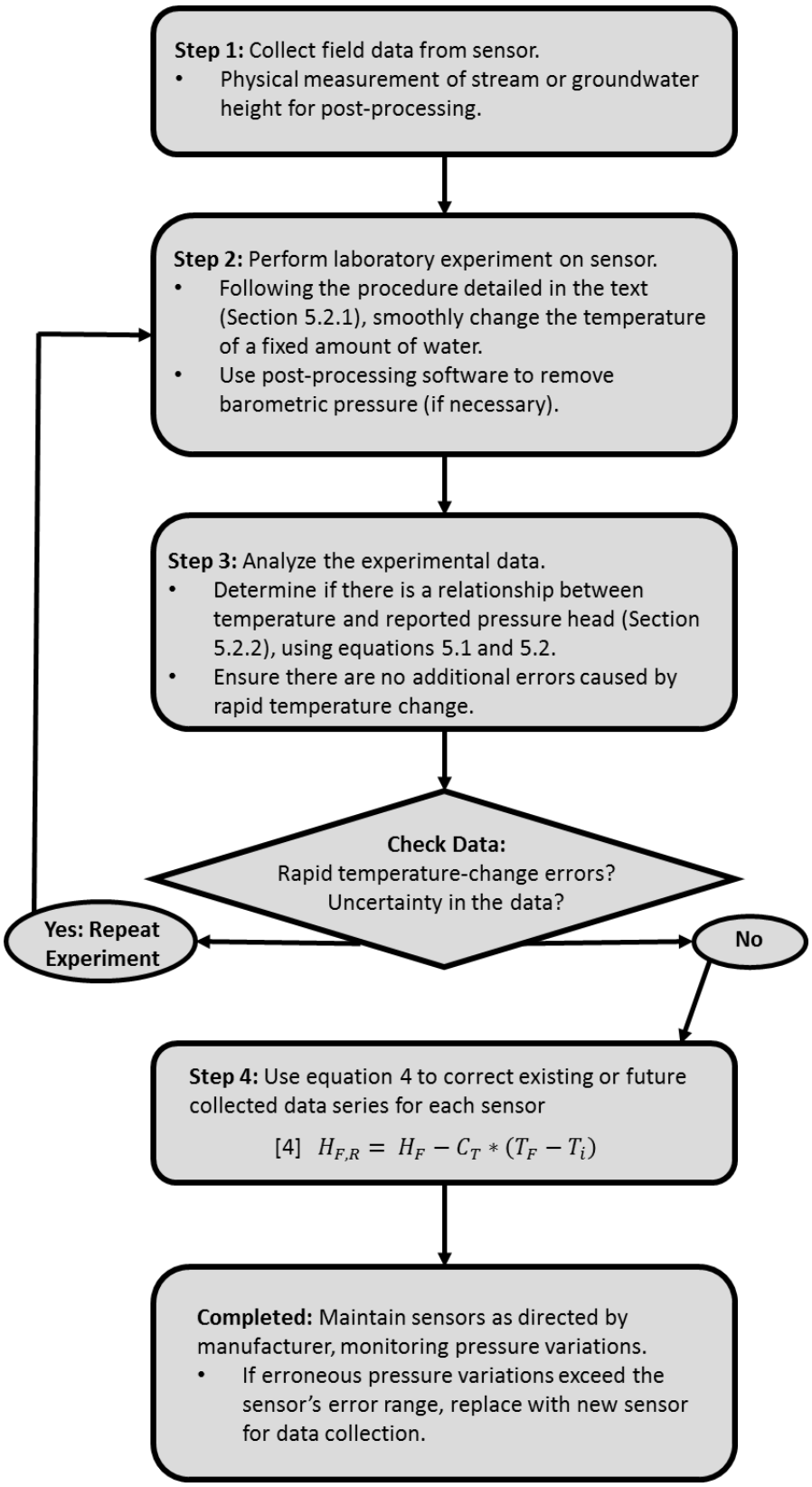

Figure 5.11. Flow chart for analyzing pressure transducer data.

5.4 Conclusions

As presented in the literature, there is evidence that some pressure transducers report artificially exaggerated pressure variations influenced by thermal artifacts. These variations follow a 24-hour cycle as the ambient temperatures fluctuate in the environment, and may be inaccurately attributed to evapotranspiration or other processes. As high resolution hydrological modeling software packages become more commonly used, these errors in field measurement datasets must be corrected to ensure accurate modeling and hydrological assessment. The work described herein established a method for correcting datasets that have been influenced by these thermal artifacts.

In this work, through laboratory experiments, comparisons with other data and field observations, some variations in readings experienced by pressure transducers were confirmed to be induced by temperature fluctuations. For field data that has been impacted by these errors, analyses of the instruments involved can yield a determination of exactly how much temperature affects each sensor. After determining such effects, more meaningful hydrographs can be produced following the process outlined in the flowchart shown in Figure 5.11.

For sensors experiencing extreme errors, it is recommended that they be replaced for future data collection; the correction procedure explained here can be used to retrieve information from previously collected data, however the absolute error may still be quite large. For sensors that are experiencing smaller pressure variations, this procedure could reduce the overall error to an acceptable range. If so, these sensors could continue to be used for field data collection with careful monitoring of the sensor drift, ensuring that the corrected data is within the associated error range for the sensor. Thus, this procedure has solved two problems in field hydrological studies: 1) the reduction of error for sensors that produce significant pressure

variations according to temperature fluctuations; and 2) a way to resolve these variations in functional sensors so they can continue to be deployed if necessary.

During the research conducted which led to this proposed methodology, other research needs were identified involving pressure transducers. Although manufacturers recommend avoiding rapid temperature changes, there may be some applications where pressure measurements are desired in an environment of rapidly changing temperatures (such as streams and water bodies receiving thermal loads during stormwater runoff or monitoring points close to thermal discharges from power plants). In these cases, it would be beneficial to know and be able to predict the pattern of pressure variation sensors report as a function of temperature change. Another future step is the ability to implement this methodology within the processing software that users are familiar with. Additionally, future work could focus on utilizing the principles discussed here to resolve existing field data without performing the laboratory experiment, if known pressure head values are available. Although these procedures will increase the accuracy and prolong the life of pressure transducers, researchers should be mindful of the variety of issues when considering the use of pressure transducers.

Chapter 6 – Conclusions and Recommendations

6.1 Conclusions

This dissertation presented research that was motivated by the need to evaluate impacts of stormwater runoff from roadways into small streams. Part of this work was done to address the objectives of project number 930-837R for the funding agency, the Alabama Department of Transportation. The overarching objective of this ALDOT project was to assess the impacts of the existing roadway (I-59) on the receiving water body, the LCC. Over the duration of this research, further insights into the complex relationship between groundwater tables and stream surface water during rain events were noticed in field measurements, leading to research efforts to incorporate these into hydrological models to simulate this system. Lastly, improvements to the quality of pressure transducer data were made by the formulation and verification of a procedure to remove thermal artifacts from stream and groundwater sensors.

The initial work on assessing the impacts of I-59 focused on water quality and surface stormwater runoff upstream and downstream of the roadway. In regards to nitrogen, phosphorous, pH, temperature, salinity, and other water quality parameters, it was determined that the road had no definable impact on the concentration of these constituents in stormwater runoff, except total nitrogen concentrations. For four samples, total nitrogen downstream of I-59 was between 1 to 2.5 mg/L higher than upstream, indicating that atmospheric deposition, or organic nitrogen sources were higher in the roadway than the upstream land uses. Maximum TSS concentrations were between 50 to 200 mg/L higher at the downstream site than the upstream site of the main branch, but up to 200 mg/L lower than the upstream site of the secondary branch. Thus, no additional sediment concentrations in stormwater runoff could be observed downstream of the roadway, because they were likely exceeded by the high sediment concentrations

upstream. Data analysis of stormwater runoff comparing measured rainfall and streamflow amounts indicated higher volumetric runoff coefficients for the upstream land uses than the additional roadway area. This is a counterintuitive result because it would be expected that the roadway area and drainage features would increase the relative surface runoff because the road subcatchment has more impermeable surfaces. This finding prompted the setup of groundwater observation wells, and the setup of hydrologic models for further investigation.

Two models were developed and calibrated for investigations into the stormwater runoff mechanisms at this research location: The Gridded Surface and Subsurface Hydrologic Analysis (GSSHA) model and the Stormwater Management Model (SWMM). Because of the discretization and model differences, surface-groundwater interaction and groundwater equations varied between the two models significantly. Both SWMM and GSSHA produced similar surface water runoff and precipitation infiltration, indicating that despite the discretization differences both models calculate overland processes with similar accuracy.

Stream bank storage was determined to be a dominant process for the measured data, and produced groundwater table elevations with small error ranges for the downstream location. For the downstream site, the summary error G_{gw} was 0.0481 and 0.0597 for GSSHA and SWMM, respectively. The summary error PEH for the downstream site was 18% and -38% for GSSHA and SWMM, respectively. Both models have high errors associated with groundwater table elevations in the median. The summary error G_{gw} for the median was 0.96 and 1.23 for GSSHA and SWMM, respectively. The summary error PEH for the median was -47% and -58% for GSSHA and SWMM, respectively. It is inferred that another process was responsible for the variation of groundwater table elevations in that location, not bank storage. Though GSSHA has a more rigorous groundwater component than SWMM, error analysis of the groundwater

solutions shows that SWMM and GSSHA have comparable solutions when compared to measured data.

6.2 Limitations

Because the focus of this research was on the impact of I-59 on the LCC by measuring downstream and upstream constituents, measurements were made within the stream channel. A limitation of this approach is that water quality aspects of stormwater runoff, such as nutrient concentrations, would likely have smaller concentrations within the stream due to dilution. Because the resolution of the methods used here for some of the water quality constituents were higher than the actual concentrations, it is unknown the precise concentrations of these parameters (such as NH_3). However, without this approach, a comparison to upstream concentrations would not be possible. Additionally, due to spatial variability of rainfall, equipment malfunction and availability, there is no data showing the sediment concentration in all 3 sites at the same time. Thus, observations and discussions about sources of sediment loadings are limited.

The hydrological models setup in this research focused on event-based surface water flow rates and groundwater table fluctuations as measured in the field. In order to accurately represent the roadway in GSSHA, small grid cells (5 m x 5m) were used. This approach required longer computational time per simulation than SWMM (approximately 300x more). Because of the computational time, long term simulations were not attempted in GSSHA. Additionally, due to limited data availability, evapotranspiration was not simulated in GSSHA, and instead the initial moisture conditions were calibrated and varied for each rain event. A major limitation noted in this research for the SWMM model setup is the discretization of the groundwater component.

Small catchments are yield more accurate overland simulation, however subsurface flow between subcatchments is not currently modeled in SWMM. Thus, for this model, the groundwater domain is an idealized component and has limited use in dynamic groundwater settings.

6.3 Future Recommendations

The work discussed here demonstrated that I-59 has no measured impact on the LCC, which received stormwater runoff from the roadway and has multiple locations of intersection within the watershed. In particular, it was noted that the roadway drainage features (grass-lined swales and median) provided adequate capacity for precipitation infiltration in part due to the low slopes compared to the surrounding areas. Future work should consider how variations in roadway geometries alter stormwater runoff delivery and retention. Additionally, the data shown here evaluated water quality parameters and stormwater runoff volume and flow rates with only the currently existing I-59. Future development in the area associated with the construction of the BNB would likely alter the hydrological response to rain events, as well as water quality constituents. Thus, future work should consider the BNB post-construction hydrology and water quality of the LCC.

Future development in this region should also be considered in conjunction with hydrological modeling. In particular, because an intersection of the BNB is planned for the area, SWMM and GSSHA models can be developed with estimated roadway conditions. This would aid in considerations of channel alignment, and choices of BMP installation. Because the GSSHA groundwater solution is more robust, it is likely that it would yield better estimates of the impact of development on the groundwater table. This is particularly useful when considering

infiltration based volume reduction approaches, which is the most common approach advised by Strecker et al. (2014).

In modeled results, the groundwater table elevations were not as accurately represented in the interstate median as the downstream location. Field measurements indicated that the median captured a significant amount of precipitation in prolonged events of low intensity. A more robust evaluation of the dynamics of this system could yield more insight to the capacity of roadway medians to capture runoff. Applying Richard's infiltration equation or using a 3D groundwater solver like MODFLOW (Harbaugh, 2005) could more accurately represent this complex surface-groundwater interaction.

Stream bank storage was a dominant process in this hydrological system, as indicated by modeled and measured data. A relevant and important area to address is whether roadway ditches have a similar storage effect. This could be accomplished through experimental setups and supplemented with field measured infiltration rate data.

Lastly, although the procedure discussed in Chapter 5 for improving pressure transducer data is relatively simplistic in nature, the process can be cumbersome and require a lot of data processing. Another step towards producing high quality stream and groundwater data would be to incorporate the proposed procedure into the software provided by the manufacturer to process logged data.

References

Abi Aad, M., Suidan, M., and Shuster, W. (2010). "Modeling Techniques of Best Management Practices: Rain Barrels and Rain Gardens Using EPA SWMM-5." J. Hydrol. Eng., 10.1061/(ASCE)HE.1943-5584.0000136, 434-443.

Alabama Department of Environmental Management (ADEM). (2013). MS4 Stormwater Management Program Plan: NPDES Permit No. ALS000006. Montgomery, AL: ADEM. https://www.dot.state.al.us/dsweb/Stormwater/doc/MS4SWMPP.pdf

Alabama Water Watch (2016). AlabamaWaterWatch.com. Accessed June 6, 2016.

American Forests (2009). Urban Ecosystem Analysis: Albuquerque, New Mexico. Analysis and report prepared for the City of Albuquerque.

Amoah, J. K., Amatya, D. M., & Nnaji, S. (2013). "Quantifying watershed surface depression storage: determination and application in a hydrologic model." Hydrological Processes, 27(17), 2401-2413.

ASCE Task Committee on Definition of Criteria for Evaluation of Watershed Models of the Watershed Management Committee, Irrigation and Drainage Division (1993). "Criteria for Evaluation of Watershed Models." J. Irrig. Drain Eng., 10.1061/(ASCE)0733-9437(1993)119:3(429), 429-442.

AQEG (Air Quality Expert Group). (2004). "Nitrogen Dioxide in the United Kingdom. London." Department for Environment, Food and Rural Affairs. http://uk-air.defra.gov.uk/assets/documents/reports/aqeg/nd-summary.pdf

Barco, O. J., Ciaponi, C., & Papiri, S. (2004). "Pollution in storm water runoff. Two cases: an urban catchment and a highway toll gate area." In NOVATECH, 5th international conference on sustainable techniques and strategies in urban water management. Lyon, June. 6-10.

Barrett, M., Irish, L., Jr., Malina, J., Jr., and Charbeneau, R. (1998). "Characterization of Highway Runoff in Austin, Texas, Area." J. Environ. Eng., 10.1061/(ASCE)0733-9372(1998)124:2(131), 131-137.

Barrett, M. E., Zuber, R. D., Collins, E. R., Malina, J. F., Charbeneau, R. J., & Ward, G. H. (1993). A review and evaluation of literature pertaining to the quantity and control of pollution from highway runoff and construction.

Bing Maps. www.bingmaps.com/mapspreview. Accessed at [October, 2016].

Bisht, D. S., Chatterjee, C., Kalakoti, S., Upadhyay, P., Sahoo, M., & Panda, A. (2016). Modeling urban floods and drainage using SWMM and MIKE URBAN: a case study. Natural Hazards, 84(2), 749-776.

Burszta-Adamiak, E., & Mrowiec, M. (2013). Modelling of green roofs' hydrologic performance using EPA's SWMM. Water Science and Technology, 68(1), 36-42.

Butler, C., Vasconcelos, J. G., Zech, W. C., and M. Moore (under review). “Impacts of Roadway Runoff on a Headwater Tributary of the Cahaba River, AL.” Journal of Water Management Modeling.

Cain III, S. F., Davis, G. A., Loheide II, S. P., & Butler Jr, J. J. (2004). “Noise in pressure transducer readings produced by variations in solar radiation.” Ground water, 42 (6), 939-944.

Capea, J. N., Y. S. Tanga, N. van Dijka, L. Lovea, M. A. Suttona, and S. C. F. Palmer. (2004). “Concentrations of Ammonia and Nitrogen Dioxide at Roadside Verges, and their Contribution to Nitrogen Deposition.” Environmental Pollution 132 (3): 469–78.

Chintalapudi, S., Sharif, H. O., Yeggina, S., & Elhassan, A. (2012). Physically Based, Hydrologic Model Results Based on Three Precipitation Products.

Chintalapudi, S., Sharif, H. O., & Xie, H. (2014). Sensitivity of Distributed Hydrologic Simulations to Ground and Satellite Based Rainfall Products. Water, 6(5), 1221-1245.

Cuevas, J. G., Calvo, M., Little, C., Pino, M., Dassori, P. (2010). “Are Diurnal Fluctuations in Streamflow Real?” Journal of Hydrological Hydromechanics 58: 149-162.

Downer, C., and Ogden, F. (2002) "GSSHA user’s manual, gridded surface subsurface hydrologic analysis version 1.43 for WMS 6.1." Engineer Research and Development Center Technical Report, Vicksburg, MS.

Downer, C., and Ogden, F. (2004). "GSSHA: Model to Simulate Diverse Stream Flow Producing Processes." J. Hydrol. Eng., 10.1061/(ASCE)1084-0699(2004)9:3(161), 161-174.

Driscoll, E. D., Shelley, P. E., & Strecker, E. W. (1990). “Pollutant loadings and impacts from highway stormwater runoff.” Volume III: Analytical investigation and research report (No. FHWA-RD-88-008).

Duncan, R.S., Elliott, C.P., Fluker, B.L. and Kuhajda, B.R. (2010). Habitat use of the watercress darter (estheostoma nuchale): An endangered fish in an urban landscape. American Midland Naturalist, Vol. 164, pp. 9-21.

ESRI. (2016). World Imagery. More details at http://www.arcgis.com/home/item.html?id=10df2279f9684e4a9f6a7f08febac2a9 Accessed [October 27, 2016].

Follum, M. L., Downer, C. W., Niemann, J. D., Roylance, S. M., & Vuyovich, C. M. (2015). A radiation-derived temperature-index snow routine for the GSSHA hydrologic model. Journal of Hydrology, 529, 723-736.

Freeman, L. A., Carpenter, M. C., Rosenberry, D. O., Rousseau, J. P., Unger, R., & McLean, J. S. (2004). “Use of submersible pressure transducers in water-resources investigations.” US

Geological Survey Techniques of Water-Resources Investigations, book 8, chap. A3 [variously paged].

Gomi, T., Sidle, R. C., & Richardson, J. S. (2002). "Understanding Processes and Downstream Linkages of Headwater Systems Headwaters differ from downstream reaches by their close coupling to hillslope processes, more temporal and spatial variation, and their need for different means of protection from land use." BioScience, 52(10), 905-916.

Gribovszki, Z., Szilágyi, J., & Kalicz, P. (2010). "Diurnal fluctuations in shallow groundwater levels and streamflow rates and their interpretation–A review." Journal of Hydrology, 385(1), 371-383.

Gribovszki, Z., Kalicz, P., and Szilágyi, J. (2013). "Does the accuracy of fine-scale water level measurements by vented pressure transducers permit for diurnal evapotranspiration estimation?" Journal of Hydrology 488: 166–169.

Gubernick, B., Clarkin, K. and Furniss, M.J. (2003). Design and construction of aquatic organism passage at road-stream crossings: site assessment and geomorphic considerations in stream simulation culvert design, pp. 30-41. In: 2003 Proceedings of the International Conference on Ecology and Transportation (Irwin, C.L., Garrett, P. and McDermott, K.P., Eds.). Center for Transportation and the Environment. Raleigh, NC: North Carolina State University.

Habib, E., Malakpet, C. G., Tokay, A., & Kucera, P. A. (2008). Sensitivity of streamflow simulations to temporal variability and estimation of Z–R relationships. Journal of Hydrologic Engineering, 13(12), 1177-1186.

Habib, E. H., Meselhe, E. A., & Aduvala, A. V. (2008). Effect of local errors of tipping-bucket rain gauges on rainfall-runoff simulations. Journal of Hydrologic Engineering, 13(6), 488-496.

Habib, E., Ma, Y., & Williams, D. (2012). Development of a web-based hydrologic education tool using Google Earth resources. Geological Society of America Special Papers, 492, 431-439.

Harbaugh, A.W. (2005). "MODFLOW-2005, The U.S. Geological Survey modular ground-water model—the Ground-Water Flow Process." U.S. Geological Survey Techniques and Methods 6-A16, variously p.

Harned, D.A. (1988). Effects of highway runoff on streamflow and water quality in the Sevenmile Creek basin, a rural area in the Piedmont Province of North Carolina, United States Geological Survery, Water supply paper 2329.

Han, Y., S. Lau, M. Kayhanian and M. K. Stenstrom. (2006). "Characteristics of Highway Stormwater Runoff." Water Environment Research 78 (12): 2377–88.

Hanson, R.L., (1991). "Evapotranspiration and Droughts." in Paulson, R.W., Chase, E.B., Roberts, R.S., and Moody, D.W., Compilers, National Water Summary 1988-89--Hydrologic Events and Floods and Droughts: U.S. Geological Survey Water-Supply Paper 2375, p. 99-104.

El Hassan, A. A., Sharif, H. O., Jackson, T., & Chintalapudi, S. (2013). Performance of a conceptual and physically based model in simulating the response of a semi-urbanized watershed in San Antonio, Texas. Hydrological Processes, 27(24), 3394-3408.

Hatch, C. E., Fisher, A. T., Ruehl, C. R., & Stemler, G. (2010). "Spatial and temporal variations in streambed hydraulic conductivity quantified with time-series thermal methods." Journal of Hydrology, 389(3), 276-288.

Herngren, L., Goonetilleke, A. and Ayoko, G.A. (2006). Analysis of heavy metals in road-deposited sediments. Analytica Chemica Acta, Vol. 571, pp. 270-278.

Hoffman, E. J., G. L. Mills, J. S. Latimer and J. G. Quinn. (1984). "Urban Runoff as a Source of Polycyclic Aromatic Hydrocarbons to Coastal Waters." Environmental Science and Technology 18:580–7.

Homer, C.G., Dewitz, J.A., Yang, L., Jin, S., Danielson, P., Xian, G., Coulston, J., Herold, N.D., Wickham, J.D., and Megown, K., (2015). "Completion of the 2011 National Land Cover Database for the conterminous United States-Representing a decade of land cover change information." Photogrammetric Engineering and Remote Sensing, v. 81, no. 5, p. 345-354.

Irish, L. B., Jr., W. G. Lesso, M. E. Barrett, J .F. Malina, R. J. Charbeneau and G. H. Ward. (1995). "An Evaluation of the Factors Affecting the Quality of Highway Runoff in the Austin, Texas Area." Technical Report CRWR 264. Austin, TX: University of Texas at Austin, Center for Research in Water Resources. http://www.crwr.utexas.edu/reports/pdf/1995/rpt95-9.pdf

Jang, S., Cho, M., Yoon, J., Yoon, Y., Kim, S., Kim, G., ... & Aksoy, H. (2007). Using SWMM as a tool for hydrologic impact assessment. Desalination, 212(1), 344-356.

James, W., Rossman, L., and James, R. (2016). "User's guide to SWMM 5." CHI Press Publication R242. ISBN: 978-0-9808853-5-4.

Johnson, M. L., I. Werner, P. G. Green, S. Fong, L. Deanovic and C. C. Fessler. (2007). "Toxicity of Stormwater from Transportation Facilities." Prepared for The Department of Transportation. Davis, CA: University of California, Davis.

Jones, J. A., Swanson, F. J., Wemple, B. C. and Snyder, K. U. (2000). "Effects of Roads on Hydrology, Geomorphology, and Disturbance Patches in Stream Networks." Conservation Biology, 14: 76–85. doi:10.1046/j.1523-1739.2000.99083.x

Jones, N., Nelson, J., Swain, N., Christensen, S., Tarboton, D., & Dash, P. (2014). Tethys: A Software Framework for Web-Based Modeling and Decision Support Applications. In 7th International Congress on Environmental Modelling and Software, DP Ames, NWT Quinn, and AE Rizzoli (Editors). iEMSs, San Diego, California (pp. 170-177).

Julien, P. Y., Saghafian, B., & Ogden, F. L. (1995). RASTER-BASED HYDROLOGIC MODELING OF SPATIALLY-VARIED SURFACE RUNOFF1. JAWRA Journal of the American Water Resources Association, 31(3), 523-536.

Kahklen, K., and J. Moll. (1999). "Measuring Effects of Roads on Groundwater: Five Case Studies." Pages 24. San Dimas, California: U.S. Department of Agriculture Forest Service, San Dimas Technology and Development Center.

Kalin, L., & Hantush, M. M. (2006). "Hydrologic modeling of an eastern Pennsylvania watershed with NEXRAD and rain gauge data." Journal of Hydrologic Engineering, 11(6), 555-569.

Kayhanian, M. and Stenstrom, M.K. (2005). Mass loading of first flush pollutants with treatment strategy simulations. Transportation Research Record 1904, pp. 1-11.

LaBadie, K. (2010). Identifying Barriers to Low Impact Development and Green Infrastructure in the Albuquerque Area. Albuquerque, New Mexico: The University of New Mexico, 2010. 8-43. Web. Accessed 15 Jul. 2013.

Lambin, Eric F., and Patrick Meyfroidt (2011). "Global land use change, economic globalization, and the looming land scarcity." Proceedings of the National Academy of Sciences 108, no. 9. 3465-3472.

Lau, S.L., Ma, J.S., Kayhanian, M. and Stenstrom, M.K. (2004). First flush of organics in highway runoff. Global Solutions for Urban Drainage, pp. 1-12.

Lee, J.Y., Kim, H., Kim, Y. and Han, M.Y. (2011). Characteristics of the event mean concentration (EMC) from rainfall runoff on an urban highway. Environmental Pollution, Vol. 159, pp. 884-888.

Li, Y., Lau, S.L, Kayhanian, M. and Stestrom M.K. (2005). Particle size distribution in highway runoff. Journal of Environmental Engineering, Vol. 131, pp. 1267-1276.

Li, B., Yu, Z., Liang, Z., & Acharya, K. (2014). Hydrologic response of a high altitude glacierized basin in the central Tibetan Plateau. Global and Planetary Change, 118, 69-84.

Line., D.E., M.B. Shaffer, and J. Blackwell. (2009) "Effects of Highway Construction in Sedgefield Lakes and Kings Mill Continued." Final Report. Raleigh, NC: NC State University, Biological and Agricultural Dept, 9 January 2009. 3-5. Web. Report No. FHWA/NC/2008-17

Liong, S. Y., Chan, W. T., & Lum, L. H. (1991). “Knowledge-based system for SWMM runoff component calibration.” Journal of Water Resources Planning and Management, 117(5), 507-524.

Liu, Z. and Higgins, C. W. (2015). “Does temperature affect the accuracy of vented pressure transducer in fine-scale water level measurement?” Geoscientific Instrumentation Methods and Data Systems 4: 65-73.

Marsalek, J., Q. Rochfort, B. Brownlee, T. Mayer and M. Servos. (1999). “An Exploratory Study of Urban Runoff Toxicity.” Water Science Technology 39 (12): 33–9.

McCutcheon, M., & Wride, D. (2013). Shades of Green: Using SWMM LID Controls to Simulate Green Infrastructure. Journal of Water Management Modeling, R246-15, 289-301.

McDonald, M. G., and Harbaugh, A. W. (1988). “A modular three-dimensional finite-difference ground-water flow model.” Techniques of Water-Resources Investigations of the United States Geological Survey, U.S. Geological Survey. Book 6, Chapter A1.

McLaughlin, D. L., & Cohen, M. J. (2011). “Thermal artifacts in measurements of fine-scale water level variation.” Water Resources Research, 47(9).

Mein, R. G., C. L. Larson. (1973). “Modeling infiltration during a steady rain.” Water Resources Research, 92, 384–394.

Moore, M., Butler, C., Vasconcelos, J. (2015) “Assessing the Impacts of Stormwater Runoff from I-59 to a Headwater Stream in Central Alabama.” Journal of Water Management Modeling. DOI: 10.14796/JWMM.C383.

Moynihan, K. P., & Vasconcelos, J. G. (2014). “SWMM Modeling of a Rural Watershed in the Lower Coastal Plains of the United States.” Journal of Water Management Modeling.

National Atmospheric Deposition Program. (2014). NADP Program Office, Illinois State Water Survey.

National Oceanic and Atmospheric Administration (NOAA). (2002) C”limatography of the United States, No. 81: Monthly Station Normals of Temperature, Precipitation, and Heating

and Cooling Degree Days 1971–2000." Asheville, NC: National Oceanic and Atmospheric Administration; National Environmental Satellite, Data, and Information Service; National Climatic Data Center. http://nsstc.uah.edu/aosc/files/ALnorm.pdf

Negishi, J. N., Sidle, R. C., Ziegler, A. D., Noguchi, S., & Rahim, N. A. (2008). "Contribution of intercepted subsurface flow to road runoff and sediment transport in a logging-disturbed tropical catchment." Earth Surface Processes and Landforms, 33(8), 1174-1191.

Nyholm, T., Rasmussen, K. R., & Christensen, S. (2003)." Estimation of stream flow depletion and uncertainty from discharge measurements in a small alluvial stream." Journal of Hydrology, 274(1), 129-144.

Ogden, F. L., Raj Pradhan, N., Downer, C. W., & Zahner, J. A. (2011). Relative importance of impervious area, drainage density, width function, and subsurface storm drainage on flood runoff from an urbanized catchment. Water Resources Research, 47(12).

Ogden, F.L. Evidence of equilibrium peak runoff rates in steep tropical terrain on the island of Dominica during Tropical Storm Erika, August 27, 2015. J. Hydrol. (2016), http://dx.doi.org/10.1016/j.jhydrol.2016.08.041

Onset Company Corporation. U20-001-01 Logger Manual (2014). Accessed at (10/2015) http://www.onsetcomp.com/products/data-loggers/u20-001-01

Peterson, E. W., & Wicks, C. M. (2006). Assessing the importance of conduit geometry and physical parameters in karst systems using the storm water management model (SWMM). Journal of hydrology, 329(1), 294-305.

Pitt, R. (2007). "Water Sample Collection Methods. Module 3 of Experimental Design and Field Sampling." Tuscaloosa, AL: University of Alabama Department of Civil, Construction, and Environmental Engineering. http://rpitt.eng.ua.edu/Class/Classes.shtml

Pitt, R., Maestre, A., and Morquecho, R. (2004). “The national stormwater quality database (NSQD, version 1.1).” In 1st Annual Stormwater Management Research Symposium Proceedings. pp. 13-51.

Pradhan, N. R., A. R. Byrd, M. Jourdan, and J. Ellis. 2016. Development of predictive relationships for the estimates of a return period flood effects in ungaged basins. ERDC/CHL CHETN-VIII-8. Vicksburg, MS: U.S. Army Engineer Research and Development Center.

Rai, P. K., Chahar, B. R., & Dhanya, C. T. (2016). GIS-based SWMM model for simulating the catchment response to flood events. Hydrology Research, nh2016260.

Reed, S., Koren, V., Smith, M., Zhang, Z., Moreda, F., Seo, D. J., and D.M.I.P. participants (2004). “Overall distributed model intercomparison project results.” Journal of Hydrology, 298(1), 27-60.

Rosa, D. J., Clausen, J. C., & Dietz, M. E. (2015). Calibration and verification of SWMM for low impact development. JAWRA Journal of the American Water Resources Association, 51(3), 746-757.

Schueler, T. R., P. A. Kumble and M. A. Heraty. (1992). “Current Assessment of Urban Best Management Practices: Techniques for Reducing Non-Point Source Pollution in the Coastal Zone.” Washington, DC: Metropolitan Washington Council of Governments, Department of Environmental Programs, Anacostia Restoration Team.

Seibert, J., & McDonnell, J. J. (2002). “On the dialog between experimentalist and modeler in catchment hydrology: Use of soft data for multicriteria model calibration.” Water Resources Research, 38(11).

Shaheen, D. G. (1975). “Contributions of Urban Roadways to Water Pollution.” Washington, DC: U. S. Environmental Protection Agency Office of Research and Development. EPA-600/2-75-004.

Sharif, H., Chintalapudi, S., Hassan, A., Xie, H., and Zeitler, J. (2010). "Physically Based Hydrological Modeling of the 2002 Floods in San Antonio, Texas." J. Hydrol. Eng., 10.1061/(ASCE)HE.1943-5584.0000475, 228-236.

Sharif, H. O., Hassan, A. A., Bin-Shafique, S., Xie, H., & Zeitler, J. (2010). Hydrologic Modeling of an Extreme Flood in the Guadalupe River in Texas1

Smith, B. K., Smith, J. A., Baeck, M. L., & Miller, A. J. (2015). Exploring storage and runoff generation processes for urban flooding through a physically based watershed model. Water Resources Research, 51(3), 1552-1569.

Soil Survey Staff, Natural Resources Conservation Service, United States Department of Agriculture. Web Soil Survey. Available online at http://websoilsurvey.nrcs.usda.gov/. Accessed [June/15/2015].

Spane, F. A. (2002). “Considering barometric pressure in groundwater flow investigations.” Water resources research, 38(6), 14-1.

State Climate Office of North Carolina, NC State University. CRONOS [internet database] available at http://climate.ncsu.edu/cronos/. Accessed February 02, 2016.

Steele County. Water Management Plan Update. (2016) Available online at http://www.co.steele.mn.us/departments/environmental_services/docs/Steele_County_Water_Plan_2011_Amendment_FinalVersion.pdf. Accessed [01/27/2016].

Strecker, Eric, et al. (2014) “Volume Reduction of Highway Runoff in Urban Areas.” NCHRP Report 802. No. NCHRP Project 25-41.

Sun, Y. W., Wei, X. M., & Pomeroy, C. A. (2011). Global analysis of sensitivity of bioretention cell design elements to hydrologic performance. Water Science and Engineering, 4(3), 246-257.

Szilágyi, J., Gribovszki, Z., Kalicz, P., & Kucsara, M. (2008). "On diurnal riparian zone groundwater-level and streamflow fluctuations." Journal of Hydrology, 349(1), 1-5.

Taylor, J. R. (1982). "An Introduction to Error Analysis: The Study of Uncertainties in Physical Measurements." 327 pp. Univ. Sci. Books, Mill Valley, Calif.

Temprano, J., Arango, Ó., Cagiao, J., Suárez, J., & Tejero, I. (2006). Stormwater quality calibration by SWMM: A case study in Northern Spain. water SA, 32(1), 55-63.

Thomson, N. R., McBean, E. A., Mostrenko, I. B., & Snodgrass, W. J. (1994). "Characterization of stormwater runoff from highways." Current Practices in Modelling the management of stormwater impacts, CRC Publishers, 141-157.

Thompson, D. B. (2006). "The Rational Method." http://drdbthompson.net/writings/rational.pdf (Accessed October, 2016).

Tian, Y., Zheng, Y., Wu, B., Wu, X., Liu, J., & Zheng, C. (2015). Modeling surface water-groundwater interaction in arid and semi-arid regions with intensive agriculture. Environmental Modelling & Software, 63, 170-184.

Trescott, P. C., & Larson, S. P. (1976). "Documentation of finite-difference model for simulation of three-dimensional ground-water flow." No. 76-591. US Geological Survey.

Trimble Report, County, B. (2013) "Wolf Bay Watershed Study." Available at baldwincountyal.gov. Accessed [05/13/2016].

Tsihrinris, V.A., and Hamid, R. (1997). Modeling and management of urban stormwater runoff quality: A Review. Water Resources Management, Vol. 11, pp. 137-164.

Tsihrintzis, V. A., and Hamid, R. (1998). “Runoff quality prediction from small urban catchments using SWMM.” Hydrological Processes, 12(2), 311-329.

USGS. http://water.usgs.gov/edu/watercycle.html (accessed October 27, 2016)

Van Griensven, A., Thomas Meixner, S. Grunwald, T. Bishop, M. Diluzio, and R. Srinivasan. (2006). "A global sensitivity analysis tool for the parameters of multi-variable catchment models." Journal of hydrology 324, no. 1: 10-23.

Viessman, Jr., W. and Lewis, G. L. (2003) “Introduction to Hydrology.” Pearson Education, Inc., Upper Saddle River, New Jersey, USA.

Wang, X., Liu, T., Yang, D., Qu, Z., Clary, C., and Wunneburger, C. (2011). "Simulating Hydrologic Effects of Raised Roads within a Low-Relief Watershed." J. Hydrol. Eng., 10.1061/(ASCE)HE.1943-5584.0000351, 585-597.

Warwick, J. and Tadepalli, P. (1991). "Efficacy of SWMM Application." J. Water Resour. Plann. Manage., 10.1061/(ASCE)0733-9496(1991)117:3(352), 352-366.

Watts, R.D., R.W. Compton, J.H. McCammon, C.L. Rich, and S.M. Wright. (2005). “Distance to the nearest road in the conterminous United States.” Fact Sheet 2005-3011. Fort Collins, CO: U.S. Geological Survey. 2p.

Wesseling, P. (2009). “Principles of computational fluid dynamics” (Vol. 29). Springer Science & Business Media.

Wheeler, A. P., P. L. Angermeier and A. E. Rosenberger (2006). “Impacts of New Highways and Subsequent Landscape Urbanization on Stream Habitat and Biota.” Reviews in Fisheries Science 13 (3): 141–64.

White, K. D. and C. Bernhard (2014). “Vegetated Filter Strip Performance Evaluation for Cost-Effective Roadway Runoff Treatment in Alabama.” ALDOT Research Project 930-811R (Final Report). 70 p.

Wright, D., Smith, J., & Baeck, M. L. (2013, April). Rainfall and Flood Frequency Analysis Using High-Resolution Radar Rainfall Fields and Stochastic Storm Transposition. In EGU General Assembly Conference Abstracts (Vol. 15, p. 5468).

Wu, J. S., C. J. Allan, W. L. Saunders and J. B. Evett. (1998). “Characterization and Pollutant Loading Estimation for Highway Runoff.” Journal of Environmental Engineering 124:584–92.

Wu, J. Y., Thompson, J. R., Kolka, R. K., Franz, K. J., & Stewart, T. W. (2013). Using the Storm Water Management Model to predict urban headwater stream hydrological response to climate and land cover change. Hydrology and Earth System Sciences, 17(12), 4743.

Yang, L., Smith, J. A., Baeck, M. L., & Zhang, Y. (2016). Flash flooding in small urban watersheds: Storm event hydrologic response. Water Resources Research.

Zhang, G., Guhathakurta, S., Dai, G., Wu, L., & Yan, L. (2013). The control of land-use patterns for stormwater management at multiple spatial scales. Environmental management, 51(3), 555-570.

Zhang, Y., and W. Shuster, W. (2014). “The Comparative Accuracy of Two Hydrologic Models in Simulating Warm-Season Runoff for Two Small, Hillslope Catchments.” JAWRA Journal of the American Water Resources Association, 50(2), 434-447.

Zhang, L., Jin, X., He, C., Zhang, B., Zhang, X., Li, J., Zhao, C., Tian, J., and C. DeMarchi (2016). "Comparison of SWAT and DLBRM for Hydrological Modeling of a Mountainous

Watershed in Arid Northwest China." J. Hydrol. Eng., 10.1061/(ASCE)HE.1943-5584.0001313, 04016007.

Zhu, J., Young, M., Healey, J., Jasoni, R., and J. Osterberg (2011). "Interference of river level changes on riparian zone evapotranspiration estimates from diurnal groundwater level fluctuations." Journal of Hydrology, 403(3), 381-389.

Zoppou, C. (2000). "Review of urban storm water models." Environmental Modelling and Software. Vol. 16, 195-231.

Appendix

Biomonitoring form from the LCC, upstream of I-59.

Alabama Water Watch
STREAM BIOMONITORING DATA FORM

☐ online

Group Name: _____

Collector(s): Cat, Mitchell, Dr V, Douglas Address: _____

City: _____ State: _____ Zip: _____ Phone #: _____

Sample Date: 3/23/15 Sample Time: _____ ~~AWW~~ Site Code: 3-I-59 Wes

Watershed: _____ Waterbody: _____ County & State: _____

Sampling site location: _____

(Notify the AWW office about any changes in sampling site location.)

Waterbody condition: ☐ Adequate Depth ☐ Inadequate Depth ☐ Dry ☐ No Access

Tidally influenced streams and rivers: ☐ Rising Tide ☐ Falling Tide ☐ Uncertain

Max of 10 to identify

Group I Taxa	Letter Code *	Group II Taxa	Letter Code *	Group III Taxa	Letter Code *
Stonefly	1R A	Dragonfly	4 C	Midge	5 C
Mayfly	1R A	Damselfly	4 C	Aquatic Worm	5 C
Caddisfly	10+ A	Cranefly	1 R	Leech	Ø
Riffle Beetle	4C	Blackfly	—	Pouch Snail***	Ø
Water Penny Beetle	2 R	Filtering Caddisfly**	10+ A		
Snail	10+ A	Hellgramite	Ø		
		Scud	1 R		
		Sowbug	10+ A		
		Crayfish	Ø		
		Asiatic Clam	Ø		
Number of Taxa= 6		Number of Taxa= 6		Number of Taxa= 2	
Multiply by 3 = 18		Multiply by 2 = 12		Multiply by 1 = 2	
(Index Value)		(Index Value)		(Index Value)	

* **Letter Code**: **R** = 1 to 3 (Rare); **C** = 4 to 9 (Common); **A** = 10 or more (Abundant)

** Filtering Caddisflies are in the Family Hydropsychidae (gills on abdomen; common caddisfly)
*** Pouch snails are in the Family Physidae (shell opens to the left; air-breathing snail)

STREAM BIOTIC INDICES		STREAM QUALITY ASSESSMENT (*Check box corresponding to Cumulative Index Value*)			
Total Number of Taxa (*Sum of Number of Taxa in each group*)	13	**POOR** <11	☐	**FAIR** 11-16	☐
Cumulative Index Value (*Sum of Index Values for each group*)	32	**GOOD** 17-22	☐	**EXCELLENT** >22	☑

Page 1 of 2

Biomonitoring form from the LCC, downstream of I-59.

Alabama Water Watch

STREAM BIOMONITORING DATA FORM

☐ online

Group Name: _____

Collector(s): Cat, Mitchell, Dr V., Douglas Address: _____

City: Trussville State: _____ Zip: _____ Phone #: _____

Sample Date: _____ Sample Time: _____ ~~AWW~~ Site Code: 1-I-59 E

Watershed: _____ Waterbody: _____ County & State: _____

Sampling site location: _____

(Notify the AWW office about any changes in sampling site location.)

Waterbody condition: ☑ Adequate Depth ☐ Inadequate Depth ☐ Dry ☐ No Access

Tidally influenced streams and rivers: ☐ Rising Tide ☐ Falling Tide ☐ Uncertain

Group I Taxa	Letter Code *	Group II Taxa	Letter Code *	Group III Taxa	Letter Code *
Stonefly	10 A	Dragonfly	3R	Midge	2R
Mayfly	6C	Damselfly	2R	Aquatic Worm	3R
Caddisfly	3R	Cranefly	-0-	Leech	
Riffle Beetle	3R	Blackfly	-0-	Pouch Snail***	
Water Penny Beetle	Ø	Filtering Caddisfly**	3R		
Snail (right opening)	10 A	Hellgramite	4C		
Cased Caddisfly	5C	Scud	4C		
		Sowbug	-0-		
		Crayfish	2R		
		Asiatic Clam	2R		

Number of Taxa= 10
Multiply by 3 = 12 (Index Value)

Number of Taxa= 7
Multiply by 2 = 14 (Index Value)

Number of Taxa= 2
Multiply by 1 = 2 (Index Value)

* **Letter Code: R** = 1 to 3 (Rare); **C** = 4 to 9 (Common); **A** = 10 or more (Abundant)

** Filtering Caddisflies are in the Family Hydropsychidae (gills on abdomen; common caddisfly)
*** Pouch snails are in the Family Physidae (shell opens to the left; air-breathing snail)

STREAM BIOTIC INDICES		STREAM QUALITY ASSESSMENT (*Check box corresponding to Cumulative Index Value*)			
Total Number of Taxa (*Sum of Number of Taxa in each group*)	15	POOR <11	☐	FAIR 11-16	☐
Cumulative Index Value (*Sum of Index Values for each group*)	29	GOOD 17-22	☐	EXCELLENT >22	☑

Page 1 of 2